Pat1 promotes processing body assembly by enhancing the phase separation of the DEAD-box ATPase Dh1 and RNA

Ruchika Sachdev[1], Maria Hondele[1], Miriam Linsenmeier[1], Pascal Vallotton[1], Christopher F. Mugler[1,2,3], Paolo Arosio[1], and Karsten Weis [1, 4]

[1] ETH Zurich, 8093 Zurich, Switzerland

[2] University of California, Berkeley, Berkeley CA, 94720, USA

[3] Current address: Amyris Inc. 5885 Hollis Street, Emeryville, 94608, California, USA

[4] To whom correspondence should be addressed

Email: karsten.weis@bc.biol.ethz.ch

Competing interests:

The authors have declared that no competing interests exist.

Abstract

Processing bodies (PBs) are cytoplasmic mRNP granules that assemble via liquid-liquid phase separation and are implicated in the decay or storage of mRNAs. How PB assembly is regulated in cells remains unclear. We recently identified the ATPase activity of the DEAD-box protein Dhh1 as a key regulator of PB dynamics and demonstrated that Not1, an activator of the Dhh1 ATPase and member of the CCR4-NOT deadenylase complex inhibits PB assembly *in vivo* [Mugler et al., 2016]. Here, we show that the PB component Pat1 antagonizes Not1 and promotes PB assembly via its direct interaction with Dhh1. Intriguingly, *in vivo* PB dynamics can be recapitulated *in vitro*, since Pat1 enhances the phase separation of Dhh1 and RNA into liquid droplets, whereas Not1 reverses Pat1-Dhh1-RNA condensation. Overall, our results uncover a function of Pat1 in promoting the multimerization of Dhh1 on mRNA, thereby aiding the assembly of large multivalent mRNP granules that are PBs.

Introduction

Cells are often subjected to severe environmental fluctuations such as nutrient deficiency, temperature changes or osmotic shock. To cope with stresses, a variety of mechanisms have evolved allowing cells to respond acutely and survive. These include changes in the gene expression program, which are often driven by robust transcriptional responses. Yet cells must also inactivate old mRNAs that may interfere with adaptation to the new condition, and therefore, post-transcriptional regulation and RNA turnover are critical to enable rapid changes in gene expression (Ashe et al., 2000; Mager and Ferreira, 1993).

The post-transcriptional fate of eukaryotic mRNAs is tightly linked to the complement of proteins that associate with it to form mRNPs (messenger ribonucleoproteins). For example, the presence of the m^7G cap structure at the 5' end is crucial for eIF4E binding, while Pab1 binds the 3' poly-A tail, both of which protect the mRNA against degradation and promote translation initiation. On the other hand, mRNA turnover is thought to initiate via deadenylation by the Ccr4/Pop2/Not1 complex (Muhlrad and

46 Parker 1992; Meyer et al., 2004; Sheth and Parker, 2004), followed by cap removal by the decapping
47 enzyme Dcp1/2 and 5'-3' degradation of the transcript by the exonuclease Xrn1 (Coller and Parker
48 2004; Larimer and Stevens, 1990). Thus, the processes of mRNA translation and decay are coupled and
49 act antagonistically (Radakrishnan et al., 2016; Beelman and Parker, 1994; Schwartz and Parker, 1999;
50 Schwartz and Parker, 2000; Sun et al,. 2012; Hu et al., 2009; Chan et al., 2018)

51 The balance between mRNA translation and decay is not only temporally but also spatially controlled.
52 For instance in yeast, upon glucose starvation, the majority of cellular translation halts and
53 untranslated mRNA as well as many factors of the RNA decay machinery concentrate in large
54 cytoplasmic mRNP granules, so called processing bodies [PBs] (Brengues et al., 2005; Sheth and Parker,
55 2003; Teixeira et al., 2005). PBs contain major components of the 5'-3' RNA decay pathway, e.g. Dcp1/2
56 and Xrn1, as well as activators of decapping - namely, the DEAD-box ATPase Dhh1, Pat1, Edc3 and the
57 Lsm1-7 complex. PBs presumably form around mRNAs sequestered away from active translation, and
58 in support of this, inhibition of translation initiation leads to induction of PBs (Frank and Anderson,
59 2008; Chan et al., 2018; Teixeira et al., 2005; Lui et al., 2010). On the contrary, inhibition of translation
60 elongation, for example by the drug cycloheximide which traps mRNA on ribosomes, and prevents
61 their influx into PBs, has the opposite effect and leads to PB disassembly (Texeria et al., 2005; Mugler
62 et al., 2016).

63 In consequence, PBs have been implicated in a variety of post-transcriptional processes such as
64 translational repression (Holmes et al., 2004; Coller and Parker, 2005), mRNA decay (Sheth and Parker,
65 2003; Cougot et al., 2004; Mugler et al., 2016), mRNA storage (Brengues et al., 2005; Bhattacharya et
66 al., 2006), and in higher eukaryotes, micro RNA-mediated repression (Liu et al., 2005; Pillai et al., 2005).
67 PBs and related mRNP granules such as stress granules, P granules in germ cells, neuronal granules etc.
68 form in a number of different species from yeast to mammals, and in a variety of cell types and
69 biological contexts, suggesting that these structures are crucial for cellular function or survival (Barbee
70 et al., 2006; Seydoux and Braun, 2006). Indeed, there is evidence that PBs can be essential for cell
71 survival under stress. For instance, cells unable to form PBs show a drastic loss in viability in stationary

72 phase (Ramachandran et al., 2011; Shah et al., 2013). However, the precise role of PBs in the regulation
73 of gene expression is a matter of debate and in order to understand PB function it is critical to examine
74 how PBs assemble and are regulated.

75 Numerous recent studies have shown that PBs are dynamic, membraneless organelles that assemble
76 from a variety of multivalent but weak RNA-protein, protein-protein and RNA-RNA interactions; a
77 phenomenon called liquid-liquid phase separation [LLPS]. The resulting granules are liquid-like,
78 spherical, dynamic and are dissolved by the alcohol 1,6-hexanediol, all key features of LLPS (Decker et
79 al., 2007; Fromm et al., 2012, 2014; Guo and Shorter, 2015; Mugler et al., 2016; Kroschwald et al.,
80 2015).

81 Although PB formation occurs via a plethora of multivalent protein-RNA interactions in a redundant
82 fashion (Rao and Parker, 2017), there are key players whose deletion drastically attenuates PB
83 assembly (Decker et al., 2007; Pilkington and Parker, 2007; Scheller et al., 2007). One such component
84 is the highly abundant DEAD-box ATPase Dhh1 (DDX6 in humans). Dhh1 is an enhancer of decapping
85 and is involved in the translational repression of mRNAs (Carroll et al., 2011; Coller and Parker,
86 2005; Fischer and Weis, 2002, Coller and Parker 2001). We recently showed that Dhh1 undergoes
87 phase separation *in vitro*, and controls PB dynamics *in vivo* via its RNA-stimulated ATPase activity
88 whereas the ATPase activator Not1 dissolves Dhh1 droplets *in vitro* and inhibits PB formation *in vivo.*
89 However, whether additional factors assist Dhh1 in promoting PB formation remains to be determined
90 and is the focus of this study.

91 One such candidate is the eukaryotic PB component Pat1, an evolutionarily conserved multi-domain
92 RNA binding protein that, like Dhh1, functions in both translational repression and mRNA decay
93 (Pilkington and Parker, 2008; Teixeira and Parker, 2007). In yeast, Pat1 acts as a scaffold that brings
94 together repression and decay factors (Dhh1, Edc3, Lsm1-7, Dcp1/2 etc.) via direct and/or indirect
95 interactions with mRNPs (Nissan et al., 2010). Dhh1 for example directly binds acidic residues in the N-
96 terminal domain of Pat1, an interaction that is conserved across species (Sharif et al., 2013; Conti;

97 Ozgur and Stoecklin, 2013). Deletion of *PAT1* in yeast alters the localization of PB components, whereas
98 its overexpression induces the formation of constitutive PBs even in unstressed cells (Pilkington and
99 Parker, 2007; Coller and Parker, 2005). Furthermore, it was shown that phosphorylation of Pat1 by the
100 cAMP-dependent protein kinase A (PKA) inhibits PB formation, and cells expressing a phospho-mimetic
101 mutant of Pat1 are defective in PB assembly (Ramachandran et al., 2011). However, the mechanism
102 by which Pat1 regulates PB assembly is unclear.

103 Here, we demonstrate that Pat1 promotes PB formation via Dhh1, and we show that the interaction
104 between Pat1 and Dhh1 is critical for robust PB assembly *in vivo*. Using a liquid phase separation assay
105 we can recapitulate this function of Pat1 *in vitro* as addition of recombinant Pat1, but not of a Pat1
106 variant that cannot bind Dhh1, enhances phase separation of Dhh1 and RNA. Overall, our *in vivo* and
107 *in vitro* data suggests that during stress Pat1 antagonizes the inhibitory effect of Not1 on PB assembly
108 and promotes the multimerization of Dhh1 on mRNA, leading to the formation of PBs.

109 **Results**

110 **Constitutive PB formation upon Pat1 overexpression is Dhh1 dependent**

111 The PB components Pat1 and Dhh1 were each previously shown to be required for PB formation in
112 yeast (Pilkington and Parker, 2008; Ramachandran et al., 2011; Mugler et al., 2016; Rao et al., 2017).
113 To understand the relationship between Pat1 and Dhh1 in the regulation of PB assembly, we took
114 advantage of the observation that overexpression of Pat1 leads to constitutive PB formation (Coller
115 and Parker 2005). This allowed us to characterize their respective regulatory contributions without
116 external influences such as nutrient starvation signals. As expected, Pat1 overexpression from its
117 endogenous locus using the galactose promoter in the presence of Dhh1 led to the formation of
118 constitutive PBs, as visualized by co-localization of Dhh1-GFP and Dcp2-mCherry foci (Figure 1A). No
119 foci were formed when Pat1 was not overexpressed or when we overexpressed the human influenza
120 hemagglutinin (HA) tag alone (Figure 1- figure supplement 1A). Notably, when Pat1 was overexpressed
121 in cells that lack Dhh1, a drastic reduction in the number of PBs was observed, as visualized by the

122 *bona fide* PB marker Edc3-GFP and its co-localization with Dcp2-mCherry (Figure 1A, B). This
123 demonstrates that formation of constitutive PBs upon Pat1 overexpression requires Dhh1.

124 **Pat1 and Dhh1 interaction is essential for PB assembly**

125 Pat1 is an 88 kDa protein that consists of an N-terminal un-structured domain (Pat1-N) followed by a
126 proline-rich stretch plus middle domain and a C-terminal globular fold (Pat1-C). The N-terminal domain
127 of Pat1 directly binds Dhh1's RecA2 core via a conserved DETF motif (Sharif et al., 2013; Ozgur and
128 Stoecklin, 2013). Furthermore, Pat1's C-terminus harbors two serine residues that are phosphorylated
129 by the cAMP-dependent protein kinase A (PKA) negatively regulating the interaction with Dhh1 and PB
130 formation (Ramachandran et al., 2011).

131 In order to understand how these Pat1 domains influence liquid-liquid phase separation and PB
132 assembly, we wanted to characterize various Pat1 mutants both *in vivo* and *in vitro*. Unfortunately, we
133 were unable to recombinantly express functional, full-length Pat1. Based on published crystal
134 structures and *in vitro* interaction studies, we therefore developed a minimal Pat1 construct
135 encompassing both N- and C-terminal domains that we refer to as Pat1-NC [amino acids: 5-79 (N) and
136 456-787 (C) connected with a $(GGS)_4$ linker] (Figure 1C). The N-terminal fragment of Pat1 (amino acids
137 5-79) was crystallized and shown to directly bind to Dhh1 (Sharif et al., 2013) whereas the C-terminus
138 of Pat1 (amino acids 456-787) contains the PKA phosphorylation sites and mediates the interaction
139 with the LSM-complex and RNA (Sharif and Conti, 2013, Fourati et al., 2014, Charenton et al., 2017,
140 Ramachandran et al., 2011, Pilkington and Parker, 2008).

141 To investigate whether this *PAT1-NC* construct is functional *in vivo* and behaves similar to wild-type
142 Pat1, we took advantage of the temperature-sensitive growth defect of a *PAT1* deletion mutant
143 (Fourati et al., 2014). Like full-length Pat1, expression of the *PAT1-NC* construct fully restored growth
144 of *pat1Δ* cells at 37° C (Figure 1- figure supplement 1B and 1C). In addition, we also tested if the
145 expression of *PAT1-NC* is able to rescue the synthetic lethality that was observed in *pat1Δ edc3Δ scd6Δ*

146 cells (Fourati et al., 2014). The expression of *PAT1-NC* rescued the growth phenotype of *pat1Δ edc3Δ*
147 *scd6Δ* cells at 37°C to a similar extent as achieved by wild-type *PAT1* (Figure 1- figure supplement 1D).

148 Furthermore, cells expressing the *PAT1-NC* construct when starved of glucose induced PBs to a similar
149 level as wild-type *PAT1* (Figure 1D, E) indicating full functionality *in vivo.* The PBs in the *PAT1-NC*
150 expressing cells rapidly dissolved upon re-addition of glucose demonstrating that they are reversible
151 and dynamic rather than anomalous granules (Figure 1D). In addition, Pat1-NC-GFP itself localized to
152 PBs upon stress in a reversible manner (Figure 1- figure supplement 1E). Finally, when we
153 overexpressed Pat1-NC using a GAL promoter, robust PBs were induced in the absence of stress (Figure
154 1F, G). Taken together our data suggest that the *PAT1-NC* construct is fully functional *in vivo*.

155 We next examined whether Pat1-NC can interact with Dhh1 *in vitro*, and as expected, Pat1-NC
156 displayed strong binding to full-length Dhh1 in a GST pull down assay (Figure 2A). However, this
157 interaction was completely abolished for a Pat1-NC variant in which the N-terminal DETF motif was
158 mutated to four alanines [Pat1$^{4A\text{-}Dhh1}$, see supplemental table S2B for a list of all mutants used in this
159 study] (Figure 2A).

160 We next investigated the effect of the *pat1$^{4A\text{-}Dhh1}$* mutant in the context of the full-length protein on
161 PB formation *in vivo*. While cells expressing *pat1$^{4A\text{-}Dhh1}$* showed a mild growth defect compared to the
162 wild type *PAT1*, they grew significantly better than *pat1Δ* cells, indicating that this protein is at least
163 partially functional (Figure 2- figure supplement 1A). To examine whether the interaction between
164 Pat1 and Dhh1 is required for PB formation, we monitored PB assembly upon stress in the absence of
165 glucose in wild-type (*PAT1*) or the *pat1$^{4A\text{-}Dhh1}$* background. As expected, the number of PBs was
166 drastically reduced in the complete absence of Pat1, as visualized by Dhh1-GFP (Figure 2- figure
167 supplement 1B). Importantly, *pat1$^{4A\text{-}Dhh1}$* expressing cells also demonstrated a drastic reduction in PB
168 number compared to cells expressing *PAT1* (Figure 2B, C) and the Pat1$^{4A\text{-}Dhh1}$-GFP protein itself showed
169 a significant defect in localizing to PBs (Figure 2D, E).

170 To assure that the Pat1$^{4A\text{-}Dhh1}$ mutant is stably expressed we checked its protein levels using Western
171 blotting and observed that the mutant expresses to similar levels as wild-type Pat1 (Figure 2- figure
172 supplement 1C). Moreover, in the Pat1$^{4A\text{-}Dhh1}$ mutant cells, the expression levels of Dhh1 were
173 comparable to the Dhh1 levels in cells harboring a wild-type copy of Pat1 (Figure 2- figure supplement
174 1D). This demonstrates that the defect in PB formation in cells expressing the Pat1$^{4A\text{-}Dhh1}$ binding
175 mutant is specifically due to impaired Pat1 function.

176 We were unable to overexpress the *Pat1$^{4A\text{-}Dhh1}$* mutant in yeast. In order to investigate PB formation
177 independently of carbon starvation stress, we therefore treated cells with the drug hippuristanol,
178 which inhibits the eukaryotic translation initiation factor eIF4A (Bordeleau, M.E., et al., 2006). In
179 consequence, hippuristanol prevents translation initiation and robustly induces PB formation within
180 minutes in cells expressing wild-type *PAT1* (Chan et al., 2018) [Figure 2F, Video 1]. Cells expressing
181 *pat1$^{4A\text{-}Dhh1}$* however, did not show PB formation until 2hrs after hippuristanol addition (Figure 2F and
182 Video 2).

183 It cannot be excluded that the Pat1$^{4A\text{-}Dhh1}$ mutant might interfere with the binding of Pat1 to some
184 other factor with a role in PB formation in addition to Dhh1. We therefore also employed a
185 complementary approach wherein we examined mutants on Dhh1 that impair interaction with Pat1.
186 Two such Dhh1 mutants have been described: Dhh1 Mut3A (Dhh1^{S292DN294D}) and Dhh1 Mut3B
187 (Dhh1^{R295D}) that partially or completely abolish binding to Pat1, respectively (Sharif et al., 2013). Cells
188 expressing either wild-type Dhh1, Dhh1^{S292DN294D}, Dhh1^{R295D} or lacking Dhh1 altogether were starved of
189 glucose and PB assembly was assessed. Whereas the Dhh1 variants expressed as well as wild-type
190 Dhh1 (Figure 3- figure supplement 1), we observed a drastic reduction in the number of PBs in both
191 Dhh1^{S292DN294D}, Dhh1^{R295D} cells (Figure 3A, B), and as published before also in *dhh1Δ* cells (Figure 3A, B,
192 Mugler et al., 2016). The Dhh1^{R295D} had a more severe PB formation defect compared to the
193 Dhh1^{S292DN294D} aligning with the *in vitro* binding abilities of these Dhh1 mutants to Pat1 (Sharif et al.,
194 2013).

195 To test PB formation independently of carbon starvation stress in these Pat1-binding mutants of Dhh1,
196 we used the drug hippuristanol as before. Dhh1 wild-type cells when treated with hippuristanol formed
197 PBs within minutes as judged by the co-localization of Dhh1-GFP and Dcp2-mCherry foci (Figure 3 C, D
198 and video 3). However, both the Dhh1^{S292DN294D} and Dhh1^{R295D} mutants did not form robust PBs until 3
199 hours of hippuristanol treatment exhibiting a phenotype similar to *dhh1Δ* cells (Figure 3 C, D and videos
200 4, 5, 6). Taken together, our data reveal that the Pat1-Dhh1 interaction is pivotal for robust PB
201 assembly.

202 **Pat1 phosphorylation status influences RNA binding**

203 Pat1 is a target of the cAMP-dependent protein kinase A (PKA) and phosphorylation of two serines
204 (amino acids 456/457) in the C-terminus of Pat1 under glucose-rich conditions was previously shown
205 to negatively regulate PB formation (Ramachandran et al., 2011). In agreement with the published
206 literature, cells expressing the *pat1^{EE}* mutant showed a defect in PB formation (Figure 4- figure
207 supplement 1A, B and Ramachandran et al., 2011). To better understand how Pat1 phosphorylation
208 controls PB assembly, we sought to characterize the influence of the phosphorylation status of Pat1
209 on PB formation in the absence of stress. Overexpression of *PAT1$^{WT/SS}$* (WT= wild-type) and *pat1^{AA}* (non-
210 phosphorylatable) led to constitutive PB formation as visualized by Dhh1-GFP and Dcp2-mCherry
211 positive foci. However, upon overexpression of *pat1^{EE}* (phospho-mimetic), foci number was reduced
212 (Figure 4 A, B). The Pat1^{EE}-GFP mutant was expressed as well as wild-type Pat1-GFP and had no effect
213 on Dhh1 expression (Figure 2- figure supplement 1C and 1D) emphasizing that the phospho-mimetic
214 mutant specifically impairs Pat1 function.

215 Pull-down experiments from cell extracts previously suggested that PKA-dependent phosphorylation
216 of Pat1 diminishes its interaction with Dhh1 (Ramachandran et al., 2011). To test whether this effect
217 is direct, we performed pull-down assays with the recombinant Pat1-NC protein and the Pat1-NC^{EE}
218 variant. However, in this assay there was no significant difference in Dhh1 binding between Pat1-NC
219 and Pat1-NC^{EE} (Figure 2A). Since the strong DETF binding site in Pat1-N might mask any weaker

220 interaction in Pat1-C, we also tested for direct binding of Pat1-C to Dhh1 but were unable to detect
221 any interaction (Figure 4C), indicating that the DETF-motif in Pat1-N provides the major interaction
222 surface for Dhh1.

223 Pat1-C was previously shown to bind RNA (Pilkington and Parker, 2008; Chowdhury et al., 2014). We
224 therefore tested whether RNA binding is regulated by PKA-dependent phoshphorylation by performing
225 RNA oligo gel shift assays using recombinant proteins. Whereas wild-type Pat1-C robustly binds the
226 RNA oligo and shifts it to higher molecular weight in a native PAGE gel, Pat1^{EE} displayed a significantly
227 reduced RNA shift (quantified in Figure 4D). Taken together, our *in vivo* and *in vitro* results on the
228 phospho-mimetic Pat1^{EE} mutant suggest that in addition to Pat1-Dhh1 binding, also the interaction
229 between Pat1 and RNA is important for PB formation.

230 **Pat1 and Not1 act antagonistically *in vivo***

231 Our lab previously showed that Not1 promotes PB disassembly by activating the ATPase activity of
232 Dhh1, and cells expressing a Not1 mutant that cannot bind to Dhh1 (*not1$^{9X\text{-}Dhh1}$*) form constitutive PBs
233 in non-stressed cells. Yet these PBs are less intense and fewer in number than those formed upon
234 glucose starvation (Mugler et al., 2016), indicating that additional mechanisms prevent PB formation
235 in glucose-replete conditions.

236 Since in glucose-rich media PB assembly is also inhibited by the PKA-dependent phosphorylation of
237 Pat1 (Ramachandran et al., 2011), we wanted to test whether expression of the non-phosphorylatable
238 *pat1^{AA}* variant enhances PB formation in the *not1$^{9X\text{-}Dhh1}$* strain background. While expression of *pat1^{AA}*
239 alone was not sufficient to induce constitutive PBs as observed before (Ramachandran et al., 2011 and
240 Figure 4- figure supplement 1A, B), expression of *pat1^{AA}* in the presence of *not1$^{9X\text{-}Dhh1}$* significantly
241 increased the number of constitutive PBs compared to cells expressing *not1$^{9X\text{-}Dhh1}$* alone (Figure 5A and
242 B). Yet, these PBs are still not as bright and numerous as in stressed wild-type cells. Interestingly, PB
243 intensity strongly increased when these strains were further treated with hippuristanol, a drug that

244 blocks initiation and liberates mRNA molecules from polysomes. The percentage of large PBs was
245 highest in the *pat1*^{AA} + *not1*$^{9X\text{-}Dhh1}$ strain, followed by the *not1*$^{9X\text{-}Dhh1}$ and then *pat1*^{AA} (Figure 5A, B).

246 Overall, this suggests that there are at least three determinants that act cooperatively to enhance the
247 formation of PBs: (a) direct interactions between Pat1-Dhh1 and Pat1-RNA; (b) lack of Not1 binding to
248 Dhh1 and in consequence low Dhh1 ATPase activity (Mugler et al., 2016); and (c) the availability of PB
249 client mRNAs that are not engaged in translation. Furthermore, our results suggest that Pat1 and Not1
250 act antagonistically on PB dynamics. Whereas Pat1 binding to Dhh1 enhances the assembly of PBs, the
251 interaction of Not1 with Dhh1 promotes PB disassembly, likely through activation of the ATPase
252 activity of Dhh1.

253 **Pat1 promotes PB assembly by enhancing the phase separation of Dhh1 and RNA**

254 At least two mechanisms of how Pat1 promotes PB formation via Dhh1 could be envisioned: first, Pat1
255 could slow the ATPase cycle of Dhh1, for example by preventing Not1 binding and/or inhibiting ATP
256 hydrolysis, second, Pat1 could directly promote oligomerization and condensation of Dhh1 on RNA.

257 To test the first hypothesis, we used an *in vitro* ATPase assay using purified protein components in
258 which Not1 robustly stimulates the ATPase activity of Dhh1 (Mugler et al., 2016). However, we did not
259 observe a significant inhibition of the Not1-stimulated ATPase activity upon addition of Pat1-NC (Figure
260 6- figure supplement 1A), suggesting that Pat1 does not directly interfere with the mechanism of
261 ATPase activation.

262 We had previously shown that PB dynamics are regulated by the ATPase activity of Dhh1 (Carroll et al.,
263 2011; Mugler et al., 2016). To test Pat1's effect on the Dhh1 ATPase cycle *in vivo,* we therefore also
264 examined the turnover of PBs that form upon Pat1 overexpression. The drug cycloheximide (CHX) traps
265 mRNAs on polysomes and thereby stops the supply of new RNA clients to PBs. Since active Dhh1
266 constantly releases mRNA molecules from PBs, a lack of mRNA influx eventually leads to their
267 disassembly and in consequence the catalytic dead mutant of Dhh1 that is locked in the ATP- state
268 (Dhh1^{DQAD}) inhibits PB disassembly and was shown to have negligible turnover rates (Mugler et al.,

269 2016; Kroschwald et al., 2015). We observed that PBs formed upon Pat1 overexpression were more
270 dynamic than PBs formed in the presence of Dhh1^{DQAD} and their dis-assembly kinetics was comparable
271 to PBs formed upon stress in a wild-type *DHH1* background (Figure 6- figure supplement 1B, C and
272 Videos 7, 8, 9). Thus, overall, our *in vitro* and *in vivo* findings are not consistent with the conclusion
273 that Pat1 blocks the ATPase activation of Dhh1.

274 The second hypothesis is that Pat1 promotes higher-order mRNP assembly by directly or indirectly
275 promoting Dhh1 oligomerization, thereby acting as a scaffold and providing additional protein-protein
276 or protein-RNA interactions (Coller and Parker, 2005; Roy and Parker, 2017). We have previously
277 shown that recombinant Dhh1 can undergo liquid-liquid phase separation (LLPS) in the presence of
278 RNA and ATP, and that these Dhh1 droplets can recapitulate aspects of *in vivo* PB dynamics. (Mugler
279 et al., 2016). We therefore utilized this *in vitro* system to test Pat1's impact on the phase separation
280 behavior of Dhh1.

281 Dhh1 droplets were assembled from purified components as described previously (Mugler et al.,
282 2016). Interestingly, while no LLPS of Pat1-NC alone was detected (Figure 6- figure supplement 2A),
283 addition of increasing concentrations of wild-type Pat1-NC strongly enhanced the LLPS of Dhh1 in the
284 presence of ATP and RNA as judged by an increase in the area * intensity of Dhh1 droplets (Figure 6A).
285 Furthermore, Pat1-NC itself enriched in Dhh1 droplets, suggesting that Pat1 and Dhh1 co-oligomerize
286 with RNA to form a composite phase-separated compartment (Figure 6A).

287 In order to test if the enhancement in phase separation of Dhh1 via Pat1 is RNA-dependent, we
288 perfomed this experiment also in the absence of RNA. Interestingly, we did not observe any Dhh1
289 droplets upon addition of increasing concentrations of Pat1-NC when RNA was omitted from the
290 reaction (Figure 6- figure supplement 2B) suggesting that under these *in vitro* conditions RNA plays a
291 critical role in the Pat1-promoted enhancement of Dhh1 oligomerization and higher-order phase
292 separation. Consistent with this, the Pat1-N- terminus alone which cannot bind to RNA also does not

293 enhance the phase separation of Dhh1 even in the presence of RNA and ATP (Figure 6- figure
294 supplement 2C).

295 Overall, our *in vitro* data suggests that a combination of both the Pat1-N (binding to Dhh1) and Pat1-C
296 (binding to RNA) is critically required to enhance the phase separation of Dhh1 and promote higher-
297 order oligomeric mRNP structures akin to *in vivo* PBs.

298 To test the specificity of LLPS stimulation, we tested the Pat1$^{4A\text{-}Dhh1}$ (Dhh1 binding) and Pat1^{EE} (phospho-
299 mimetic) mutants both of which drastically reduce PB formation *in vivo* (see Figure 2B, 4A, B and Figure
300 4- figure supplement 1A). Consistent with the *in vivo* results, Dhh1-RNA droplet formation was either not
301 at all or only mildly stimulated upon addition of these Pat1 variants (Figure 6A).

302 We previously demonstrated that the MIF4G domain of Not1 prevents formation of Dhh1-RNA
303 droplets, presumably by activating the ATPase cycle of Dhh1 (Mugler et al., 2016). We therefore next
304 analyzed whether the Pat1-Dhh1 droplets are still responsive to Not1. Similar to what we observed *in*
305 *vivo* (Figure 5), Not1^{MIF4G} also diminishes formation Dhh1 droplets in the presence of Pat1 *in vitro*
306 (Figure 6B).

307 Taken together our results suggest that Pat1 enhances the multivalency of protein-protein and
308 protein-RNA interactions in a Dhh1-Pat1 mRNP and in consequence promotes the formation of higher-
309 order, liquid-like mRNP droplets akin to *in vivo* PBs.

310 ***In vitro* phase separated droplets mimic the stoichiometry of PB components *in vivo***

311 To examine how well our *in vitro* droplets resemble *in vivo* PBs we investigated the stoichiometric ratio
312 of Dhh1:Pat1 in these granules. In order to determine the stoichiometry *in vivo,* we measured the
313 number of PBs and the fluorescence intensity of GFP-tagged Dhh1 and Pat1 in these foci. Briefly, we
314 glucose starved both Pat1-GFP and Dhh1-GFP expressing cells to induce PBs (Figure 7- figure
315 supplement 1A) and used the single particle tracking software Diatrack to count the number and
316 intensity of PBs in an unbiased and automated manner in each strain [Vallotton et al., 2013].
317 Surprisingly, despite the fact that the cellular concentration of Pat1 is ten-times lower than Dhh1

318 (Figure 7- figure supplement 1B), the ratio of the two PB components was approximately 2:1+/-0.18
319 (Dhh1:Pat1) after 0.5-4 hours of starvation (Figure 7A). Extended starvation resulted in enhanced Dhh1
320 recruitment to PBs until reaching a Dhh1:Pat1 ratio of 2.5:1+/- 0.23, suggesting that PB composition
321 matures over time (Figure 7A).

322 In order to determine the stoichiometry of Pat1 and Dhh1 droplets *in vitro*, we imaged Dhh1-mCherry
323 and Pat1-GFP droplets with a confocal microscope (Figure 7- figure supplement 1C). The protein
324 concentration of both Dhh1 and Pat1 in the droplet was calculated from a standard curve determined
325 from values measured for different concentrations of the respective soluble fluorophores (Figure 7B).
326 Remarkably, we found a stoichiometric ratio of 2.7:1 +/- 0.13 of Dhh1 to Pat1 in the *in vitro* phase-
327 separated droplets, closely resembling the Dhh1:Pat1 ratio of mature PBs *in vivo* (Figure 7B).

328 Thus, while other mRNA decay factors also contribute to PB formation *in vivo*, our data demonstrate
329 that with a minimal number of constituents, namely Dhh1, RNA, ATP and Pat1 higher-order dynamic
330 liquid droplets can be formed *in vitro*. The *in vitro* droplets recapitulate various properties of PBs
331 formed *in vivo* such as (a) the stoichiometry of PB components, and (b) the dynamics of Pat1-
332 stimulated assembly and Not1-stimulated disassembly of *in vivo* PBs identifying Pat1 as an important
333 player in PB formation promoting LLPS via Dhh1.

334 **Discussion**

335 **Tug-of-war model between Pat1 and Not1 to regulate PB dynamics**

336 The ability of proteins and RNA to undergo liquid-liquid phase separation (LLPS) has emerged as an
337 essential fundamental biological process allowing cells to organize and concentrate their cellular
338 components without the use of membranes. Yet, how these membraneless organelles assemble, are
339 kept dynamic and are regulated remains enigmatic. One such cellular phase-separated compartment
340 is the PB and our results presented here together with our prior work (Mugler et al., 2016) identify and
341 characterize both positive and negative regulators of PB assembly and provides novel insight into the
342 regulation of membraneless organelle formation.

343 Overall, our work uncovers a function of Pat1 as an enhancer of PB formation that acts via Dhh1 and
344 counteracts the inhibitory function of Not1. Based on our results, we propose that there are at least
345 three inputs that cooperatively regulate PB dynamics *in vivo* (Figure 7C). First, the availability of mRNA
346 clients acting as seeding substrates to initiate PB formation. mRNA availability is inversely proportional
347 to the translation status, which is regulated by different stress responses and the metabolic state of
348 the cell (Figure 2C). Second, the activity of cAMP-dependent PKA negatively regulates PB assembly in
349 nutrient-rich conditions, at least in part through phosphorylation of Pat1. However, since expression
350 of non-phosphorylatable Pat1^{AA} at endogenous levels (in contrast to overexpression) is not sufficient
351 to induce PBs, Pat1 availability appears to be limiting (Figure 5, 4A, and Figure 4- figure supplement 1A
352 and Ramachandran et al., 2011). Third, activation of the Dhh1 ATPase cycle by the CCR4-Not1
353 deadenylation complex stimulates mRNA release and negatively regulates PB assembly. It is of note
354 that Not1 itself might also be subject to post-translational regulation, in response to metabolic state
355 and/or cell cycle stages of the cell (Mugler et al., 2016; Braun et al., 2014).

356 In this model, a tug-of-war between Pat1 and Not1 regulates PB assembly and disassembly: whereas
357 a tight Pat1-Dhh1 interaction in the presence of RNA clients, promotes PB formation, Not1, induces PB
358 turnover via stimulating the ATPase activity of the DEAD box ATPase Dhh1 (Figure 7C). Remarkably,
359 our *in vivo* findings are corroborated *in vitro* wherein, Pat1 enhances the LLPS of Dhh1 and RNA, a step
360 critical for the assembly of large mRNP granules, and by contrast, Not1 reverses the LLPS of Pat1-Dhh1-
361 RNA droplets (Figure 6 and 7C). Furthermore, the observed stoichiometry of Dhh1 and Pat1 in PBs is
362 recapitulated in our *in vitro* phase separation assay (Figure 7A, B).

363 **The interaction between Pat1 and Dhh1 is critical for PB assembly**

364 Inducing PB formation by Pat1 overexpression or hippuristanol treatment allowed us to dissect distinct
365 mechanisms that govern PB assembly and characterize the crucial role of the Pat1-Dhh1 interaction in
366 this process. The benefit of these modes of PB formation are that they bypass the characteristic
367 stresses associated with PB formation, such as nutrient starvation, that might have more widespread

368 and confounding effects on translation, mRNA degradation, or on the regulation of other PB
369 components.

370 Our experiments reveal that Pat1 functions in PB formation through Dhh1 since PB induction by Pat1
371 overexpression is strictly dependent on the presence of Dhh1 (Figure 1A). Furthermore, a mutant in
372 the DETF motif in the N-terminus of Pat1 mediating direct binding to Dhh1 (Pat1$^{4A\text{-}Dhh1}$ variant) and
373 mutants of Dhh1 that abolish Pat1 binding fail to promote PB assembly (Figure 2). These results were
374 further confirmed using the drug hippuristanol that inhibits translation initiation wherein PBs were
375 induced in wild-type cells but not in cells expressing the Pat1$^{4A\text{-}Dhh1}$ mutant, and the Dhh1 mutants that
376 abolish Pat1 binding (Dhh1^{R295D} and Dhh1^{S292DN294D}) [Figure 2F, 3C and Chan et al., 2018]. This suggests
377 that high mRNA load alone is inadequate for PB formation and that a direct physical interaction
378 between Pat1 and Dhh1 is obligatory as well. Since the DETF motif in Pat1 is conserved across evolution
379 and was suggested to regulate PB assembly in human cells as well (Sharif et al., 2013; Ozgur and
380 Stoecklin, 2013), the Pat1-Dhh1 interaction likely plays a critical role in PB formation across species.

381 Our results seem to be at odds with a previous publication, which suggests that Pat1 acts
382 independently of Dhh1 to promote PB formation (Coller and Parker 2005). However, in this study Pat1
383 was overexpressed from a plasmid, in the presence of the endogenous copy. When recapitulating
384 these conditions, we observed that PB components mislocalize to the nucleus [observed by DAPI and
385 a nuclear rim marker, see Figure 7- figure supplement 2A, B] and it is possible that in the absence of
386 additional organelle markers, this nuclear accumulation was misinterpreted as PB formation.

387 **Pat1 enhances the LLPS of Dhh1, thereby promoting PB formation**

388 How does Pat1 enhance PB formation? One hypothesis is that Pat1 directly counteracts the Not1-
389 stimulated ATPase activation of Dhh1, but we do not favor such a model since i) Pat1 does not inhibit
390 Dhh1's ATPase activity at physiological protein ratios *in vitro* (Figure 6- figure supplement 1A), ii)
391 Not1^{MIF4G} dissolves Pat1-Dhh1 condensates, while droplets formed from catalytic-dead Dhh1^{DQAD} are

392 Not1-resistant (Figure 6 and Mugler et al., 2016), and iii) *in vivo*, PBs formed upon Pat1 overexpression
393 are much more dynamic than those formed from Dhh1^{DQAD} (Figure 7- figure supplement 1B).

394 Instead, our data are consistent with a model in which Pat1 promotes PB assembly by directly
395 enhancing the LLPS of Dhh1. DDX6, the human homolog of Dhh1 can oligomerize (Lange et al., 2012),
396 and given the fact that both DDX6 and Dhh1 are found in molar excess over mRNA, we propose that
397 Pat1 functions as a scaffold, providing additional multivalent interactions with Dhh1 and RNA, thereby
398 aiding in the fusion of Dhh1 LLPS droplets and promoting assembly of microscopically-detectable
399 mRNP condensates (Figure 6). Interestingly, both functional binding to Dhh1 in Pat1-N and RNA-
400 binding in Pat1-C are required for this mechanism as individually mutations in each of the domains
401 alter PB assembly *in vivo* and fail to enhance Dhh1's phase separation *in vitro*. Rather, Pat1-N alone
402 diminishes the extent of LLPS (Figure 6- figure supplement 2C). It is interesting to note that Pat1-N was
403 previously shown to interfere with the ability of Dhh1 to interact with RNA (Sharif et al., 2013) and we
404 thus speculate that Pat1-N might outcompete RNA from Dhh1, and in the absence of the C-terminal
405 Pat1 RNA-binding site destabilize droplets. This might explain why RNA-binding by Pat1's C-terminus
406 that is under the regulation of PKA (Figure 4A, B, Figure 4- figure supplement 1A) is critical for LLPS and
407 PB assembly. *In vivo*, we find that the Pat1$^{4A\text{-}Dhh1}$ (Dhh1 binding mutant) and Pat1^{EE} (phospho-mimetic
408 mutant) not only have a drastically reduced number of PBs, but also much lower intensity (reduced by
409 7 and 8 fold respectively, Figure 7- figure supplement 2C) compared to Pat1 wild-type PBs.

410 Our recent findings also show that the un-structured poly-Q rich C-terminal tail of Dhh1 is required for
411 PB formation *in vivo* and Dhh1 LLPS *in vitro* (Hondele et al., *submitted*). Thus, Pat1 might potentially
412 enhance Dhh1 multimerization via the low complexity tails of Dhh1. Structural studies will now be
413 needed to clarify how Pat1 facilitates oligomerization and PB formation of the Dhh1-Pat1- RNA
414 complex.

415 **The emerging importance of liquid-liquid phase separation in diverse aspects of cell biology and the**
416 **power of *in vitro* reconstitution systems**

417 As non-membrane bound organelles, it is of interest to understand how cells assemble large RNP
418 granules and regulate their dynamics. PBs are prominent membraneless cellular compartments, which
419 have been shown to be not only involved in numerous aspects of mRNA turnover, but also crucial for
420 survival under various cellular stresses. With an *in vitro* phase separation tool in hand that faithfully
421 reconstitutes certain aspects of PB formation, we are now in a position to dissect how PBs form and
422 characterize their biophysical behavior. This will aid us not only in elucidating key components of PB
423 formation, but also help us elucidate the function of PBs in regulating mRNA turnover.

424 At this stage, our in *vitro* systems are limited to Dhh1, Pat1, Not1 and RNA and for the sake of simplicity;
425 we present a model only depicting the role of Pat1 and Dhh1 in PB formation (Figure 7C). However, it
426 is important to note that several additional PB components have been characterized. For example, this
427 includes Ecd3, members of the Lsm1-7 complex, or Dcp2 that play crucial roles either alone or together
428 with Pat1 and Dhh1 in PB assembly. Both Edc3 and Lsm4 contain low complexity-domains that were
429 shown to be critical for PB formation *in vivo*, and it was recently demonstrated a threshold
430 concentration of low-complexity domain containing proteins is required for robust PB assembly
431 (Protter et al., 2018). In addition, it was previously shown that both Pat1 (C-terminus) and the Lsm1-
432 7 complex individually have low RNA binding ability but a reconstituted Lsm1-7-Pat1-C complex
433 displays an enhanced ability to bind RNA (Chowdhury et al., 2014). This might suggest that *in vivo* the
434 Pat1-C- terminus functions together with the Lsm1-7 complex to bind RNA and enhance PB formation.
435 Furthermore, it cannot be excluded that direct binding of Dcp2 to the C-terminus of Pat1 also regulates
436 PB assembly and RNA turnover (Fourati et al., 2014). It will thus be critical to examine additional PB
437 components in future experiments and to evaluate how they function together with Pat1 and Dhh1 in
438 order to understand the complex interplay of various inputs that regulate PB assembly and dynamics.
439 Nonetheless, based on our data and the aforementioned literature evidence we propose that Pat1
440 provides a central PB scaffold and participates in an intricate network of protein-protein and protein-
441 RNA interactions that promote PB assembly and influence RNA turnover rates *in vivo*.

442 The physical basis of LLPS has attracted a great deal of attention recently, at least in part because of
443 the critical role that proper mRNP assembly plays in pathological neurodegenerative diseases and
444 stress responses (Ramaswami et al., 2013; Alberti and Hyman 2016; Patel et al., 2015; Aguzzi and
445 Altmeyer, 2016; Hyman et al., 2014). An important challenge is to understand how these granules are
446 kept dynamic and functional under some conditions whereas the formation of solidified and aberrant
447 aggregates are triggered under others. Robust *in vitro* reconstitution systems that can recapitulate
448 mRNP granule assembly, dynamics and stoichiometry will be invaluable in addressing these research
449 questions and increase our understanding of the molecular mechanism of how cells age and deal with
450 stress.

451 **Materials and methods**

Key Resources Table				
Reagent type (species) or resource	**Designation**	**Source or reference**	**Identifiers**	**Additional information**
strain, strain background (Yeast: *Saccharomyces cerevisiae*)	W303	SGD:https://www.yeastgenome.org/strain/S000203491	KWY XYZ	MATa/MATα {leu2-3,112 trp1-1 can1-100 ura3-1 ade2-1 his3-11,15} [phi+]
strain, strain background (*Escherichia coli*)	*E.Coli* DH5α	Thermo Fisher Scientific	18258012	
strain, strain background (*Escherichia coli*)	*E.Coli* BL21 star (DE3)	Thermo Fisher Scientific	C601003	
genetic reagent ()				Please see table S1, S2A
antibody	mouse-anti-GFP	Roche	Cat# 11814460001, RRID: AB_390913	Western blot: 1:1000
antibody	rabbit-anti-Hxk1	US Biological	Cat# H2035-01, RRID:	Western blot: 1:3000

			AB_2629457, Salem, MA	
antibody	IRdye 680RD goat-anti-rabbit	LI-COR Biosciences	Cat# 926–68071, RRID: AB_10956166	Western blot: 1:5000
antibody	IRdye 800 donkey-anti-mouse	LI-COR Biosciences	Cat# 926–32212, RRID: AB_621847	Western blot: 1:10000
antibody	Rabbit-anti-Dhh1	in house	#100	Western blot: 1:5000
recombinant DNA reagent				Please see table S2B
chemical compound, drug	hippuristanol	kind gift from Junichi Tanaka, University of the Ryukyus	hippuristanol	10uM in DMSO
chemical compound, drug	cycloheximide	Sigma-Aldrich, CH	CAS Number 66-81-9	50ug/ml in DMSO
software, algorithm	Diatrack	http://www.diatrack.org/	Diatrack	used for counting PB number and intensity
software	fiji/imagej	NIH	https://fiji.sc/	adjusting brightness, contrast and making final figures

The details regarding all the yeast strains used in this study are in Supplementary table S1. Supplementary table S2A contains all the plasmids used in this study. Table Supplementary S2B contains the mutants used in this study and Table S2C describes the entire DNA oligos used for this manuscript.

Construction of yeast strains and plasmids

S. cerevisiae strains used in this study are derivatives of W303 and are described in table S1. ORF deletion strains and C-terminal epitope tagging of ORFs was done by PCR-based homologous recombination, as previously described (Longtine et al., 1998). Plasmids for this study are described in table S2A. Mutations in Pat1 were generated by introducing the mutation in the primer used to

462 amplify the respective Pat1 regions and stitched together with the selection marker from the plasmid
463 (table S2B). Mutations in Dhh1 and Not1 were generated as in Mugler et al., 2016. Primer sequences
464 for strain construction are listed in table S2C.

465 **Overexpression of Pat1 wild-type and mutants**

466 The samples were grown overnight in synthetic media containing 2% raffinose, diluted to OD_{600} = 0.05
467 or 0.1 the following day, and grown to mid-log phase (OD_{600}= 0.3–0.4). The culture was split into two
468 and to one-half galactose was added to 2% final concentration and the corresponding protein induced
469 for 2-3 hours. The cells in both raffinose and galactose were imaged using a wide-field fluorescence
470 microscope.

471 **PB induction and disassembly kinetics**

472 PBs were induced via glucose starvation stress. Samples were grown overnight in synthetic media
473 containing 2% glucose, diluted to OD_{600} = 0.05 or 0.1 the following day, and grown to mid-log phase
474 (OD_{600}= 0.3–0.8). Cells were harvested by centrifugation and washed in ¼ volume of fresh synthetic
475 media +/− 2% glucose, then harvested again and re-suspended in 1 volume of fresh synthetic media
476 +/− 2% glucose and grown 30 min at 30°C. Cells were then transferred onto Concanavalin A-treated
477 MatTek dishes (MatTek Corp., Ashland, MA) and visualized at room temperature. For cycloheximide
478 experiments, final concentration of 50ug/mL (Sigma-Aldrich, CH) were used to examine PB disassembly
479 kinetics. For PB induction and to determine the kinetics of PB assembly we used hippuristanol (a
480 generous gift of Junichi Tanaka, University of the Ryukyus) at a final concentration of 10µM.

481 **Wide-field fluorescence microscopy**

482 Cells were transferred onto Concanavalin A-treated MatTek dishes (MatTek Corp., Ashland, MA) and
483 visualized at room temperature. Microscopy was performed using an inverted epi-fluoresence
484 microscope (Nikon Ti) equipped with a Spectra X LED light source and a Hamamatsu Flash 4.0 sCMOS
485 camera using a 100x Plan-Apo objective NA 1.4 and the NIS Elements software. Representative images
486 were processed using ImageJ software. Brightness and contrast were adjusted to the same values for
487 images belonging to the same experiment and were chosen to cover the whole range of signal

488 intensities. Image processing for PB analysis was performed using Diatrack 3.05 particle tracking
489 software (Vallotton et al., 2013) as described below.

490 **Automated image analysis for PB quantification**

491 In order to quantify PB formation in live cells, we used an automated image analysis in a manner similar
492 to Mugler et al., 2016. First, PBs were counted using Diatrack 3.05 particle tracking software using local
493 intensity maxima detection, followed by particle selection by intensity thresholding and particle
494 selection by contrast thresholding with a value of 5% (Vallotton et al., 2017). To speed up the analysis,
495 we renamed all our images in a form that can be recognized as a time-lapse sequence by Diatrack, and
496 placed them all in a single directory, such that they all will be analyzed using exactly the same image
497 analysis parameters. Renaming and copying was done by a custom script (supplementary code 1),
498 which also performed cell segmentation using a method adapted from (Hadjidemetriou et al., 2014).
499 Briefly, the method first detects all edges using a Laplacian edge detection step, and then traces
500 normals to those edges in a systematic manner. These normals tend to meet at the cell centre where
501 the high density of normals is detected, serving as seeds to reconstruct genuine cells. Our script thus
502 counts cells and reports their number for each image - information which is output to an excel table.
503 The results from Diatrack PB counting are imported from a text file into that table, and the number of
504 PB is divided by the number of cells for each image.

505 **Protein purification**

506 Dhh1 and Not1 were purified as described previously (Mugler et al., 2016). V5-Pat1-C, GST-Pat1-N and
507 GST-Pat1-NC constructs as described in Supplementary table S2A were cloned into pETM-CN vectors.
508 These expression vectors were transformed into chemically competent *E. coli* BL21 DE3 under the
509 selection of ampicillin and chloramphenicol. Pre-cultures were grown in LB at 37°C over-night, and
510 diluted 1:100 into rich medium the next morning. Cells were grown at 37°C to an OD_{600} of 0.6 and
511 induced with 200 mM IPTG (final concentration). Cells were then grown overnight at 18°C, harvested
512 and resuspended in 30 mL lysis buffer (500mM (Pat1-C, Pat1-N) or 300 mM NaCl (Pat1-NC), 25 mM
513 Tris-HCl pH 7.5, 10 mM imidazole, protease inhibitors, 10% glycerol) per cell pellet from 2 L of culture.

514 After cell lysis by EmulsiFlex (Avestin Inc, Ottawa, CA), the 6xHis tagged proteins were affinity extracted
515 with Ni^{2+} sepharose in small columns, dialyzed into storage buffer (MH200G (Pat1-C, Pat1-N): 200 mM
516 NaCl, 25 mM Tris pH 7.5 (RT), 10% glycerol, 2 mM DTT), MH300G (Pat1-NC): same with 300mM NaCl)
517 with simultaneous protease cleavage of the His-tag and GST-tag (unless required for pull-down assays)
518 and further purified by size exclusion with a Superdex 200 column on an AEKTA purifier (both GE Life
519 Sciences, Marlborough, MA) in storage buffer. Protein expression levels, His eluates and gel filtration
520 fractions were analyzed by SDS-PAGE. Clean Superdex elution fractions were pooled, concentrated
521 using Millipore Amicon Centrifugation units and snap frozen as ~ 20 µl aliquots in siliconized tubes in
522 liquid nitrogen.

523 **ATPase assays**

524 ATPase assays were performed according as described (Montpetit et al., 2011) with the following
525 modifications: final concentration 2 µM Dhh1-mCherry was mixed with 0.5 µM Not1 and Pat1-mCherry
526 (1 and 3µM) as indicated and protein volumes equalized with storage buffer (MH200G). 2 µL 10x
527 ATPase buffer (300 mM HEPES-KOH pH 7.5, 1 M NaCl, 20 mM $MgCl_2$), 4 µL 10 mg/ml polyU (unless
528 indicated otherwise), RNase inhibitors, 13.3 µL 60% glycerol, 2.7 µL 10 mg/mL BSA, were added to a
529 final volume of 36 µL. Reactions were set up in triplicate in a 96-well NUNC plate. The assay was
530 initiated by the addition of 40 µL of a master mix containing 1x ATPase buffer, 2.5 mM ATP (from a
531 100 mM stock in 0.5 M HEPES-KOH pH 7.5), 1 mM DTT, 6 mM phosphoenolpyruvate, 1.2 mM NADH
532 (from a 12 mM stock in 25 mM HEPES-KOH pH 7.5) and 125–250 units / mL PK/LDH. NADH absorption
533 was monitored with a CLARIOstar plate reader (BMG Labtech, Ortenberg, Germany) at 340 nm in 30 s
534 intervals for 400 cycles.

535 ***In vitro* liquid droplet reconstitution assay**

536 Reactions were pipetted in 384-well microscopy plates (Brooks 384 well ClearBottom Matriplate, low
537 glass). Proteins were diluted to 50 µM (Dhh1) or 100 µM (Not1, Pat1) stocks with storage buffer and

538 mixed as droplets at the side of the well; volumes were equalized to 5 µl with storage buffer. Next, a
539 master mix of 12.5 µl 150 mM KCl buffer (150 mM KCl, 30 mM HEPES-KOH pH 7.4, 2 mM $MgCl_2$), 2µl
540 ATP reconstitution mix (40 mM ATP, 40 mM $MgCl_2$, 200 mM creatine phosphate, 70 U/mL creatine
541 kinase), 2.5 µl 2mg/ml polyU (in H_2O) as an RNA analog, 1 µl 1M HEPES-KOH pH 6.4 buffer and 2 ml
542 10mg/ml BSA were added and mixed by pipetting, the droplets still at the side of the well, since this
543 later on produced more equal droplet distribution. First imaging was performed after 20 minutes
544 incubation at room temperature; just prior to imaging, droplets were spun down at 100 g for 1
545 minute. For subsequent analysis, plates were stored in the fridge. Pictures displayed were recorded
546 after 1 hour incubation.

547 **Stoichiometry analysis of Dhh1 and Pat1 in PBs *in vivo***

548 In order to estimate the relative amount of Dhh1 to that of Pat1 in PBs *in vivo*, we labelled both proteins
549 with eYGFP in two separate strains, and imaged them in exactly the same conditions after inducing
550 carbon (glucose) starvation stress for indicated times (Figure 6A). Using exactly the same endogenous
551 probe for both proteins allowed us to deduce ratios of abundances directly from ratios of intensities
552 (no spectral corrections are necessary). We then measured the intensity of the 10 brightest PBs as a
553 function of time and in both cases took the median intensity value as representative of the more visible
554 PBs (at least 10 PBs were present in every image for both strains and at each time point). Finally, we
555 divided the median value obtained for Dhh1 by that for Pat1 and plotted that ratio as a function of
556 time post-stress.

557 **Stoichiometry of Dhh1 and Pat1 in phase-separated *in vitro* droplets**

558 For the analysis of the *in vitro* phase transition of Dhh1 in the presence of Pat1, 2 µM mCherry-tagged
559 Dhh1 and 4 µM GFP-tagged Pat1-NC were added to 0.1 mg/mL polyU and 5 mM ATP in 150 mM KCl,
560 30 mM HEPES-KOH, pH 7.4 and 2 mM $MgCl_2$. After 1 hour incubation, the phase-separated droplets
561 were imaged in both the mCherry and the GFP channel by confocal fluorescence microscopy (Leica TCS
562 SP8) with a 63x NA 1.4 oil objective (Leica). The protein concentration was evaluated from the

563 fluorescence intensity via a standard curve obtained by measuring a series of samples at different
564 known concentrations for each fluorophore. The size distributions were obtained by analyzing the
565 images obtained by fluorescence microscopy with an in-house code written in Matlab.

566 **GST pull-down assays**

567 25 µl of 100 µM recombinant purified GST Pat1-NC was bound to 30 µl GST-slurry (Sigma), and one
568 aliquot of GST-beads was included without added Pat1-NC as negative control. Reactions were
569 incubated for 30mins rotating at 4°C and washed 4-times with wash buffer (300 mM NaCl, 10 mM Tris
570 pH 7.5, 0.05 % NP40). 4 µl 250 µM Dhh1 was added in 500 µl wash buffer and incubated rotating at
571 4°C for 1 hour. Reactions were washed 5-times, proteins eluted by boiling with 4x SDS loading buffer
572 and separated on a 12% acrylamide gel and stained with Coomassie. For V5-pulldown assays, the bait
573 (15 µl 100 µM Pat1-C construct) was bound to 15 ml V5-slurry (Sigma), the bait 3 µl 200 µM Dhh1-
574 mCherry, and incubation / wash buffers as above with salt concentration as indicated in the blot. Final
575 washes were only performed three times.

576 **Native PAGE**

577 Proteins were diluted to 20 µM. 0, 2 or 4 µl of protein solution was filled to 4 µl with storage buffer
578 (200mM NaCl, 25mM Tris pH 7.5, 10% glycerol, 2 mM DTT). Proteins were mixed with a master mix
579 containing per reaction 2 µl 10x ATPase buffer (300 mM HEPES-KOH pH 7.5, 1 M NaCl, 20 mM MgCl2),
580 0.3 µl Cy5-labeled *in vitro* transcribed RNA oligo (29nt, 1.1 µg/µl), 2 µl 2.5M NaCl, 13.7 µl H2O and 3 µl
581 60% glycerol. Reactions were incubated on ice for 20 min and separated on a precast Bis-Tris Native
582 gradient Gel (Invitrogen) in 1x running buffer (50 mM Bis-Tris 50 mM Tricine pH 6.8) at 100V 4C for
583 about 2.5hrs.

584 **Growth curve and spotting assays**

585 Overnight yeast cultures were grown in permissive conditions in SCD media. Growth curves were
586 acquired using CLARIOstar automated plate reader (BMG Labtech, Ortenberg, Germany) at 30°C in 24-
587 well plastic dishes (Thermo Fisher) from overnight pre-cultures diluted 1:125 in the specified synthetic

588 liquid media. For spotting assays on plates the indicated strains were grown overnight at 25°C to
589 saturation. Next day equal number of ODs for each strain was spotted (with a 1:10 series dilution) on
590 YPD plates and incubated at 25°C, 30°C and 37°C for 2-3 overnights.

591 **Western blotting**

592 For Western blot analysis, roughly 5 OD_{600} units of log growing cells were harvested and treated with
593 0.1M NaOH for 15 mins at room temperature. The samples were vortexed in between and finally
594 centrifuged to remove the NaOH. SDS sample buffer was added and homogenates were boiled.
595 Proteins were resolved by 4–12% Bolt Bis-Tris SDS PAGE (Thermo Fischer, Waltham, MA), then
596 transferred to nitrocellulose membrane (GE Life Sciences, Marlborough, MA). Membranes were
597 blocked in PBS with 5% non-fat milk, followed by incubation with primary antibody overnight.
598 Membranes were washed four times with PBS with 0.1% Tween-20 (PBS-T) and incubated with
599 secondary antibody for 45 min. Membranes were imaged and protein bands quantified using an
600 infrared imaging system (Odyssey; LI-COR Biosciences, Lincoln, NE). The following primary antibodies
601 were used for detection of tagged proteins at the indicated dilutions: rabbit-anti-Dhh1 (1:5000) as
602 described in (Fischer and Weis, 2002), (Weis Lab ETH Zurich Cat# Weis_001, RRID:AB_2629458),
603 mouse-anti-GFP (1:1000) (Roche Cat# 11814460001, RRID:AB_390913), and rabbit-anti-Hxk1 (1:3000)
604 (US Biological Cat# H2035-01, RRID:AB_2629457, Salem, MA). IRdye 680RD goat-anti-rabbit (LI-COR
605 Biosciences Cat# 926–68071, RRID:AB_10956166) and IRdye 800 donkey-anti-mouse (LI-COR
606 Biosciences Cat# 926–32212, RRID:AB_621847) were used as secondary antibodies.

607 **ACKNOWLEDGEMENTS**

608 We would like to thank Justine Kusch and the ETHZ ScopeM facility for technical assistance with
609 confocal microscopy, Elisa Dultz, Carmen Weber, Stephanie Heinrich, Mostafa Zedan, Sarah Khawaja
610 Evgeny Onishchenko, Annemarie Kralt and Jan Nagler for their critical reading of this manuscript and
611 members of the Weis lab for helpful discussions and comments. We would like to thank Bram Hofland
612 for assisting in cloning of yeast constructs. We would also like to thank the Séraphin lab for sharing

613 their yeast strains. M.H. was supported by a Human Frontier Science Program (HFSP) postdoctoral
614 fellowship (LT000914/2015) and an ETH postdoctoral fellowship (FEL-37-14-2). This work was
615 supported by NIH/NIGMS (R01GM058065 and R01GM101257 to K.W.) and the Swiss National Science
616 Foundation (SNF 31003A_159731 and 31003A_179275 to K.W.).

617

618 **Figure legends**

619 **Figure 1. (A) Overexpression (OE) of Pat1 leads to constitutive PB formation but only in the presence**
620 **of Dhh1.** Cells co-expressing the indicated PB components were grown in synthetic complete (SC)
621 raffinose media to exponential growth phase after which Pat1 was overexpressed via addition of
622 galactose. Cells in both raffinose and galactose were observed by fluorescence microscopy. In all Pat1
623 OE strains the endogenous promoter of Pat1 was replaced by the galactose 1-10 promoter (*p-GAL-*
624 *PAT1*). Scale bar: 5µm. (B) Quantification of images in A depicting number of PBs/cell. N=3 biological
625 replicates with >800 cells/replicate. Error bars: SEM. (C) **Pat1-NC (AA 5-79 + 456-587) is functional *in***
626 ***vivo*.** Cartoon of the Pat1-NC construct (see text for details). **(D) *PAT1-NC* induces PB formation upon**
627 **stress *in vivo***. Cells co-expressing the indicated the PB components in *PAT1* full length or *PAT1-NC*
628 background were grown in synthetic complete (SCD) media to exponential growth phase then shifted
629 to glucose-rich or glucose-starvation conditions for 30 minutes and observed by fluorescence
630 microscopy. PBs induced in the *PAT1-NC* background were dissolved by addition of 2% glucose
631 demonstrating reversibility. Scale bar: 5µm. (E) Quantification of images shown in A depicting number
632 of PBs/cell. Bars: SEM. N=3 biological replicates with >800 cells/replicate. **(F) *PAT1-NC* (AA 5-79 + 456-**
633 **587) OE leads to constitutive PB induction**. *p(GAL)-PAT1* or *p(GAL)-PAT1-NC* cells expressing Dhh1-
634 GFP were grown in SC raffinose media to exponential growth phase after which Pat1 OE was induced
635 with galactose. Scale bar: 5µm. (G) Graph depicts Dhh1 PBs/cell, SEM. N= 3 biological replicates with
636 >800 cells/replicate. [Diatrack 3.05 and cell segmentation using in house Matlab code was used for the
637 quantification of PB and cell numbers respectively for all the experiments shown in the manuscript].

638 **Figure 1- figure Supplement 1. (A) Controls for the Pat1 OE, relating to Figure 1.** Upper panel: *PAT1*
639 (endogenous promoter) cells expressing Dhh1-GFP were grown in (SC) raffinose media to exponential
640 growth phase after which galactose was added and cells were imaged by fluorescence microscopy.
641 Lower Panel: *p(GAL)-HA pat1Δ* (Hemagglutinin tag) OE does not lead to constitutive PB formation.
642 Scale bar: 5µm**. (B) *PAT1-NC* rescues the *pat1Δ* growth phenotype**. *PAT1, pat1Δ* and *PAT1-NC* cells
643 were grown overnight in SCD media to saturation and the next day the different strains were
644 inoculated to OD 0.1 in SCD. Absorbance based growth measurements were recorded for 24 hours.
645 The growth curve depicts O.D. 600 nm versus time. **(C) *PAT1-NC* rescues the thermosensitive growth**
646 **phenotype of *pat1Δ*.** Cells expressing *PAT1-NC*, *PAT1* and cells lacking *PAT1* were grown to saturation
647 in SCD media overnight and the next day spotted on YPD plates at the indicated temperatures. Growth
648 was monitored after 2-3 days of incubation. The phenotype was confirmed with three biological
649 replicates. **(D) *PAT1-NC* fully rescues the growth phenotype in *pat1Δ edc3Δ scd6Δ* cells at 37°C.** Cells
650 expressing *PAT1 edc3Δ scd6Δ*, *pat1Δ edc3Δ scd6Δ* and *PAT1-NC edc3Δ scd6Δ* were grown to saturation
651 in SCD media overnight and the next day spotted on YPD plates at the indicated temperatures. Growth
652 was monitored after 2-3 days of incubation. The phenotype was confirmed with three biological
653 replicates. **(E) Pat1-NC localizes to PBs upon stress *in vivo*.** Cells co-expressing Pat1-NC-GFP and Dcp2-
654 mCherry as an additional PB marker were grown in SCD media to exponential growth phase then
655 shifted to glucose-rich or glucose-starvation conditions for 30 minutes and observed by fluorescence
656 microscopy. After visualization 2% final concentration of glucose was added for one hour to
657 demonstrate reversibility and dissolution of Pat1-NC PBs. Scale bar: 5µm.

658 **Figure 2. (A) Recombinant Pat1-NC$^{4A\text{-}Dhh1}$ is defective for Dhh1 binding.** GST pull-down with GST-Pat1-
659 NC and mutants thereof as matrix-bound bait and Dhh1 as prey. After 1h of binding at 4°C, the samples
660 were washed 5 times with a buffer containing 300 mM NaCl and visualized by Coomassie staining after
661 separation on a 12 % acrylamide gel. **(B) Expression of *pat1$^{4A\text{-}Dhh1}$* (Dhh1 binding mutant) leads to a**
662 **drastic reduction in PB formation.** Cells co-expressing the indicated PB components in the *PAT1* or
663 *pat1$^{4A\text{-}Dhh1}$* background were grown in SCD media to exponential growth phase, then shifted to glucose-

664 rich or glucose-starvation conditions for 30 minutes and observed by fluorescence microscopy. Scale
665 bar: 5µm. (C) Quantification of images in B depicting number of PBs/cell, (Dhh1-GFP PBs co-localizing
666 with Dcp2-mCherry) are shown, three biological replicates, bars: SEM. **(D) Pat1$^{4A\text{-}Dhh1}$-GFP mutant is**
667 **defective for PB localization.** Cells expressing either Pat1-GFP or the Pat1$^{4A\text{-}Dhh1}$-GFP mutant were
668 grown in SCD media to exponential growth phase then shifted to glucose-rich or glucose-starvation
669 conditions for 30 minutes and observed by fluorescence microscopy. Scale bar: 5µm. (E) Quantification
670 of images shown in D depicting number of PBs/cell. N= 3 biological replicates with >500 cells/replicate.
671 Error bars: SEM. (F) ***pat1$^{4A\text{-}Dhh1}$* mutant is defective in PB formation upon hippuristanol treatment.**
672 Cells expressing either *PAT1* or the *pat1$^{4A\text{-}Dhh1}$* were grown in SCD media to exponential growth phase
673 after which they were treated with 10uM hippuristanol for 2hrs. The kinetics of PB formation was
674 monitored using Dhh1-GFP and its co-localization with Dcp2-mCherry. Quantification of PBs/cell is
675 depicted. Stills from the live imaging time course are shown. N= 2 biological replicates, two technical
676 replicates each with >300 cells/replicate, SD.

677 **Figure 2- figure Supplement 1. (A) *pat1$^{4A\text{-}Dhh1}$* mutant has a slight growth defect.** *PAT1*, *pat1Δ* and
678 *pat1$^{4A\text{-}Dhh1}$* cells were grown overnight in SCD media to saturation and the next day the different strains
679 were inoculated to OD 0.1 and growth curves were recorded for 24 hours. The growth curve depicts
680 O.D. 600 nm versus time. **(B) *pat1Δ* abolishes PB formation.** Cells expressing Dhh1-GFP in *pat1Δ or*
681 *PAT1* strains were grown in SCD media to exponential growth phase then shifted to glucose-rich or
682 glucose-starvation conditions for 30 minutes and observed by fluorescence microscopy. The graph
683 depicts the number of PBs/cell. N=2 biological replicates, 300 cells per replicate, SD. **(C) Pat1$^{4A\text{-}Dhh1}$ and**
684 **Pat1^{EE} are expressed to similar levels as wild-type Pat1.** Pat1-GFP, Pat1$^{4A\text{-}Dhh1}$–GFP and Pat1^{EE}-GFP
685 expressing cells were grown in SCD media to exponential growth phase and protein levels were
686 measured using Western blot with an anti-GFP antibody. Hexokinase was used as a loading control.
687 The graph depicts the expression levels of different Pat1 mutants normalized to the loading control.
688 N=2 biological replicates. SD shown. **(D) Dhh1 expression in different Pat1 mutants is comparable to**
689 **Dhh1 expression in wild-type Pat1.** Pat1-GFP, Pat1$^{4A\text{-}Dhh1}$–GFP and Pat1^{EE}-GFP expressing cells were

690 grown in SCD media to exponential growth phase and Dhh1 protein levels were measured using
691 Western blot with an anti-Dhh1 antibody. A non-specific band detected by the antibody was used as
692 an internal control. The graph depicts the expression levels of Dhh1 in Pat1 mutants normalized to the
693 internal control. N=2 biological replicates. SD shown.

694 **Figure 3: (A) Expression of two distinct Pat1 binding mutants, Dhh1^{R295D} and Dhh1^{S292DN294D}, leads to**
695 **a drastic reduction in PB formation.** Cells co-expressing the indicated PB components in either Dhh1,
696 Dhh1^{R295D} or Dhh1^{S292DN294D} cells were grown in SCD media to exponential growth phase, then shifted
697 to glucose-rich or glucose-starvation conditions for 30 minutes and observed by fluorescence
698 microscopy. Scale bar: 5µm. (B) Quantification of images in A depicting number of Dhh1 positive and
699 Dcp2 positive PBs/cell; N= 4 biological replicates with >300 cells/replicate, SEM. (C) **Dhh1^{R295D} and**
700 **Dhh1^{S292DN294D} mutants are defective in PB formation upon hippuristanol treatment.** Cells expressing
701 either *Dhh1,* Dhh1^{R295D}, Dhh1^{S292DN294D} or *dhh1Δ*, were grown in SCD media to exponential growth phase
702 after which they were treated with 10uM hippuristanol for 3hrs. The kinetics of PB formation was
703 monitored using Dhh1-GFP and its co-localization with Dcp2-mCherry. (D) Quantification of PBs/cell.
704 Stills from the live imaging time course are shown. N= 3 biological replicates with >300 cells/replicate,
705 SEM.

706 **Figure 3- figure supplement 1: Dhh1 mutants that abolish Pat1 binding are expressed at similar levels**
707 **to wild-type Dhh1.** Dhh1-GFP, Dhh1^{R295D}–GFP and Dhh11^{S292DN294D}-GFP expressing cells were grown in
708 SCD media to exponential growth phase and protein levels were measured using Western blot with an
709 anti-GFP antibody. Hexokinase was used as a loading control. The graph depicts the expression levels
710 of different Dhh1 mutants normalized to the loading control. N=2 biological replicates. SD shown.

711 **Figure 4. (A, B) Overexpression (OE) of *p(GAL)-PAT1^{WT}*(wild-type) and *p(GAL)-pat1^{AA}* (non-**
712 **phosphorylatable) leads to constitutive PB formation but OE of *p(GAL)-pat1^{EE}* (phospho-mimetic)**
713 **does not.** Cells co-expressing the indicated PB components were grown in SC raffinose media to
714 exponential growth phase after which OE of different Pat1 alleles was induced by galactose addition.

715 Cells were imaged using fluorescence microscopy. Quantification of images shown in C depicting
716 number of PBs/cell. Scale bar: 5µm, SEM. N=3 biological replicates with >800 cells/replicate. (C) **Pat1-**
717 **C-terminal domain does not bind Dhh1.** V5 pull-down with V5-Pat1-C and V5-Pat1-C^{EE} as matrix-bound
718 bait and Dhh1-mCherry as prey. After 1h of binding at 4°C, the samples were washed 4 times with a
719 buffer containing NaCl as indicated and visualized by Coomassie staining after separation on a 12 %
720 acrylamide gel. **(D) Pat1-C^{EE} weakens the interaction with RNA compared to Pat1-C.** Recombinant
721 Pat1-C (WT) and Pat1-C^{EE} were incubated with a Cy5-labeld 29nt RNA oligo in the presence of 300mM
722 NaCl and separated on a NativePage gradient gel. The fluorescence of the oligo was detected by LI-
723 COR imaging. Reactions were performed in triplicate and the intensity of the upper shifted RNA oligo
724 band was quantified. Equal input of the Pat1-C proteins was verified by acrylamide PAGE and
725 Coomassie staining. Error bars: SD.

726 **Figure 4- figure supplement 1. (A) *PAT1* and *pat1* ^{AA} lead to PB induction upon stress, which is**
727 **drastically reduced in the *pat1*^{EE} background.** (A) Cells expressing the indicated GFP-PB markers (in
728 the *PAT1*$^{WT/SS}$, *pat1*^{AA} and *pat1*^{EE} backgrounds) were grown in SCD media to exponential growth phase
729 then shifted to glucose-rich (left panel) or glucose-starvation conditions (right panel) for 30 minutes
730 and observed by fluorescence microscopy. Scale bar: 5µm. (B) Quantification of images shown in A
731 depicting PBs/cell. Bars: SEM, N= 3 biological replicates with >800 cells/replicate.

732 **Figure 5. (A) *not1*$^{9X\text{-}Dhh1}$ (Dhh1 binding mutant) combined with *pat1*^{AA} (non-phosphorylatable Pat1)**
733 **enhances constitutive PB formation.** Cells expressing either *not1*$^{9X\text{-}Dhh1}$ or *pat1*^{AA} or the combination
734 of both mutants were grown in SCD media to exponential growth phase and PBs visualized by
735 fluorescence microscopy using Dcp2-mCherry as a *bona fide* PB marker. Scale bar: 5µm. (B) The graph
736 depicts the number of Dcp2 positive PBs/cell. N= 3 biological replicates with >500 cells visualized in
737 each replicate, bars: SEM.

738 **Figure 6. Pat1 WT but not Pat1$^{4A\text{-}Dhh1/EE}$ mutant enhances the phase separation of Dhh1 and RNA *in***
739 ***vitro*.** (A) 4 µM Dhh1-mCherry was mixed with 3.2 mM ATP and 0.2 mg/ml polyU as RNA-analog in a

740 150mM KCl buffer. Pat1-NC-GFP and mutants thereof were added in increasing concentrations, as
741 indicated. mCherry and GFP intensities are scaled identically in all images displayed. Representative
742 images, scale bar 25 µm. Quantification of the droplet intensity multiplied by area (mCherry and GFP
743 channels separately normalized to Dhh1 alone and Pat1 4µM respectively) of three technical replicates
744 of the reactions displayed in Figure 5A, mean and standard deviation. (B) **Not1 prevents droplet**
745 **formation also in the presence of Pat1**. Proteins were mixed as indicated, and droplet formation
746 induced by addition of low salt buffer, ATP and polyU. Scale bar 25 mM, quantification (intensity
747 multiplied by area) of two biological replicates (one to three technical replicates each), mean and
748 standard deviation.

749 **Figure 6- figure supplement 1. (A) Pat1 does not inhibit the Not1^{MIF4G}-stimulatd ATPase activity of**
750 **Dhh1**. ATPase reactions were performed under saturating concentrations of polyU using a Not1^{MIF4G}
751 concentration that stimulates Dhh1 to 0.75 V_{max}. Pat1 was added to either 2- and 6-fold excess over
752 Not1. Three biological replicates (each of three technical replicates); mean and standard deviation of
753 k_{cat} values. The values are corrected for blank (that is Pat1 alone or Not1 alone). P values are obtained
754 from a two-tailed t-test. **(B) Pat1 OE PBs are more dynamic than the Dhh1^{DQAD} PBs.** Cells expressing
755 Dcp2-mCherry in the *p(GAL)-PAT1* OE strain were grown in (SC) raffinose to exponential growth phase
756 after which galactose was added to 2% final concentration for 2hrs to induce PBs. Then the cells were
757 treated with 50µg/ml cycloheximide (CHX) and disappearance of Dcp2-mCherry PBs per cell was
758 monitored for 90 minutes by fluorescence microscopy. In order to study PB dynamics in the *DHH1* and
759 *dhh1 ^{DQAD}* background cells were grown as described before except PBs were induced by carbon
760 starvation and their disassembly monitored by CHX. Each time point shows a representative image. (C)
761 The graph shows the foci number per cell measurements for Dcp2-mCherry normalized to 1 to account
762 for differences in PB formation under different PB induction conditions. Scale bar: 5µm. N=2 biological
763 replicates with >200 cells counted per experiments. Error bars: SD.

764 **Figure 6- figure supplement 2.** (A) **Pat1 by itself does not phase separate *in vitro*.** Reactions are
765 performed in the presence of ATP and polyU at indicated protein concentrations. N= three technical

766 replicates. (B) **Enhancement of Dhh1's phase separation by Pat1 is RNA-dependent**. Reactions are
767 performed in the presence of ATP but absence of polyU at indicated protein concentrations. N= three
768 technical replicates (C) **Pat1-N terminus does not enhance the phase separation of Dhh1.** Reactions
769 are performed in the presence of ATP and polyU at indicated protein concentrations. Quantification
770 (intensity multiplied by area of droplets) of three technical replicates, mean and standard deviation.

771 **Figure 7. Stoichiometry of Pat1 and Dhh1 in PBs *in vivo* and in liquid droplets *in vitro*.** (A) Pat1-GFP
772 and Dhh1-GFP expressing cells were grown in SCD media to exponential growth phase and then shifted
773 to SC (minus glucose) for the indicated time points. PB formation was visualized by fluorescence
774 microscopy. Graph depicts the ratio of Dhh1: Pat1 in PBs *in vivo*. N= 3 biological replicates, SEM. (B)
775 Calibration curves to determine the protein concentration of Dhh1-mCherry and Pat1-NC-GFP within
776 the droplets: the fluorescence intensity of homogeneous solutions of the respective proteins was
777 measured at different protein concentrations (blue circles). The unknown protein concentration was
778 determined by linear fitting of this calibration curve (violet circle). Confocal fluorescence microscopy
779 images of phase-separated droplets of Dhh1-mCherry in the absence and presence of Pat1-GFP are
780 shown. Scale bar: 20µM. **(C) Tug-of-war model between Pat1 and Not1 to regulate PB dynamics.**
781 Model depicting three inputs that cooperatively regulate PB formation. The solid black arrows on the
782 left show interaction between the Pat1 N-terminus with the RecA2 core of Dhh1, Pat1 C-terminus with
783 RNA, Dhh1 interaction with RNA and potential Dhh1-Dhh1 interactions via low-complexity
784 unstructured tails. The dotted grey arrows on the right demonstrate multivalent interactions in a PB
785 driven by the LLPS of Dhh1 and RNA (a process enhanced by Pat1). Colors: green: inputs that promote
786 PB assembly, red factors that negatively regulate PB formation. Violet: Dhh1, light green: Pat1-NC,
787 blue: RNA.

788 **Figure 7- figure supplement 1. (A) Images of the Pat1-GFP and Dhh1-GFP stoichiometry**. Cells
789 expressing Pat1-GFP and Dhh1-GFP were grown in SCD media to exponential growth phase then
790 shifted to glucose-starvation conditions for different time points as indicated and PBs were imaged by

791 fluorescence microscopy. Images are representative for each times. Scale: 5µM. (B) Dhh1-GFP and
792 Pat1-GFP expressing cells (used for imaging in A) were grown in SCD media to exponential growth
793 phase and protein levels were measured using Western blot with an anti-GFP antibody. Hexokinase
794 was used as a loading control. The graph depicts the expression levels of Dhh1 and Pat1 normalized to
795 the loading control. (C) **Size distributions of *in vitro* assembled Dhh1 and Pat1 LLPS droplets** (relating
796 to Figure 6B). In presence of Pat1, the droplet size increases and the size distribution shifts to larger
797 radii. Moreover, the number of droplets decreases, thereby indicating that the droplets have higher
798 propensity to fuse in presence of Pat1. Scale bar: 20µm.

799 **Figure 7- figure supplement 2. OE of Pat1 in the presence of the endogenous copy of Pat1 [*p-PAT1*
800 **+p(GAL)-*PAT1*] leads to the nuclear localization of PB components.** (A) Cells expressing Dhh1-GFP [*p-*
801 *PAT1* +p(GAL)-*PAT1* background] were grown in SC raffinose media to exponential growth phase after
802 which Pat1 OE was induced with galactose. Localization of Dhh1-GFP to the nucleus was confirmed by
803 co-localization with DAPI staining after 2hrs of *PAT1* or $pat1^{AA}$ OE. White arrows depict the co-
804 localization of Dhh1-GFP and DAPI. Scale bar: 5µm. N= 2 biological replicates. (B) HDEL Td tomato was
805 used as a marker of the nuclear rim, scale bar: 5µm. **(C) PBs formed in $pat1^{4A\text{-}Dhh1}$ and $pat1^{EE}$ expressing
806 cells are less intense than PBs formed in *PAT1* wild-type cells.** Graph showing the average intensity
807 of PBs (obtained from Figure 2B and S3).

808 **Supplementary file 1**: is the supplementary table 1, which contains details regarding all the yeast
809 strains used in this study.

810 **Supplementary file 2:** Supplementary table S2A contains all the plasmids used in this study. Table
811 Supplementary S2B contains the mutants used in this study and Table S2C describes the entire DNA
812 oligos used for this manuscript.

813 **Source code File 1:** contains the MATLAB script to count the yeast cell number in an automated
814 manner.

815

816 **Video legends**

817 Video 1: **Hippuristanol induces PBs in cells expressing wild-type *PAT1***. The video depicts PB formation
818 (Dhh1-GFP and Dcp2-mCherry co-localization) in cells expressing wild-type *PAT1* upon hippuristanol
819 treatment. (2hrs video, 5 min intervals; video played at 7 fps). Each frame is a single plane.

820 Video 2: **Hippuristanol fails to induce PBs in cells expressing *pat1$^{4A\text{-}Dhh1}$* mutant.** The video depicts
821 failure to form PBs (Dhh1-GFP and Dcp2-mCherry co-localization) in cells expressing *pat1$^{4A\text{-}Dhh1}$* upon
822 hippuristanol treatment. (2hrs video, 5 min intervals; video played at 7 fps). Each frame is a single
823 plane.

824 Video 3: **Hippuristanol induces PBs in cells expressing wild-type *Dhh1***. The video depicts PB formation
825 (Dhh1-GFP and Dcp2-mCherry co-localization) in cells expressing wild-type Dhh1 upon hippuristanol
826 treatment. (3hrs video, 5 min intervals; video played at 7 fps). Each frame is a single plane.

827 Video 4: **Hippuristanol does not induce PBs in cells expressing the Dhh1^{S292DN294D} mutant**. The video
828 depicts PB formation (Dhh1^{S292DN294D} -GFP and Dcp2-mCherry co-localization) in cells expressing
829 Dhh1^{S292DN294D} mutant wild- upon hippuristanol treatment. (3hrs video, 5 min intervals; video played
830 at 7 fps). Each frame is a single plane.

831 Video 5: **Hippuristanol fails to induce PBs in cells expressing the Dhh1^{R295D} mutant**. The video depicts
832 PB formation (Dhh1^{R295D}-GFP and Dcp2-mCherry co-localization) in cells expressing Dhh1^{R295D} mutant
833 wild- upon hippuristanol treatment. (3hrs video, 5 min intervals; video played at 7 fps). Each frame is
834 a single plane.

835 Video 6: ***dhh1Δ* cells do not form PBs upon hippuristanol treatment.** The video depicts PB formation
836 (Dcp2-mCherry co-localization) in cells lacking *dhh1* upon hippuristanol treatment. (3hrs video, 5 min
837 intervals; video played at 7 fps). Each frame is a single plane.

838 Video 7: **Cycloheximide treatment causes wild-type PB disassembly.** Dcp2-mCherry expressing cells
839 in the *DHH1* background were grown in (SC) raffinose media to exponential growth phase, after which

840 galactose was added to 2% final concentration for 2hrs and then starved for 30 mins to allow PBs to
841 form. The cells were then treated with 50 µg/mL cycloheximide for 90 mins and disappearance of foci
842 was monitored using fluorescence microscopy. (5 min intervals; video played at 7 fps). Each frame is a
843 single plane.

844 Video 8: **Cycloheximide treatment causes Pat1 OE PB disassembly albeit faster than PB disassembly**
845 **in cells expressing *dhh1*^{DQAD}.** Cells expressing Dcp2-mCherry in the *p(GAL)-PAT1* OE strain were grown
846 in (SC) raffinose to exponential growth phase, after which galactose was added to 2% final
847 concentration for 2hrs to allow PBs to form. Thereafter, the cells were treated with 50µg/mL
848 cycloheximide (CHX) for 90 mins and disappearance of foci was monitored using fluorescence
849 microscopy. (5 min intervals; video played at 7 fps). Each frame is a single plane.

850 Video 9: **Cycloheximide treatment of *dhh1* ^{DQAD} PBs.** Dcp2-mCherry expressing cells in the *dhh1*^{DQAD}
851 mutant background were grown in (SC) raffinose to exponential growth phase, after which galactose
852 was added to 2% final concentration for 2hrs. The cells were then carbon starved for 30 mins to allow
853 PBs to form after which, 50 µg/mL cycloheximide was added and disappearance of foci was monitored
854 for 90 mins using fluorescence microscopy. (5 min intervals; video played at 7 fps). Each frame is a
855 single plane.

856

857 **SUPPLEMENTARY TABLE S1**

858 **Yeast strains in this study**

Strain #	Genotype
KWY165	*MAT a ade2-1 can1-100 GAL phi+ his3-11,15 ura3-1 leu2-3, 112 trp1-1*
KWY276	*MAT a ade2-1 can1-100 GAL phi+ his3-11,15 ura3-1 leu2-3, 112 trp1-1 dhh1::DHH1-GFP-HisMX6*

KWY1972	*MAT a ade2-1 can1-100 GAL phi+ his3-11,15 ura3-1 leu2-3, 112 trp1-1 dcp2::DCP2-mCherry-NatMX6*
KWY1973	*MAT a ade2-1 can1-100 GAL phi+ his3-11,15 ura3-1 leu2-3, 112 trp1-1 dhh1::DHH1-HisMX6 GFP dcp2::DCP2-mCherry-NatMX6*
KWY2226	*MAT a ade2-1 can1-100 GAL phi+ his3-11,15 ura3-1 leu2-3, 112 trp1-1 pat1Δ::KanMX6*
KWY3238	*MAT alpha ade2-1 can1-100 GAL phi+ his3-11,15 ura3-1 leu2-3, 112 trp1-1 dhh1Δ::KanMX6 dcp2::DCP2-mCherry-NatMX6 pDHH1-GFP-URA3*
KWY3239	*MAT alpha ade2-1 can1-100 GAL phi+ his3-11,15 ura3-1 leu2-3, 112 trp1-1 dhh1Δ::KanMX6 dcp2::DCP2-mCherry-NatMX6 pDHH1^{DQAD}-GFP-URA3*
KWY3280	*MAT a ade2-1 can1-100 GAL phi+ his3-11,15 ura3-1 leu2-3, 112 trp1-1 pat1::PAT1-GFP-HisMX6*
KWY4901	*MAT alpha ade2-1 can1-100 GAL phi+ his3-11,15 ura3-1 leu2-3, 112 trp1-1 dhh1Δ::KanMX6 dcp2::DCP2-mCherry-NatMX6 pDHH1$^{5X\text{-}Not}$-GFP-URA3*
KWY5157	*MAT alpha ade2-1 can1-100 GAL phi+ his3-11,15 ura3-1 leu2-3, 112 trp1-1 dhh1Δ::TRP dhh1Δ::KanMX6*
KWY5221	*MAT alpha ade2-1 can1-100 GAL phi+ his3-11,15 ura3-1 leu2-3, 112 trp1-1 dhh1Δ::TRP pat1Δ::KanMX6 pDHH1 GFP-URA3*
KWY5224	*MAT alpha ade2-1 can1-100 GAL phi+ his3-11,15 ura3-1 leu2-3, 112 trp1-1 dhh1Δ::TRP pat1Δ::KanMX6 pDHH1^{DQAD}-GFP-URA3*

KWY5227	*MAT alpha ade2-1 can1-100 GAL phi+ his3-11,15 ura3-1 leu2-3, 112 trp1-1 dhh1Δ::TRP pat1Δ::KanMX6 pDHH1^{RNA3X}-GFP-URA3*
KWY5230	*MAT alpha ade2-1 can1-100 GAL phi+ his3-11,15 ura3-1 leu2-3, 112 trp1-1 dhh1Δ::TRP pat1Δ::KanMX6 pDHH1$^{DQAD/RNA3X}$-GFP-URA3*
KWY5601	*MAT a ade2-1 can1-100 GAL phi+ his3-11,15 ura3-1 leu2-3, 112 trp1-1 pat1:: PAT1-HisMX6 dhh1::DHH1 GFP-URA3*
KWY5603	*MAT a ade2-1 can1-100 GAL phi+ his3-11,15 ura3-1 leu2-3, 112 trp1-1 pat1::PAT1 AA::HisMX6 dhh1::DHH1 GFP-URA3*
KWY5609	*MAT a ade2-1 can1-100 GAL phi+ his3-11,15 ura3-1 leu2-3, 112 trp1-1 pat1::PAT1 EE-HisMX6 dhh1::DHH1 GFP-URA3*
KWY5915	*MAT alpha ade2-1 can1-100 GAL phi+ his3-11,15 ura3-1 leu2-3, 112 trp1-1 dhh1Δ::TRP pat1Δ::KanMX6 edc3::EDC3-mcherry:: HisMX6 pDHH1 GFP-URA3*
KWY5917	*MAT alpha ade2-1 can1-100 GAL phi+ his3-11,15 ura3-1 leu2-3, 112 trp1-1 dhh1Δ::TRP pat1Δ::KanMX6 edc3::EDC3-mcherry:: HisMX6 pDHH1^{DQAD}-GFP-URA3*
KWY5933	*MAT alpha ade2-1 can1-100 GAL phi+ his3-11,15 ura3-1 leu2-3, 112 trp1-1 dhh1Δ::TRP pat1Δ::KanMX6 dcp2::DCP2-mcherry:: HisMX6 pDHH1 GFP-URA3*
KWY5935	*MAT alpha ade2-1 can1-100 GAL phi+ his3-11,15 ura3-1 leu2-3, 112 trp1-1 dhh1Δ::TRP pat1Δ::KanMX6 dcp2::DCP2-mcherry:: HisMX6 pDHH1^{DQAD}-GFP-URA3*
KWY5943	*MAT alpha ade2-1 can1-100 GAL phi+ his3-11,15 ura3-1 leu2-3, 112 trp1-1 pat1:: PAT14A-HisMX6*

KWY5978	*MAT alpha ade2-1 can1-100 GAL phi+ his3-11,15 ura3-1 leu2-3, 112 trp1-1 pat1:: PAT1-HisMX6 dhh1::DHH1 GFP-URA3 pGAL-PAT1-3XV5-LEU2*
KWY5980	*MAT alpha ade2-1 can1-100 GAL phi+ his3-11,15 ura3-1 leu2-3, 112 trp1-1 pat1:: PAT1-HisMX6 dhh1::DHH1 GFP-URA3 pGAL-PAT1AA-3XV5-LEU2*
KWY5983	*MAT alpha ade2-1 can1-100 GAL phi+ his3-11,15 ura3-1 leu2-3, 112 trp1-1 pat1:: PAT1-HisMX6 dhh1::DHH1 GFP-URA3 pGAL-PAT1 EE-3XV5-LEU2*
KWY6003	*MAT alpha ade2-1 can1-100 GAL phi+ his3-11,15 ura3-1 leu2-3, 112 trp1-1 pat1Δ::KanMX6 dhh1Δ::TRP pDHH1$^{5X\text{-}Not}$-GFP-URA3*
KWY6056	*MAT alpha ade2-1 can1-100 GAL phi+ his3-11,15 ura3-1 leu2-3, 112 trp1-1 pat1::PAT14A-HismX6 dhh1Δ::TRP pDHH1^{DQAD}-GFP-URA3*
KWY6058	*MAT alpha ade2-1 can1-100 GAL phi+ his3-11,15 ura3-1 leu2-3, 112 trp1-1 pat1::PAT14A-HismX6 dhh1Δ::TRP pDHH1-GFP-URA3*
KWY6180	*MAT alpha ade2-1 can1-100 GAL phi+ his3-11,15 ura3-1 leu2-3, 112 trp1-1 pGAL-PAT1 3X HA::KanMX6 dhh1::DHH1 GFP::URA3*
KWY6279	*MAT a ade2-1 can1-100 GAL phi+ his3-11,15 ura3-1 leu2-3, 112 trp1-1 pat1::PAT1-HisMX6 edc3::EDC3 GFP-URA3*
KWY6403	*MAT alpha ade2-1 can1-100 GAL phi+ his3-11,15 ura3-1 leu2-3, 112 trp1-1 pat1Δ::pGAL-3X HA::KanMX6 dhh1::DHH1 GFP URA3*

KWY6467	*MAT a ade2-1 can1-100 GAL phi+ his3-11,15 ura3-1 leu2-3, 112 trp1-1 pat1::PAT1AA-HisMX6 edc3::EDC3 GFP-URA3*
KWY6469	*MAT a ade2-1 can1-100 GAL phi+ his3-11,15 ura3-1 leu2-3, 112 trp1-1 pat1::PAT1AA-HisMX6 dcp2::DCP2 GFP-URA3*
KWY6471	*MAT a ade2-1 can1-100 GAL phi+ his3-11,15 ura3-1 leu2-3, 112 trp1-1 pat1::PAT1-HisMX6 dcp2::DCp2 GFP-URA3*
KWY6478	*MAT a ade2-1 can1-100 GAL phi+ his3-11,15 ura3-1 leu2-3, 112 trp1-1 pat1::PAT1EE-HisMX6 dcp2::DCP2 GFP-URA3*
KWY6480	*MAT a ade2-1 can1-100 GAL phi+ his3-11,15 ura3-1 leu2-3, 112 trp1-1 pat1::PAT1EE-HisMX6 edc3::EDC3 GFP-URA3*
KWY6544	*MAT a ade2-1 can1-100 GAL phi+ his3-11,15 ura3-1 trp1-1 leu2-3, 112Δ::CG-LEU2-NOT1$^{9X\text{-}Dhh1}$-TAP not1Δ::TRP1 dcp2::DCP2-mCherry-NatMX6*
KWY6604	*MAT alpha ade2-1 can1-100 GAL phi+ his3-11,15 ura3-1 leu2-3, 112 trp1-1 pat1Δ::TRP dhh1::DHH1 GFP URA3*
KWY6637	*MAT alpha ade2-1 can1-100 GAL phi+ his3-11,15 ura3-1 leu2-3, 112 trp1-1 dhh1::DHH1 GFP-URA3 dcp2::DCP2-mCherry-NatMX6 pGAL-PAT1 AA-3XV5-LEU2*
KWY6643	*MAT alpha ade2-1 can1-100 GAL phi+ his3-11,15 ura3-1 leu2-3, 112 trp1-1 pGAL-PAT1-3X HA::KanmX6 dhh1::DHH1 GFP: URA3 dcp2::DCP2-mCherry-NatMX6*
KWY6692	*MAT alpha ade2-1 can1-100 GAL phi+ his3-11,15 ura3-1 leu2-3, 112 trp1-1 pGAL-PAT1 EE-3X-HA::KanMX6 dhh1::DHH1 GFP::URA3 dcp2::DCP2-mCherry-NatMX6*

KWY6836	*MAT alpha ade2-1 can1-100 GAL phi+ his3-11,15 ura3-1 leu2-3, 112 trp1-1 pGAL-PAT1 3XHA::URA3 dhh1Δ::KanMX6 edc3::EDC3 GFP-HisMX6 dcp2::DCP2-mCherry-NatMX6*
KWY7370	*MAT a ade2-1 can1-100 GAL phi+ his3-11,15 ura3-1 leu2-3, 112 trp1-1 pat1::p-GAL- PAT1 NC-3X-HA-HYG dhh1::DHH1 GFP-URA3*
KWY7420	*MAT alpha ade2-1 can1-100 GAL phi+ his3-11,15 ura3-1 leu2-3, 112 trp1-1 pGAL-PAT1 3XHA::KanMX6 dhh1::DHH1 RNA3X GFP-HismX6*
KWY7481	*MAT a ade2-1 can1-100 GAL phi+ his3-11,15 ura3-1 leu2-3, 112 trp1-1 pat1::PAT14A GFP-URA3*
KWY7484	*MAT a ade2-1 can1-100 GAL phi+ his3-11,15 ura3-1 leu2-3, 112 trp1-1 pat1::PAT1 NC-HYG dhh1::DHH1 GFP-HisMX6 dcp2::DCP2-mCherry-NatMX6*
KWY7554	*MAT a ade2-1 can1-100 GAL phi+ his3-11,15 ura3-1 leu2-3, 112 trp1-1 pat1::PAT14A GFP-URA3 dcp2::DCP2 mcherry-KanMX6*
KWY7557	*MAT a ade2-1 can1-100 GAL phi+ his3-11,15 ura3-1 leu2-3, 112 trp1-1 pat1::PAT1N-C GFP-HismX6*
KWY7562	*MAT a ade2-1 can1-100 GAL phi+ his3-11,15 ura3-1 leu2-3, 112 trp1-1 pat1::PAT1N-C GFP-HisMX6 dcp2::DCP2 mcherry-NatMX6*
KWY7890	*MAT a ade2-1 can1-100 GAL phi+ his3-11,15 ura3-1 leu2-3, 112 trp1-1 dhh1::dhh1^{DQAD}-GFP-HisMX6 dcp2::DCP2-mCherry-NatMX6*

KWY8378	*MAT a ade2-1 can1-100 GAL phi+ his3-11,15 ura3-1 trp1-1 leu2-3, 112Δ::CG-LEU2-NOT1$^{9X\text{-}Dhh1}$-TAP not1Δ::TRP1 pat1::PAT1AA-HisMX6 dcp2::DCP2-mCherry-NatMX6*
KWY8622	*MAT a ade2-1 can1-100 GAL phi+ his3-11,15 ura3-1 leu2-3, 112 trp1-1 edc3::NatMX6 scd6::KanMX6*
KWY8624	*MAT a ade2-1 can1-100 GAL phi+ his3-11,15 ura3-1 leu2-3, 112 trp1-1 pat1:: HISMX6 edc3::NatMX6 scd6::KanMX6*
KWY8633	*MAT a ade2-1 can1-100 GAL phi+ his3-11,15 ura3-1 leu2-3, 112 trp1-1 dhh1:: dhh1^{R295D} -GFP-HisMX6 dcp2::DCP2-mCherry-NatMX6*
KWY8638	*MAT a ade2-1 can1-100 GAL phi+ his3-11,15 ura3-1 leu2-3, 112 trp1-1 dhh1:: dhh1^{S292DN294D}-GFP-HisMX6 dcp2::DCP2-mCherry-NatMX6*
KWY8753	*MAT a ade2-1 can1-100 GAL phi+ his3-11,15 ura3-1 leu2-3, 112 trp1-1 edc3::NatMX6 scd6::KanMX6 pat1::PAT1-NC-GFP::HisMX6*

859

860 SUPPLEMENTARY TABLE S2

861 A) Plasmids used in this study

Plasmid #	Description
pKW2312	pRS316 P(DHH1)-DHH1-GFP
pKW2313	pRS316 P(DHH1)-DHH1^{DQAD}-GFP
pKW2867	pRS316 P(DHH1)-DHH1$^{3X\text{-}RNA}$-GFP
pKW3040	pRS316 P(DHH1)-DHH1$^{DQAD/3X\text{-}RNA}$-GFP
pKW3333	pRS316 P(DHH1)-DHH1$^{5X\text{-}Not}$-GFP

pKW3477	pRS316 P(DHH1)-DHH1$^{DQAD/3X-RNA}$-6xHis-PP7CP
pKW3570	pFA6a-yEGFP-HIS3MX
pKW3756	pNH605-PGAL-Pat1 WT (XbaI)-3X V5
pKW3757	pNH605-PGAL- Pat1^{AA} (XbaI)-3X V5
pKW3758	pNH605-PGAL- Pat1^{EE} (XbaI)-3X V5
pKW3631	pETMCN_HisV5_Dhh1-mCherry
pKW3688	pETMCN_His_Dhh1-mCherry
pKW3641	pETMCN_HisV5_Pat1-C
pKW3702	pETMCN_HisV5_ Pat1-C^{EE}
pKW3920	pETMCN_HisTEVGST3C_Pat1-N [5-79]
pKW4225	pETMCN_GST-Pat1-NC-mCherry
pKW4356	pETMCN_GST-Pat1-NC-GFP
pKW4357	pETMCN_GST- Pat1-NC$^{4A-Dhh1}$-GFP
pKW4358	pETMCN_GST- Pat1-NC^{EE}-GFP

862

863 B) Dhh1, Pat1 and Not1 mutants used in this study

Mutant Protein	Mutation(s)
Dhh1^{DQAD}	E195Q
Dhh1$^{Q-motif}$	F66R, Q73A
Dhh1^{3X-RNA}	R322A, S340A, R370A
Dhh1^{5X-Not}	R55E, F62E, Q282E, N284E, R335E
Dhh1$^{DQAD/3X-RNA}$	E195Q, R322A, S340A, R370A

Dhh1$^{5X\text{-}Not/3X\text{-}RNA}$	R55E, F62E, Q282E, N284E, R322A, R335E, S340A, R370A
Dhh1^{R295D} (Mut3B)	R295D
Dhh1^{S292DN294D} (Mut3A)	S292D, N294D
Not1$^{9X\text{-}Dhh1}$	F791A, N795A, K804A, E823R, N834A, Y835A, K962A, F967A, E970A
Pat1^{AA}	S456A S457A
Pat1^{EE}	S456E S457E
Pat1$^{4A\text{-}Dhh1}$	D39A E40A T41A F42A
Pat1-N	Pat1-N (5-79)
Pat1-N-C	Pat1 N (5-79)- (GGS)4- C- (456-787)

C) Oligos used in this study

Oligo #	**Sequence**	**Description**
CH393	tgttcattattcatcatggaccaagccgataaaatgttatct cgt	DHH1, fw; mutagenic primer E195Q for Dhh1^{DQAD} mutant
CH394	acgagataacattttatcggcttggtccatgatgaataatga aca	DHH1, rev; mutagenic primer E195Q for Dhh1^{DQAD} mutant
CH574	atggtttttcaaaaccggcttcttcaatacccattaacagct ctcttttcaaataaaaatc	DHH1, rev; mutagenic primer F62E for Dhh1$^{5X\text{-}Not}$ mutant
CH575	cttaaatacaaagggtaatacttttgaagatttttatttgaa agaagagctgttaatgggtattttt	DHH1, fw; mutagenic primer R55E for Dhh1$^{5X\text{-}Not}$ mutant
CH576	gatttttatttgaaaagagagctgttaatgggtattgaagaa gccggttttgaaaaaccat	DHH1, fw; mutagenic primer F62E for Dhh1$^{5X\text{-}Not}$ mutant

CH577	aaaaatacccattaacagctcttctttcaaataaaaatcttc aaaagtattacccttttgtatttaag	DHH1, rev; mutagenic primer R55E for Dhh1$^{5X\text{-}Not}$ mutant
CH578	cacggttagtagaattacaaaaaataatggcttgctcaatt tcaagcttagagaataaagtatttaaacaatgtagc	DHH1, rev; mutagenic primer Q282E and N284E for Dhh1$^{5X\text{-}Not}$ mutant
CH579	gctacattgtttaaatactttattctctaagcttgaaattgag caagccattatttttgtaattctactaaccgtg	DHH1, fw; mutagenic primer Q282E and N284E for Dhh1$^{5X\text{-}Not}$ mutant
CH580	atcggagcagaccaatgtttcaaccttaccttgacgaaatt cgtgg	DHH1, rev; mutagenic primer R335E for Dhh1$^{5X\text{-}Not}$ mutant
CH581	ccacgaatttcgtcaaggtaaggttgaaacattggtctgctc cgat	DHH1, fw; mutagenic primer R335E for Dhh1$^{5X\text{-}Not}$ mutant
Ch849	atcaaattcccctcttctgatgcttaattgccccgattgcagc ctgttattgatactatt	For stitch PCRs to make Pat1 AA and EE, pringle fw
CH853	taaaaaataagggagaaaaaaaaatacatgcgtaagtac attaaaattacaggaaaaatc gaattcgagctcgtttaaac	For stitch PCRs to make Pat1 AA and EE , pringle rev
CH854	attaccgttgttgaacgcgtaagcagctcttcttctttgctta ga	For stitch PCRs to make Pat1 AA, rev
CH855	tctaagcaaagaagaagagctgcttacgcgttcaacaacg gtaat	For stitch PCRs to make Pat1 AA, fw
CH856	attaccgttgttgaacgcgtattcttctcttcttctttgcttag a	For stitch PCRs to make Pat1 EE, rev

CH857	tct aag caa aga aga aga gaa gaa tac gcg ttc aac aac ggt aat	For stitch PCRs to make Pat1 EE, fw
CH858	ttaattaacccggggatccg ttactttagttctgatatttcaccatcgcgatacaccaacccc ataac	For stitch PCRs to make Pat1 EE, rev
CH944	aacttcttcaagtcctgcttgtcccaggagggttcaggga	For stitch PCRs to make Pat1 4A GFP tagged, fw
CH945	aac ctg aac att atc acc agc agc agc agc gttcaaatagtcgttctc	For stitch PCRs to make Pat1 4A GFP tagged, rev
CH946	gaacgactatttgaac gct gct gct gct ggtgataatgttcaggttgg	For stitch PCRs to make Pat1 4A GFP tagged, fw
CH1035	tttcatggcgatgccacctggtcagtcacaaccccagtat cggatccccgggttaattaa	Dhh1, fw; C-terminal GFP tagging
CH1036	gcgtatctcaccacagtagttatttttcttagatattct gaattcgagctcgtttaaac	Dhh1 rev; C-terminal GFP tagging
CH1037	ttcagggtctaatgaattattaagcattttgcataggaag cggatccccgggttaattaa	Dcp2, fw; C-terminal mcherry tagging
CH1038	catttacagtgtgtctataaaacgtataacacttattcttga attcgagctcgtttaaac	Dcp2, rev; C-terminal mcherry tagging
CH1039	tgatcttttcgtcactgacgggtccctgctattagatttgcgg atccccgggttaattaa	Edc3, C- terminal mcherry, fw
CH1040	tatacgtatgtatccagtttaggctaaagtaattcttggtga attcgagctcgtttaaac	Edc3, C- terminal mcherry, rev

CH1116	gaggagaacgactatttgaac gct gct gct gct ggtgataatgttcaggtt	For stitch PCRs to make Pat1 4A GFP tagged, fw (pringle)
CH1117	aacctgaacattatcacc agc agc agc agc gttcaaatagtcgttctcctc	For stitch PCRs to make Pat1 4A GFP tagged, rev (pringle)
CH1550	ttccccattttatcaaaaatcatcctgccaccattttgtccaa ggatcgcactatcgccc gaattcgagctcgtttaaac	Pgal-Pat1 tagging: fw
CH1551	ttcaaagtccagaggaccatcccgcgcattaccgctattttc taacccaaagaaggacat gcactgagcagcgtaatctg	Pgal-Pat1 tagging: rev
CH1768	aaaataagggagaaaaaaaaatacatgcgtaagtacatt aaaattacaggaaaaatctta gcactgagcagcgtaatctg	K/O Pat1 in Pgal-3HA-Pat1 : rev
CH1879	aaggttttaaccggaagtaagagcagcaagaagcactagc agaacgcggccgccagctgaa	Pat1, fw; C-terminal GFP tagging
CH1878	tacatgcgtaagtacattaaaattacaggaaaaatcttatg aattcgagctcgtttaaac	Pat1, rev; C-terminal GFP tagging
UC1943	ctcttgcgttactatggtggtattattgatgctaatacgggcg cataggccactagtggatc	For pat1 delete, rev
UC1942	aaggttttaaccggaagtaagagcagcaagaagcactagc agaacgcggccgccagctgaa	For pat1 delete,fw
CH2394	ttccccattttatcaaaaatcatcctgccaccattttgtccaa ggatcgcactatcgccctcactatagggagaccggca	Pgal-Pat1 tagging: fw
CH2395	ttcaaagtccagaggaccatcccgcgcattaccgctattttc taacccaaagaaggacat cattttgagatccgggtttt	Pgal-Pat1 tagging: rev

CH2762	gggttagaaaatagcggtaatgcgcgggatggtcctctgg	For stitch PCRs to make Pat1 NC, fw
CH2768	tcgcttatttagaagtggcgcgttacttaagctcgagcataa cgtttaggaa	For stitch PCRs to make Pat1 NC, rev
CH2769	cgttatgctcgagcttaagtaacgcgccacttctaaataag cgaatttctta	For stitch PCRs to make Pat1 NC, fw
CH2790	ttaaagccttcgagcgtcccaaaaccttctcaagcaaggttt tcagtataat	For stitch PCRs to make Pat1 NC, rev
CH2791	taaaaaataagggagaaaaaaaaatacatgcgtaagtac attaaaattacaggaaaaatcttaaagccttcgagcgtccc aa	For stitch PCRs to make Pat1 NC, rev
CH2766	gacgtcccggactatgcaggatcctatccatatgacgttcc agattacgctgctcagtgcgggttagaaaatagcggtaa	For Pat1 NC HYG (pgal OE), fw
CH3005	gtacaccttgaaggaagcaaaggttttaaccggaagtaag agcagcaagaagcactagca gggttagaaaatagcggtaa	For stitch PCRs to make Pat1 NC, fw
CH3054	gggttagaaaatagcggtaatgcgcgggatggtcctctgg	For stitch PCRs to make Pat1 NC GFP tagged, fw
CH3060	catgttaattaacccggggatccgcttaagctcgagcataa cgtttaggaac	For stitch PCRs to make Pat1 NC GFP tagged, rev
CH3061	gttcctaaacgttatgctcgagcttaagcggatccccgggtt aattaacatg	For stitch PCRs to make Pat1 NC GFP tagged, fw
Ch3062	gaattcgagctcgtttaaactggatggcggcgttagtatcg aatcgacagca	For stitch PCRs to make Pat1 NC GFP tagged, rev

CH3058	gtacaccttgaaggaagcaaaggttttaaccggaagtaagagcagcaagaagcactagcagggttagaaaatagcggtaa	For stitch PCRs to make Pat1 NC GFP tagged, fw (pringle)
CH3063	taaaaaataagggagaaaaaaaaatacatgcgtaagtacattaaaattacaggaaaaatcgaattcgagctcgtttaaact	For stitch PCRs to make Pat1 NC GFP tagged, rev (pringle)
CH4227	cgccattcgcataataacttatcccaggcctaaaatacgacaagaaagaaaatagtagtaatgggttccatcaataataa	For stitch PCRs to make Dhh1^{S292DN294D}(Mut3A)-GFP and Dhh1^{R295D}(Mut3A)-GFP tagged, fw (pringle)
CH4228	ttttcttggctagtaattcgacatcgttagtagaattacaaaaaa	For stitch PCRs to make Dhh1^{R295D} Dhh1^{R295D}(Mut3A)-GFP, Dhh1^{R295D}(Mut3A)-GFP tagged,rev
CH4229	ttttttgtaattctactaacgatgtcgaattactagccaagaaaa	For stitch PCRs to make Dhh1^{S292DN294D}(Mut3A)-GFP and Dhh1^{R295D}(Mut3A)-GFP tagged,rev
CH4231	acgattagatcacaaaaaaagcgtatctcaccacagtagtttattttttcttagatattctgaattcgagctcgtttaaac	For stitch PCRs to make Dhh1^{S292DN294D}(Mut3A)-GFP, Dhh1^{R295D}(Mut3A)-GFP tagged,rev (pringle)
CH4232	ttttcttggctagtaattcgacacgatcagtatcattacaaaaaataatggcttgat	For stitch PCRs to make Dhh1^{S292DN294D}(Mut3A)-GFP tagged, rev
CH4233	atcaagccattatttttgtaatgatactgatcgtgtcgaattactagccaagaaaa	For stitch PCRs to make Dhh1^{S292DN294D}(Mut3A)-GFP tagged, fw

CH4234	ttaattaacccggggatccgatactggggttgtgactgacc aggtggcatcgccatgaaatgttc	For stitch PCRs to make Dhh1^{S292DN294D}(Mut3A)-GFP and Dhh1^{R295D}(Mut3A)-GFP tagged, rev
US5021	ttcgtacattggtctgcgccgatttattgacccgt	DHH1, fw; mutagenic primer S340A for Dhh1$^{3X\text{-}RNA}$ mutant
US5022	acgggtcaataaatcggcgcagaccaatgtacgaa	DHH1, rev; mutagenic primer S340A for Dhh1$^{3X\text{-}RNA}$ mutant
US5023	ccaaaacggcagaaacatatttacatgctattggtagatcc ggtagg	DHH1, fw; mutagenic primer R370A for Dhh1$^{3X\text{-}RNA}$ mutant
US5024	cctaccggatctaccaatagcatgtaaatatgtttctgccgt tttgg	DHH1, rev; mutagenic primer R370A for Dhh1$^{3X\text{-}RNA}$ mutant
UC6097	atcccaggcctaaaatacgacaagaaagaaaatagtagt a*atgggttccatcaataataa*	DHH1; fw; For integrating *DHH1* mutants into *dhh1Δ* strains
UC6098	tatctcaccacagtagttatttttcttagatattct*ttaatac tggggttgtgactgac*	DHH1; rv; For integrating *DHH1* mutants into *dhh1Δ* strains

References

Aguzzi, A., & Altmeyer, M. (2016). Phase Separation: Linking Cellular Compartmentalization to Disease. *Trends Cell Biol, 26*(7), 547-558. doi:10.1016/j.tcb.2016.03.004

Alberti, S., & Hyman, A. A. (2016). Are aberrant phase transitions a driver of cellular aging? *Bioessays, 38*(10), 959-968. doi:10.1002/bies.201600042

Ashe, M. P., De Long, S. K., & Sachs, A. B. (2000). Glucose depletion rapidly inhibits translation initiation in yeast. *Mol Biol Cell, 11*(3), 833-848. doi:10.1091/mbc.11.3.833

874 Barbee, S. A., Estes, P. S., Cziko, A. M., Hillebrand, J., Luedeman, R. A., Coller, J. M., . . . Ramaswami, M.
875 (2006). Staufen- and FMRP-containing neuronal RNPs are structurally and functionally related to
876 somatic P bodies. *Neuron, 52*(6), 997-1009. doi:10.1016/j.neuron.2006.10.028

877 Beelman, C. A., & Parker, R. (1994). Differential effects of translational inhibition in cis and in trans on
878 the decay of the unstable yeast MFA2 mRNA. *J Biol Chem, 269*(13), 9687-9692.

879 Bhattacharyya, S. N., Habermacher, R., Martine, U., Closs, E. I., & Filipowicz, W. (2006). Relief of
880 microRNA-mediated translational repression in human cells subjected to stress. *Cell, 125*(6), 1111-
881 1124. doi:10.1016/j.cell.2006.04.031

882 Bordeleau, M. E., Mori, A., Oberer, M., Lindqvist, L., Chard, L. S., Higa, T., . . . Pelletier, J. (2006).
883 Functional characterization of IRESes by an inhibitor of the RNA helicase eIF4A. *Nat Chem Biol, 2*(4),
884 213-220. doi:10.1038/nchembio776

885 Braun, K. A., Vaga, S., Dombek, K. M., Fang, F., Palmisano, S., Aebersold, R., & Young, E. T. (2014).
886 Phosphoproteomic analysis identifies proteins involved in transcription-coupled mRNA decay as
887 targets of Snf1 signaling. *Sci Signal, 7*(333), ra64. doi:10.1126/scisignal.2005000

888 Carroll, J. S., Munchel, S. E., & Weis, K. (2011). The DExD/H box ATPase Dhh1 functions in translational
889 repression, mRNA decay, and processing body dynamics. *J Cell Biol, 194*(4), 527-537.
890 doi:10.1083/jcb.201007151

891 Chan, L. Y., Mugler, C. F., Heinrich, S., Vallotton, P., & Weis, K. (2018). Non-invasive measurement of
892 mRNA decay reveals translation initiation as the major determinant of mRNA stability. *Elife. In press.*

893 Chowdhury, A., Kalurupalle, S., & Tharun, S. (2014). Pat1 contributes to the RNA binding activity of the
894 Lsm1-7-Pat1 complex. *Rna, 20*(9), 1465-1475. doi:10.1261/rna.045252.114

895 Coller, J. M., Tucker, M., Sheth, U., Valencia-Sanchez, M. A., & Parker, R. (2001). The DEAD box helicase,
896 Dhh1p, functions in mRNA decapping and interacts with both the decapping and deadenylase
897 complexes. *Rna, 7*(12), 1717-1727.

898 Coller, J., & Parker, R. (2004). Eukaryotic mRNA decapping. *Annu Rev Biochem, 73*, 861-890.
899 doi:10.1146/annurev.biochem.73.011303.074032

900 Coller, J., & Parker, R. (2005). General translational repression by activators of mRNA decapping. *Cell,*
901 *122*(6), 875-886. doi:10.1016/j.cell.2005.07.012

902 Charenton, C., Gaudon-Plesse, C., Fourati, Z., Taverniti, V., Back, R., Kolesnikova, O., . . . Graille, M.
903 (2017). A unique surface on Pat1 C-terminal domain directly interacts with Dcp2 decapping enzyme
904 and Xrn1 5'-3' mRNA exonuclease in yeast. *Proc Natl Acad Sci U S A, 114*(45), E9493-e9501.
905 doi:10.1073/pnas.1711680114

906 Cougot, N., Bhattacharyya, S. N., Tapia-Arancibia, L., Bordonne, R., Filipowicz, W., Bertrand, E., & Rage,
907 F. (2008). Dendrites of mammalian neurons contain specialized P-body-like structures that respond to
908 neuronal activation. *J Neurosci, 28*(51), 13793-13804. doi:10.1523/jneurosci.4155-08.2008

909 Decker, C. J., Teixeira, D., & Parker, R. (2007). Edc3p and a glutamine/asparagine-rich domain of Lsm4p
910 function in processing body assembly in Saccharomyces cerevisiae. *J Cell Biol, 179*(3), 437-449.
911 doi:10.1083/jcb.200704147

912 Ernoult-Lange, M., Baconnais, S., Harper, M., Minshall, N., Souquere, S., Boudier, T., . . . Weil, D. (2012).
913 Multiple binding of repressed mRNAs by the P-body protein Rck/p54. *Rna, 18*(9), 1702-1715.
914 doi:10.1261/rna.034314.112

915 Fischer, N., & Weis, K. (2002). The DEAD box protein Dhh1 stimulates the decapping enzyme Dcp1.
916 *Embo j, 21*(11), 2788-2797. doi:10.1093/emboj/21.11.2788

917 Fourati, Z., Kolesnikova, O., Back, R., Keller, J., Charenton, C., Taverniti, V., . . . Graille, M. (2014). The
918 C-terminal domain from S. cerevisiae Pat1 displays two conserved regions involved in decapping factor
919 recruitment. *PLoS One, 9*(5), e96828. doi:10.1371/journal.pone.0096828

920 Franks, T. M., & Lykke-Andersen, J. (2008). The control of mRNA decapping and P-body formation. *Mol*
921 *Cell, 32*(5), 605-615. doi:10.1016/j.molcel.2008.11.001

922 Fromm, S. A., Kamenz, J., Noldeke, E. R., Neu, A., Zocher, G., & Sprangers, R. (2014). In vitro
923 reconstitution of a cellular phase-transition process that involves the mRNA decapping machinery.
924 *Angew Chem Int Ed Engl, 53*(28), 7354-7359. doi:10.1002/anie.201402885

925 Fromm, S. A., Truffault, V., Kamenz, J., Braun, J. E., Hoffmann, N. A., Izaurralde, E., & Sprangers, R.
926 (2012). The structural basis of Edc3- and Scd6-mediated activation of the Dcp1:Dcp2 mRNA decapping
927 complex. *Embo j, 31*(2), 279-290. doi:10.1038/emboj.2011.408

928 Guo, L., & Shorter, J. (2015). It's Raining Liquids: RNA Tunes Viscoelasticity and Dynamics of
929 Membraneless Organelles. *Mol Cell, 60*(2), 189-192. doi:10.1016/j.molcel.2015.10.006

930 Hadjidemetriou, S., Gabrielli, B., Pike, T., Stevens, F., Mele, K., & Vallotton, P. (2014). *Detection and*
931 *Tracking of Cell Divisions in Phase Contrast Video Microscopy*. Paper presented at the Third MICCAI
932 Worshop on Microscopic Image Analysis with Applications in Biology.

933 Holmes, L. E., Campbell, S. G., De Long, S. K., Sachs, A. B., & Ashe, M. P. (2004). Loss of translational
934 control in yeast compromised for the major mRNA decay pathway. *Mol Cell Biol, 24*(7), 2998-3010.

935 Hu, W., Sweet, T. J., Chamnongpol, S., Baker, K. E., & Coller, J. (2009). Co-translational mRNA decay in
936 Saccharomyces cerevisiae. *Nature, 461*(7261), 225-229. doi:10.1038/nature08265

937 Hyman, A. A., Weber, C. A., & Julicher, F. (2014). Liquid-liquid phase separation in biology. *Annu Rev*
938 *Cell Dev Biol, 30*, 39-58. doi:10.1146/annurev-cellbio-100913-013325

939 Kroschwald, S., Maharana, S., Mateju, D., Malinovska, L., Nuske, E., Poser, I., . . . Alberti, S. (2015).
940 Promiscuous interactions and protein disaggregases determine the material state of stress-inducible
941 RNP granules. *Elife, 4*, e06807. doi:10.7554/eLife.06807

942 Larimer, F. W., & Stevens, A. (1990). Disruption of the gene XRN1, coding for a 5'----3' exoribonuclease,
943 restricts yeast cell growth. *Gene, 95*(1), 85-90.

944 Longtine, M. S., McKenzie, A., 3rd, Demarini, D. J., Shah, N. G., Wach, A., Brachat, A., . . . Pringle, J. R.
945 (1998). Additional modules for versatile and economical PCR-based gene deletion and modification in

946 Saccharomyces cerevisiae. *Yeast, 14*(10), 953-961. doi:10.1002/(sici)1097-
947 0061(199807)14:10<953::Aid-yea293>3.0.Co;2-u

948 Lui, J., Castelli, L. M., Pizzinga, M., Simpson, C. E., Hoyle, N. P., Bailey, K. L., . . . Ashe, M. P. (2014).
949 Granules harboring translationally active mRNAs provide a platform for P-body formation following
950 stress. *Cell Rep, 9*(3), 944-954. doi:10.1016/j.celrep.2014.09.040

951 Mager, W. H., & Ferreira, P. M. (1993). Stress response of yeast. *Biochem J, 290 (Pt 1)*, 1-13.

952 Montpetit, B., Thomsen, N. D., Helmke, K. J., Seeliger, M. A., Berger, J. M., & Weis, K. (2011). A
953 conserved mechanism of DEAD-box ATPase activation by nucleoporins and InsP6 in mRNA export.
954 *Nature, 472*(7342), 238-242. doi:10.1038/nature09862

955 Mugler, C. F., Hondele, M., Heinrich, S., Sachdev, R., Vallotton, P., Koek, A. Y., . . . Weis, K. (2016).
956 ATPase activity of the DEAD-box protein Dhh1 controls processing body formation. *Elife, 5*.
957 doi:10.7554/eLife.18746

958 Muhlrad, D., & Parker, R. (1992). Mutations affecting stability and deadenylation of the yeast MFA2
959 transcript. *Genes Dev, 6*(11), 2100-2111.

960 Nissan, T., Rajyaguru, P., She, M., Song, H., & Parker, R. (2010). Decapping activators in Saccharomyces
961 cerevisiae act by multiple mechanisms. *Mol Cell, 39*(5), 773-783. doi:10.1016/j.molcel.2010.08.025

962 Ozgur, S., & Stoecklin, G. (2013). Role of Rck-Pat1b binding in assembly of processing-bodies. *RNA Biol,*
963 *10*(4), 528-539. doi:10.4161/rna.24086

964 Patel, A., Lee, H. O., Jawerth, L., Maharana, S., Jahnel, M., Hein, M. Y., . . . Alberti, S. (2015). A Liquid-
965 to-Solid Phase Transition of the ALS Protein FUS Accelerated by Disease Mutation. *Cell, 162*(5), 1066-
966 1077. doi:10.1016/j.cell.2015.07.047

967 Pilkington, G. R., & Parker, R. (2008). Pat1 contains distinct functional domains that promote P-body
968 assembly and activation of decapping. *Mol Cell Biol, 28*(4), 1298-1312. doi:10.1128/mcb.00936-07

969 Pillai, R. S. (2005). MicroRNA function: multiple mechanisms for a tiny RNA? *Rna, 11*(12), 1753-1761.
970 doi:10.1261/rna.2248605

971 Protter, D. S. W., Rao, B. S., Van Treeck, B., Lin, Y., Mizoue, L., Rosen, M. K., & Parker, R. (2018).
972 Intrinsically Disordered Regions Can Contribute Promiscuous Interactions to RNP Granule Assembly.
973 *Cell Rep, 22*(6), 1401-1412. doi:10.1016/j.celrep.2018.01.036

974 Radhakrishnan, A., Chen, Y. H., Martin, S., Alhusaini, N., Green, R., & Coller, J. (2016). The DEAD-Box
975 Protein Dhh1p Couples mRNA Decay and Translation by Monitoring Codon Optimality. *Cell, 167*(1),
976 122-132.e129. doi:10.1016/j.cell.2016.08.053

977 Ramachandran, V., Shah, K. H., & Herman, P. K. (2011). The cAMP-dependent protein kinase signaling
978 pathway is a key regulator of P body foci formation. *Mol Cell, 43*(6), 973-981.
979 doi:10.1016/j.molcel.2011.06.032

980 Ramaswami, M., Taylor, J. P., & Parker, R. (2013). Altered ribostasis: RNA-protein granules in
981 degenerative disorders. *Cell, 154*(4), 727-736. doi:10.1016/j.cell.2013.07.038

982 Rao, B. S., & Parker, R. (2017). Numerous interactions act redundantly to assemble a tunable size of P
983 bodies in Saccharomyces cerevisiae. *Proc Natl Acad Sci U S A, 114*(45), E9569-e9578.
984 doi:10.1073/pnas.1712396114

985 Scheller, N., Resa-Infante, P., de la Luna, S., Galao, R. P., Albrecht, M., Kaestner, L., . . . Diez, J. (2007).
986 Identification of PatL1, a human homolog to yeast P body component Pat1. *Biochim Biophys Acta,*
987 *1773*(12), 1786-1792. doi:10.1016/j.bbamcr.2007.08.009

988 Schwartz, D. C., & Parker, R. (1999). Mutations in translation initiation factors lead to increased rates
989 of deadenylation and decapping of mRNAs in Saccharomyces cerevisiae. *Mol Cell Biol, 19*(8), 5247-
990 5256.

991 Schwartz, D. C., & Parker, R. (2000). mRNA decapping in yeast requires dissociation of the cap binding
992 protein, eukaryotic translation initiation factor 4E. *Mol Cell Biol, 20*(21), 7933-7942.

993 Seydoux, G., & Braun, R. E. (2006). Pathway to totipotency: lessons from germ cells. *Cell, 127*(5), 891-
994 904. doi:10.1016/j.cell.2006.11.016

995 Shah, K. H., Zhang, B., Ramachandran, V., & Herman, P. K. (2013). Processing body and stress granule
996 assembly occur by independent and differentially regulated pathways in Saccharomyces cerevisiae.
997 *Genetics, 193*(1), 109-123. doi:10.1534/genetics.112.146993

998 Sharif, H., Ozgur, S., Sharma, K., Basquin, C., Urlaub, H., & Conti, E. (2013). Structural analysis of the
999 yeast Dhh1-Pat1 complex reveals how Dhh1 engages Pat1, Edc3 and RNA in mutually exclusive
1000 interactions. *Nucleic Acids Res, 41*(17), 8377-8390. doi:10.1093/nar/gkt600

1001 Sheth, U., & Parker, R. (2003). Decapping and decay of messenger RNA occur in cytoplasmic processing
1002 bodies. *Science, 300*(5620), 805-808. doi:10.1126/science.1082320

1003 Sun, M., Schwalb, B., Schulz, D., Pirkl, N., Etzold, S., Lariviere, L., . . . Cramer, P. (2012). Comparative
1004 dynamic transcriptome analysis (cDTA) reveals mutual feedback between mRNA synthesis and
1005 degradation. *Genome Res, 22*(7), 1350-1359. doi:10.1101/gr.130161.111

1006 Teixeira, D., Sheth, U., Valencia-Sanchez, M. A., Brengues, M., & Parker, R. (2005). Processing bodies
1007 require RNA for assembly and contain nontranslating mRNAs. *Rna, 11*(4), 371-382.
1008 doi:10.1261/rna.7258505

1009 Tucker, M., Staples, R. R., Valencia-Sanchez, M. A., Muhlrad, D., & Parker, R. (2002). Ccr4p is the
1010 catalytic subunit of a Ccr4p/Pop2p/Notp mRNA deadenylase complex in Saccharomyces cerevisiae.
1011 *Embo j, 21*(6), 1427-1436. doi:10.1093/emboj/21.6.1427

1012 Vallotton, P., van Oijen, A. M., Whitchurch, C. B., Gelfand, V., Yeo, L., Tsiavaliaris, G., . . . Grunwald, D.
1013 (2017). Diatrack particle tracking software: Review of applications and performance evaluation. *Traffic,*
1014 *18*(12), 840-852. doi:10.1111/tra.12530

1015

Figure 1

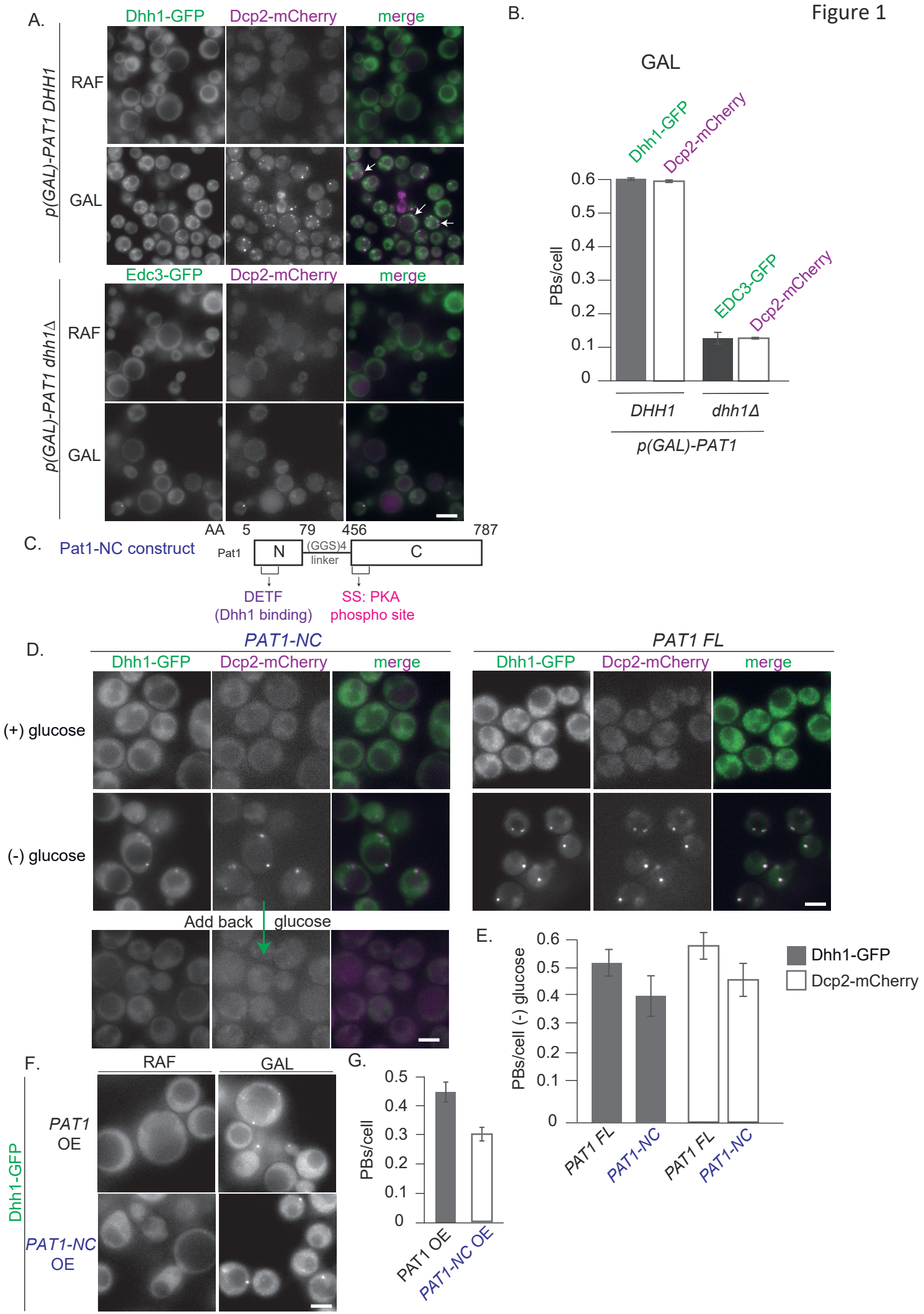
A.
Dhh1-GFP
Dcp2-mCherry
merge
p(GAL)-PAT1 DHH1
RAF
GAL
Edc3-GFP
Dcp2-mCherry
merge
p(GAL)-PAT1 dhh1Δ
RAF
GAL
B.
GAL
Dhh1-GFP
Dcp2-mCherry
EDC3-GFP
Dcp2-mCherry
PBs/cell
0.6
0.5
0.4
0.3
0.2
0.1
0
DHH1
dhh1Δ
p(GAL)-PAT1
C.
Pat1-NC construct
AA 5 79 456 787
Pat1
N
(GGS)4
linker
C
DETF
(Dhh1 binding)
SS: PKA
phospho site
D.
PAT1-NC
PAT1 FL
Dhh1-GFP
Dcp2-mCherry
merge
(+) glucose
(-) glucose
Add back glucose
E.
PBs/cell (-) glucose
0.6
0.5
0.4
0.3
0.2
0.1
0
Dhh1-GFP
Dcp2-mCherry
PAT1 FL
PAT1-NC
PAT1 FL
PAT1-NC
F.
RAF
GAL
Dhh1-GFP
PAT1 OE
PAT1-NC OE
G.
PBs/cell
0.5
0.4
0.3
0.2
0.1
0
PAT1 OE
PAT1-NC OE

Figure 2

A.

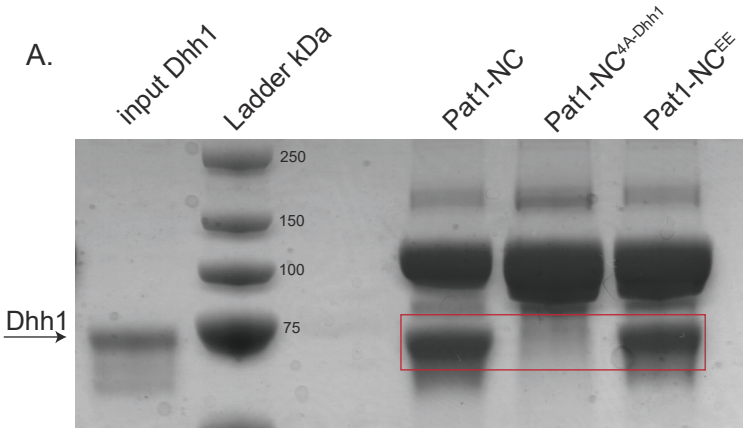

B.

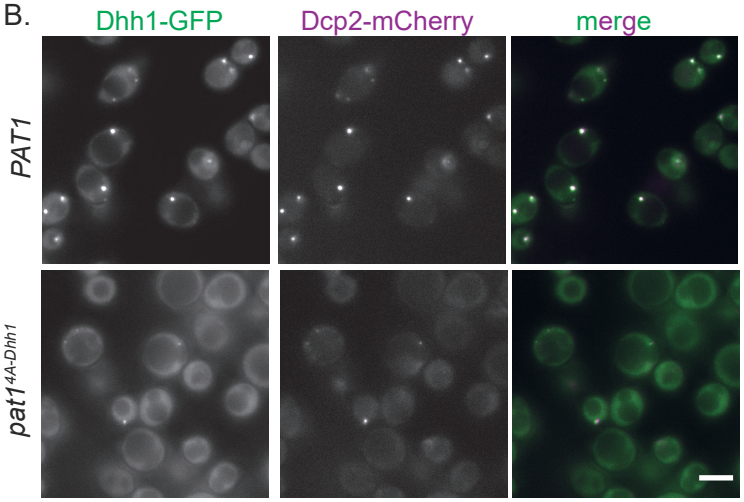

D.

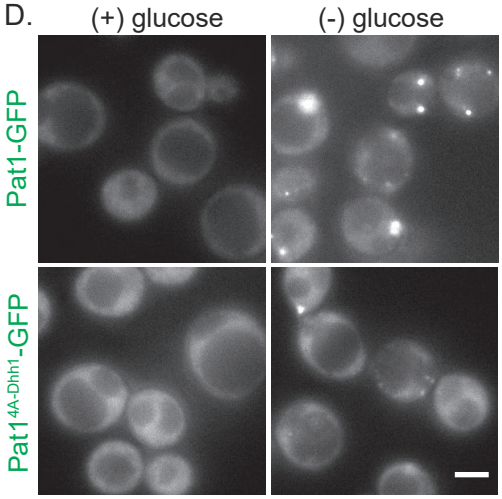

E.

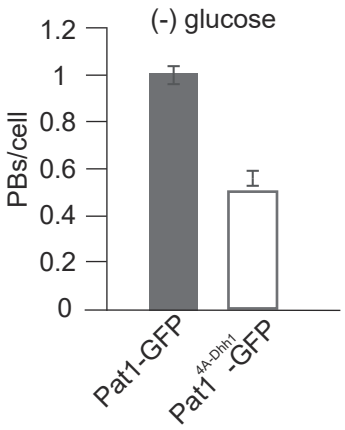

C.

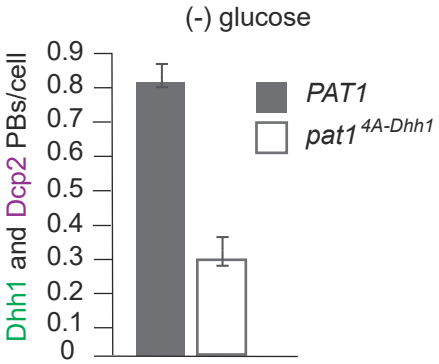

F.

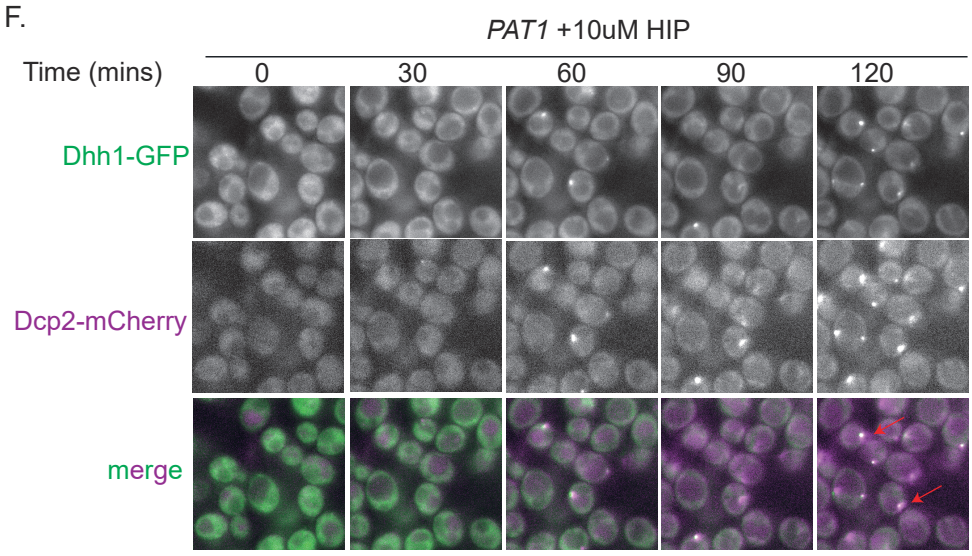

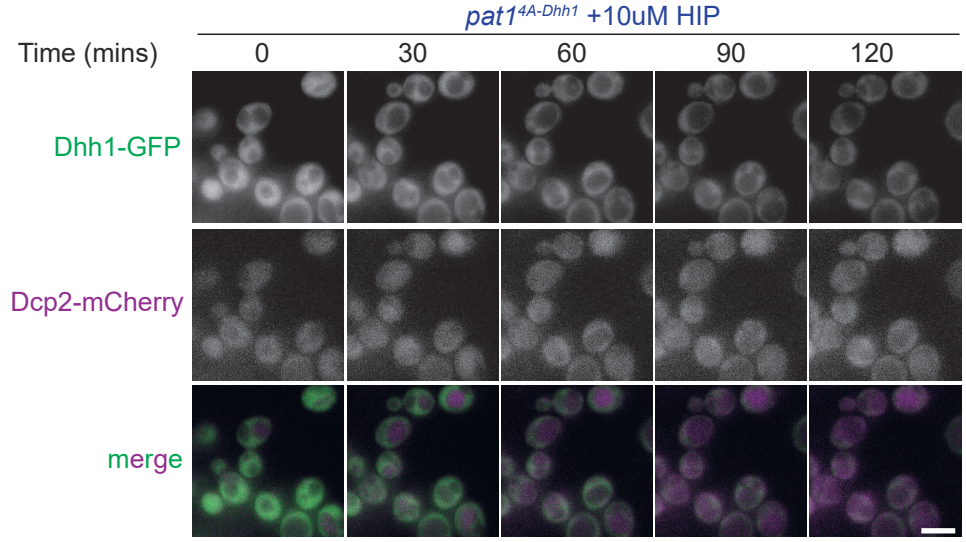

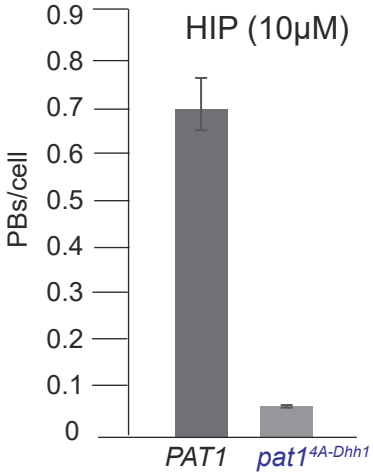

Figure 3

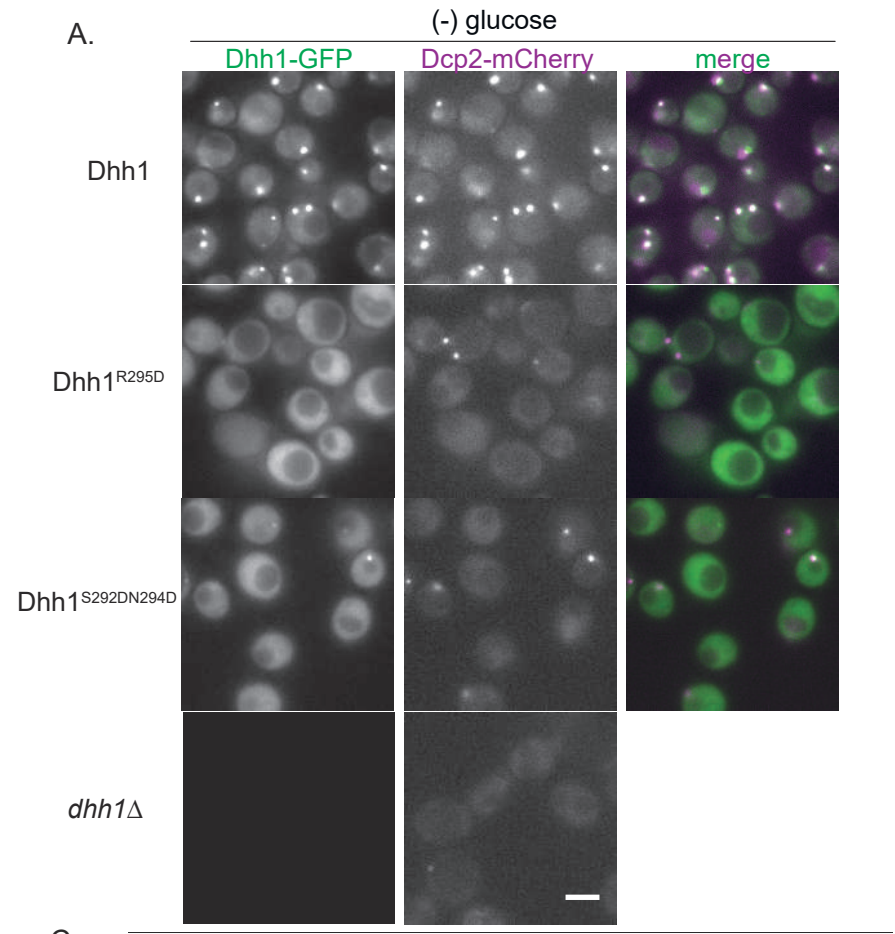
A.
(-) glucose
Dhh1-GFP
Dcp2-mCherry
merge
Dhh1
Dhh1R295D
Dhh1S292DN294D
dhh1Δ

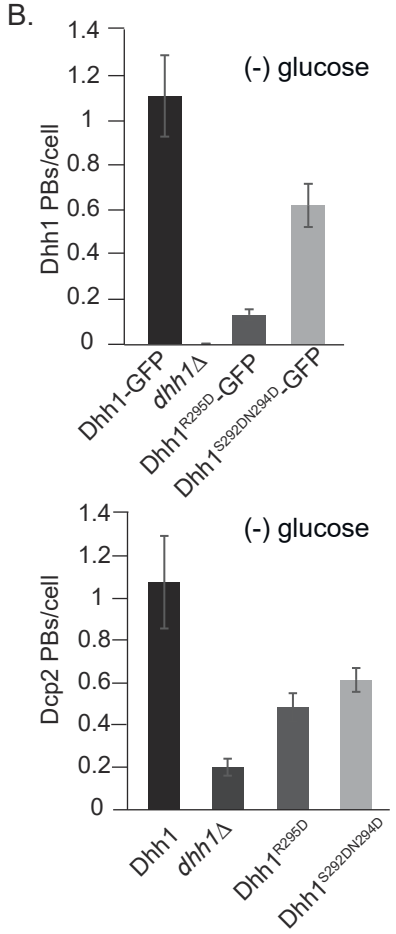
B.
(-) glucose
Dhh1 PBs/cell
1.4
1.2
1
0.8
0.6
0.4
0.2
0
Dhh1-GFP
dhh1Δ
Dhh1R295D-GFP
Dhh1S292DN294D-GFP
(-) glucose
Dcp2 PBs/cell
Dhh1
dhh1Δ
Dhh1R295D
Dhh1S292DN294D

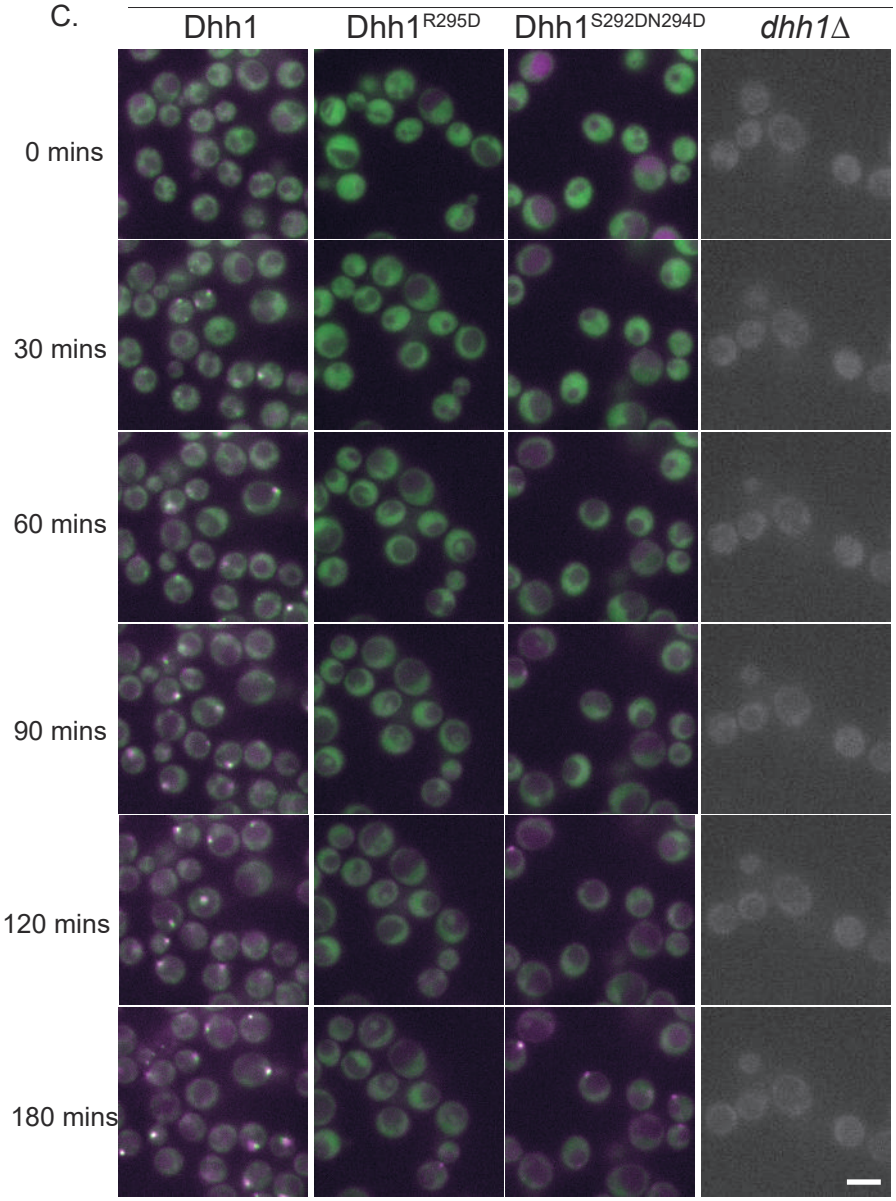
C.
Dhh1
Dhh1R295D
Dhh1S292DN294D
dhh1Δ
0 mins
30 mins
60 mins
90 mins
120 mins
180 mins

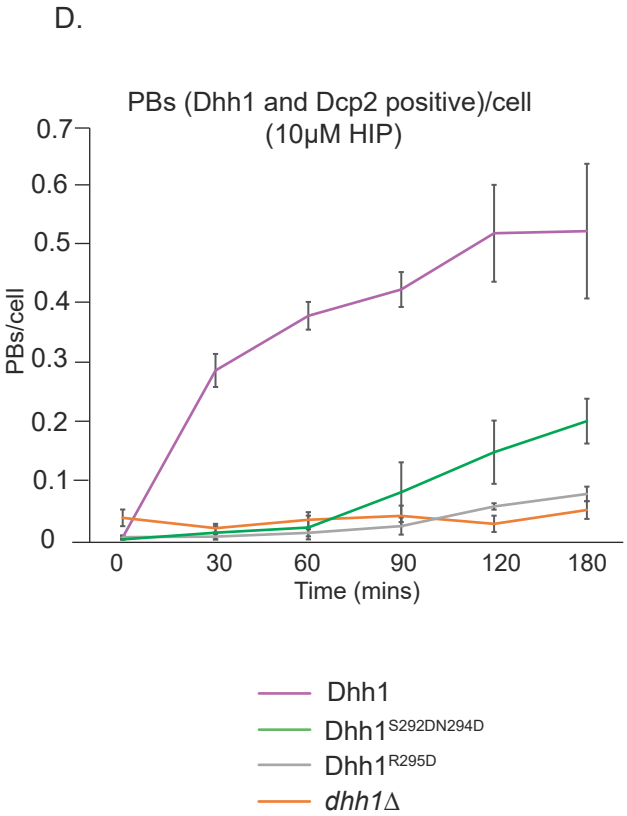
D.
PBs (Dhh1 and Dcp2 positive)/cell
(10μM HIP)
PBs/cell
0.7
0.6
0.5
0.4
0.3
0.2
0.1
0
0
30
60
90
120
180
Time (mins)
Dhh1
Dhh1S292DN294D
Dhh1R295D
dhh1Δ

Figure 4

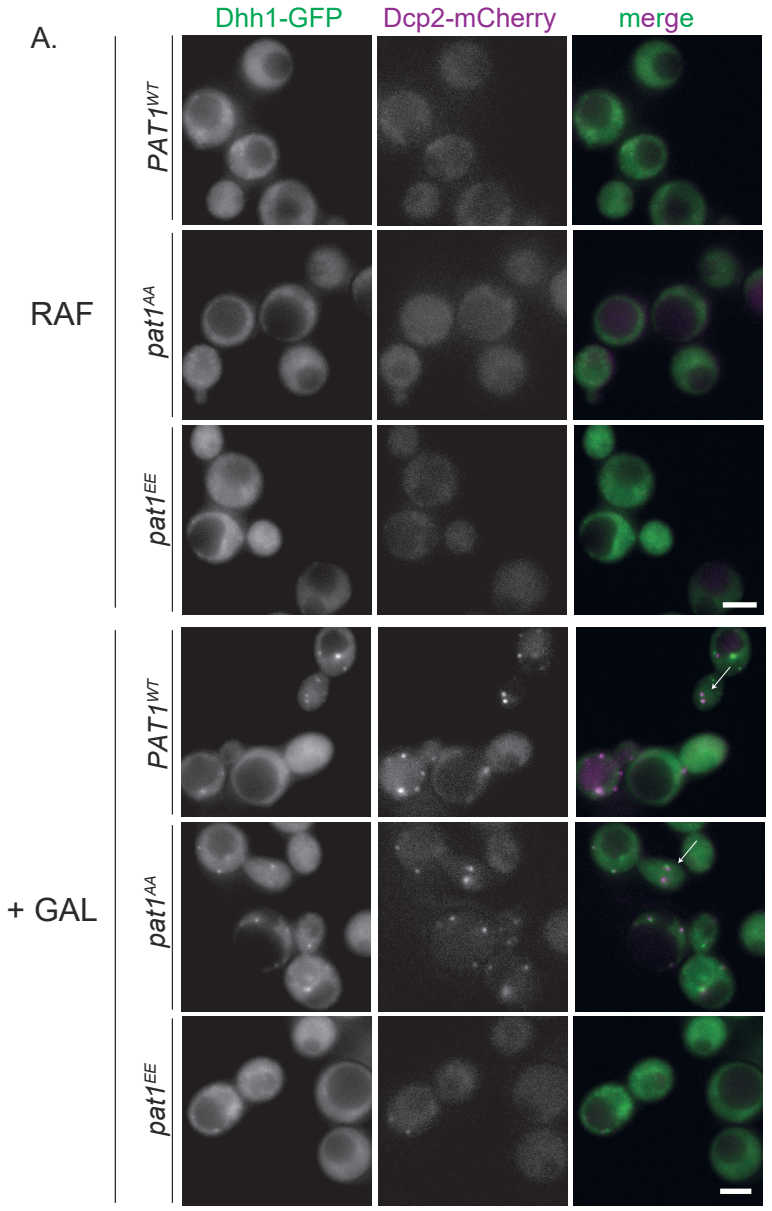
A.
Dhh1-GFP
Dcp2-mCherry
merge
RAF
+ GAL
PAT1WT
pat1AA
pat1EE

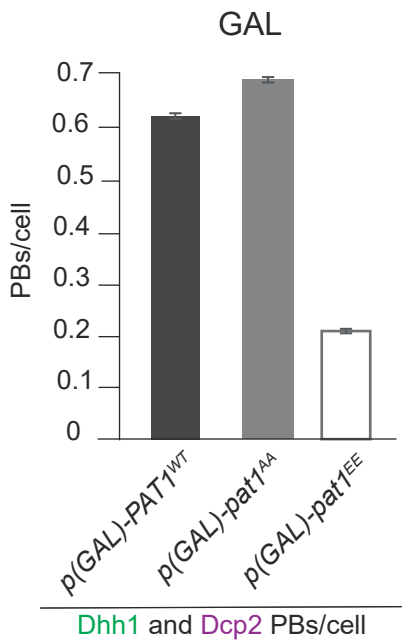
B.
GAL
PBs/cell
0.7
0.6
0.5
0.4
0.3
0.2
0.1
0
p(GAL)-PAT1WT
p(GAL)-pat1AA
p(GAL)-pat1EE
Dhh1 and Dcp2 PBs/cell

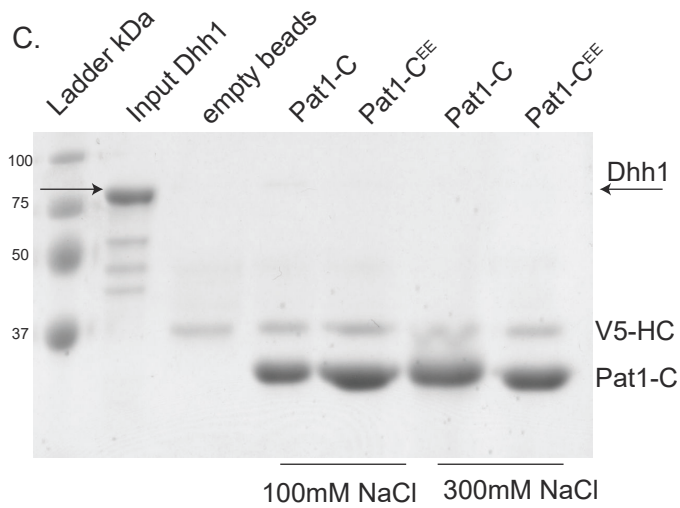
C.
Ladder kDa
Input Dhh1
empty beads
Pat1-C
Pat1-CEE
Pat1-C
Pat1-CEE
100
75
50
37
Dhh1
V5-HC
Pat1-C
100mM NaCl
300mM NaCl

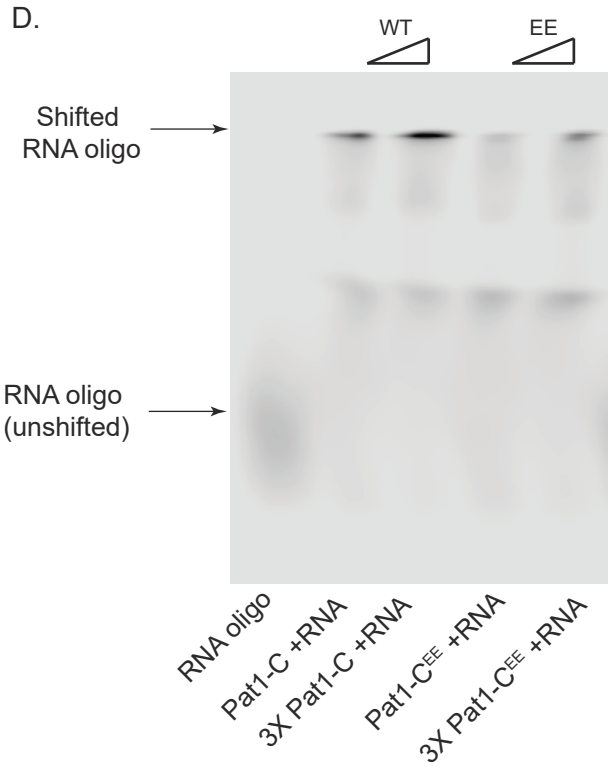
D.
WT
EE
Shifted RNA oligo
RNA oligo (unshifted)
RNA oligo
Pat1-C +RNA
3X Pat1-C +RNA
Pat1-CEE +RNA
3X Pat1-CEE +RNA

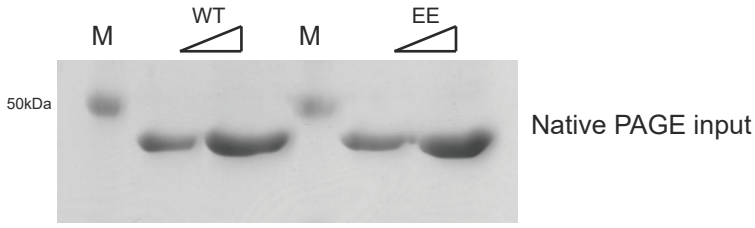
M
WT
M
EE
50kDa
Native PAGE input

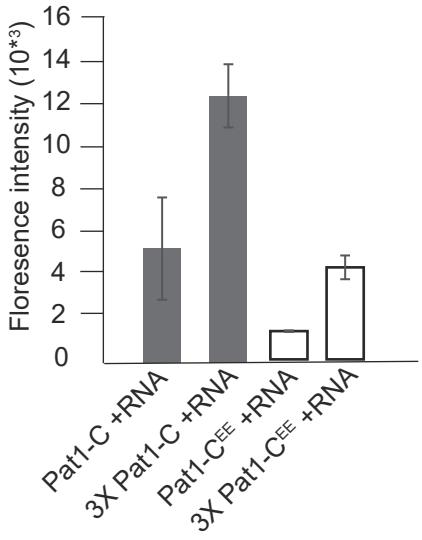
Floresence intensity (10*3)
16
14
12
10
8
6
4
2
0
Pat1-C +RNA
3X Pat1-C +RNA
Pat1-CEE +RNA
3X Pat1-CEE +RNA

Figure 5

A.

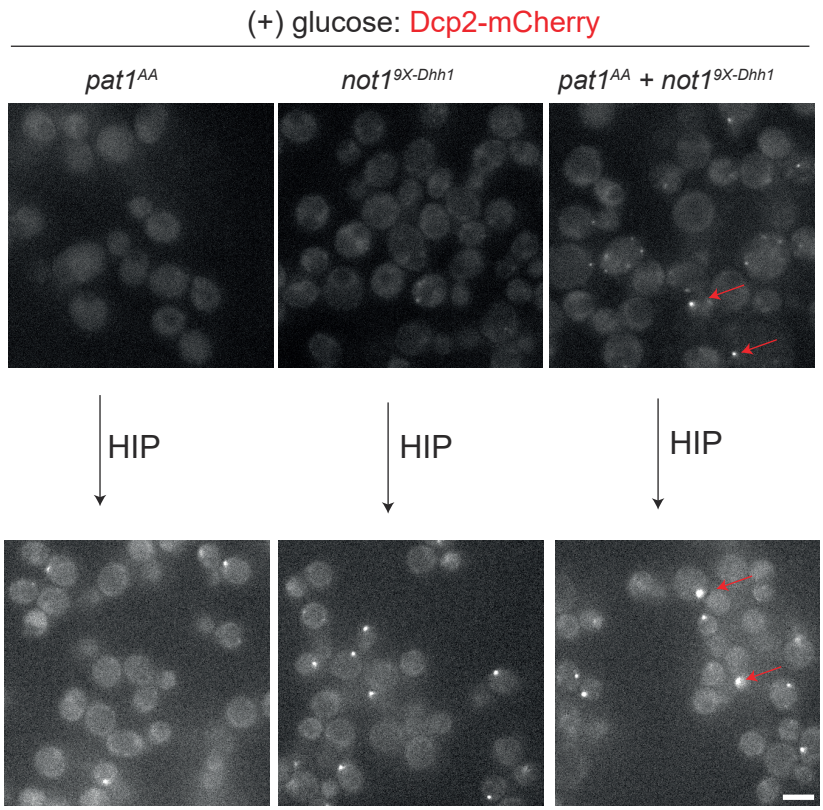
(+) glucose: Dcp2-mCherry
pat1AA
not19X-Dhh1
pat1AA + not19X-Dhh1
HIP
HIP
HIP

B.

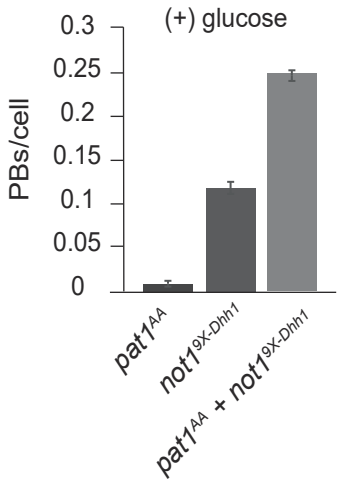
(+) glucose
PBs/cell
0.3
0.25
0.2
0.15
0.1
0.05
0
pat1AA
not19X-Dhh1
pat1AA + not19X-Dhh1

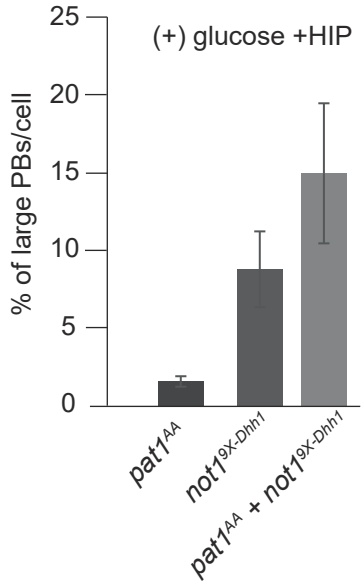
(+) glucose +HIP
% of large PBs/cell
25
20
15
10
5
0
pat1AA
not19X-Dhh1
pat1AA + not19X-Dhh1

Figure 6

A.

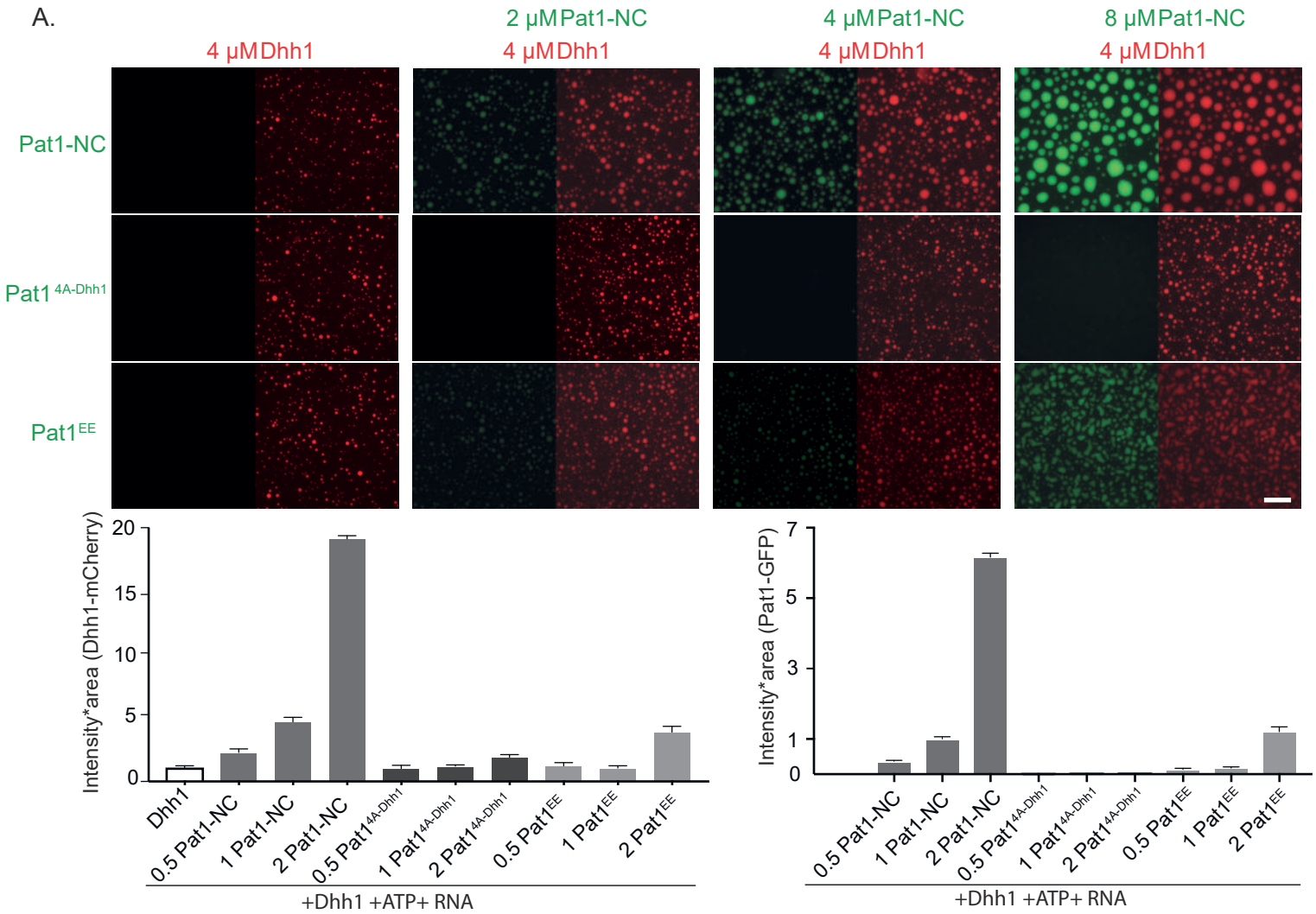
4 μM Dhh1
2 μM Pat1-NC
4 μM Dhh1
4 μM Pat1-NC
4 μM Dhh1
8 μM Pat1-NC
4 μM Dhh1
Pat1-NC
Pat1 4A-Dhh1
Pat1 EE
Intensity*area (Dhh1-mCherry)
Dhh1
0.5 Pat1-NC
1 Pat1-NC
2 Pat1-NC
0.5 Pat1 4A-Dhh1
1 Pat1 4A-Dhh1
2 Pat1 4A-Dhh1
0.5 Pat1 EE
1 Pat1 EE
2 Pat1 EE
+Dhh1 +ATP+ RNA
Intensity*area (Pat1-GFP)
0.5 Pat1-NC
1 Pat1-NC
2 Pat1-NC
0.5 Pat1 4A-Dhh1
1 Pat1 4A-Dhh1
2 Pat1 4A-Dhh1
0.5 Pat1 EE
1 Pat1 EE
2 Pat1 EE
+Dhh1 +ATP+ RNA

B.

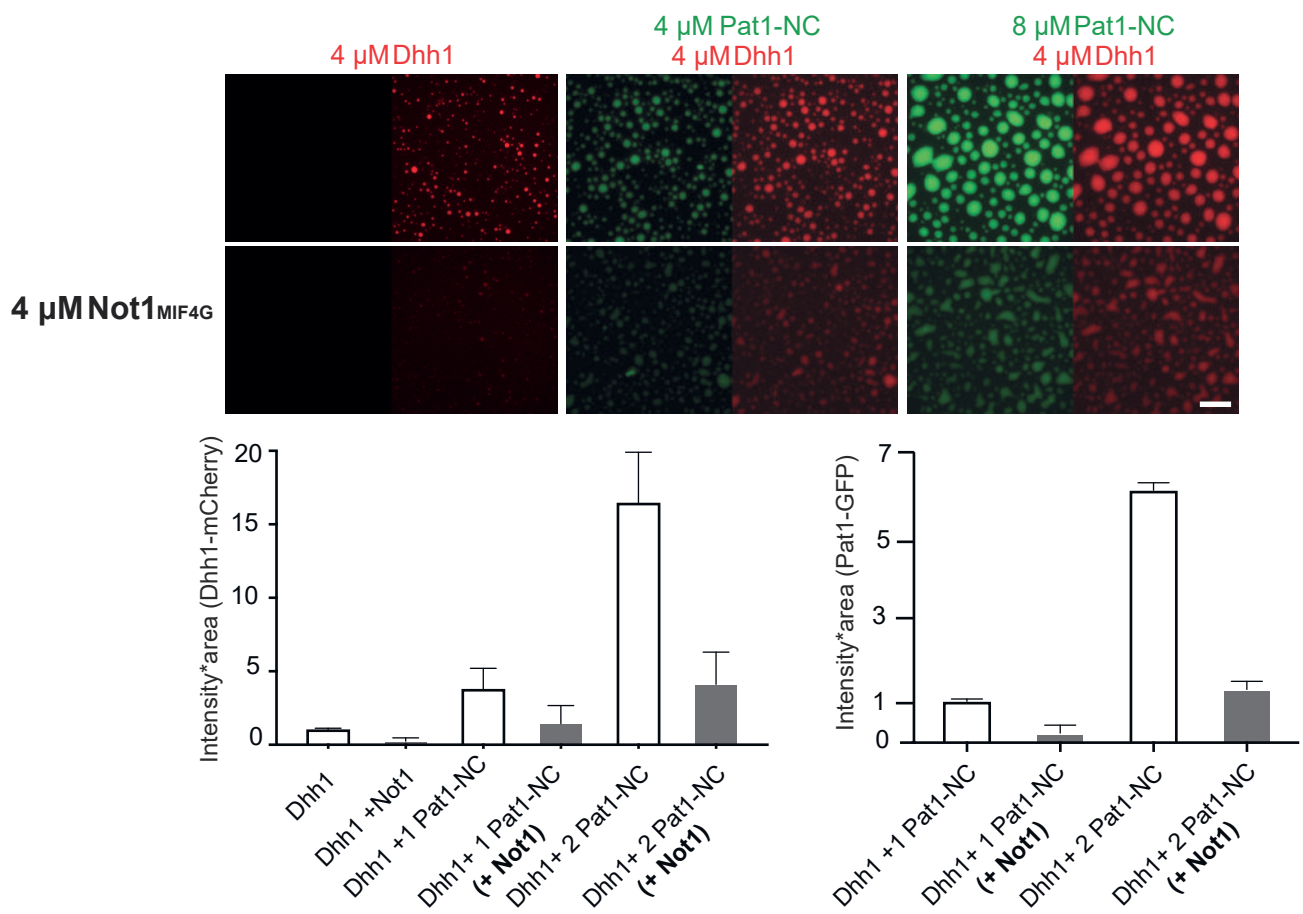
4 μM Dhh1
4 μM Pat1-NC
4 μM Dhh1
8 μM Pat1-NC
4 μM Dhh1
4 μM Not1 MIF4G
Intensity*area (Dhh1-mCherry)
Dhh1
Dhh1 +Not1
Dhh1 +1 Pat1-NC
Dhh1+ 1 Pat1-NC (+ Not1)
Dhh1+ 2 Pat1-NC
Dhh1+ 2 Pat1-NC (+ Not1)
Intensity*area (Pat1-GFP)
Dhh1 +1 Pat1-NC
Dhh1+ 1 Pat1-NC (+ Not1)
Dhh1+ 2 Pat1-NC
Dhh1+ 2 Pat1-NC (+ Not1)

Figure 7

A.

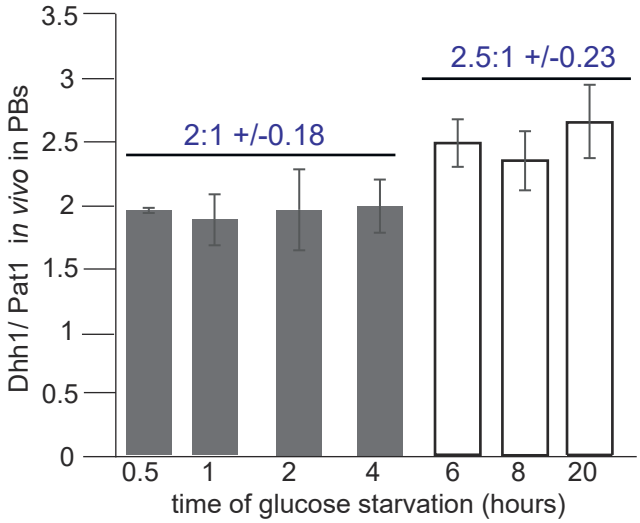

B. Stoichiometry of Dhh1/Pat1 in *in vitro* LLPS droplets

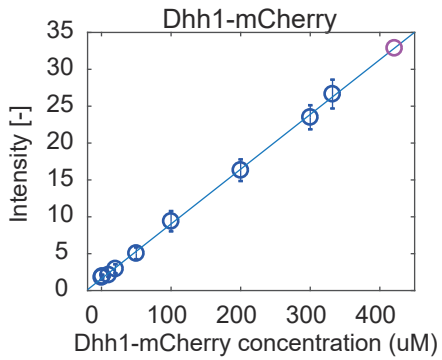

2 μM Dhh1, 5 mM ATP, 0.1 mg/ml pU

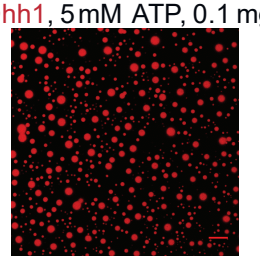

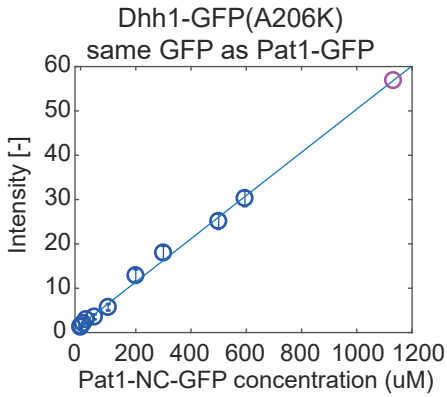

2 μM Dhh1, 5 mM ATP, 0.1 mg/ml pU + 4uM Pat1-NC

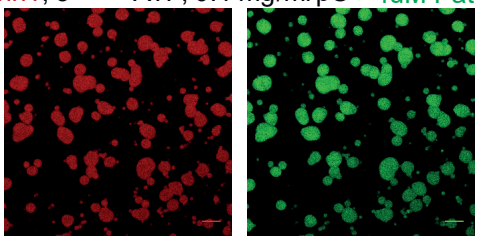

Dhh1:Pat1 in *in vitro* droplets= 2.7:1+/- 0.13

C. Tug of war model between Pat1 and Not1 to promote PB assembly and Disassembly respectively

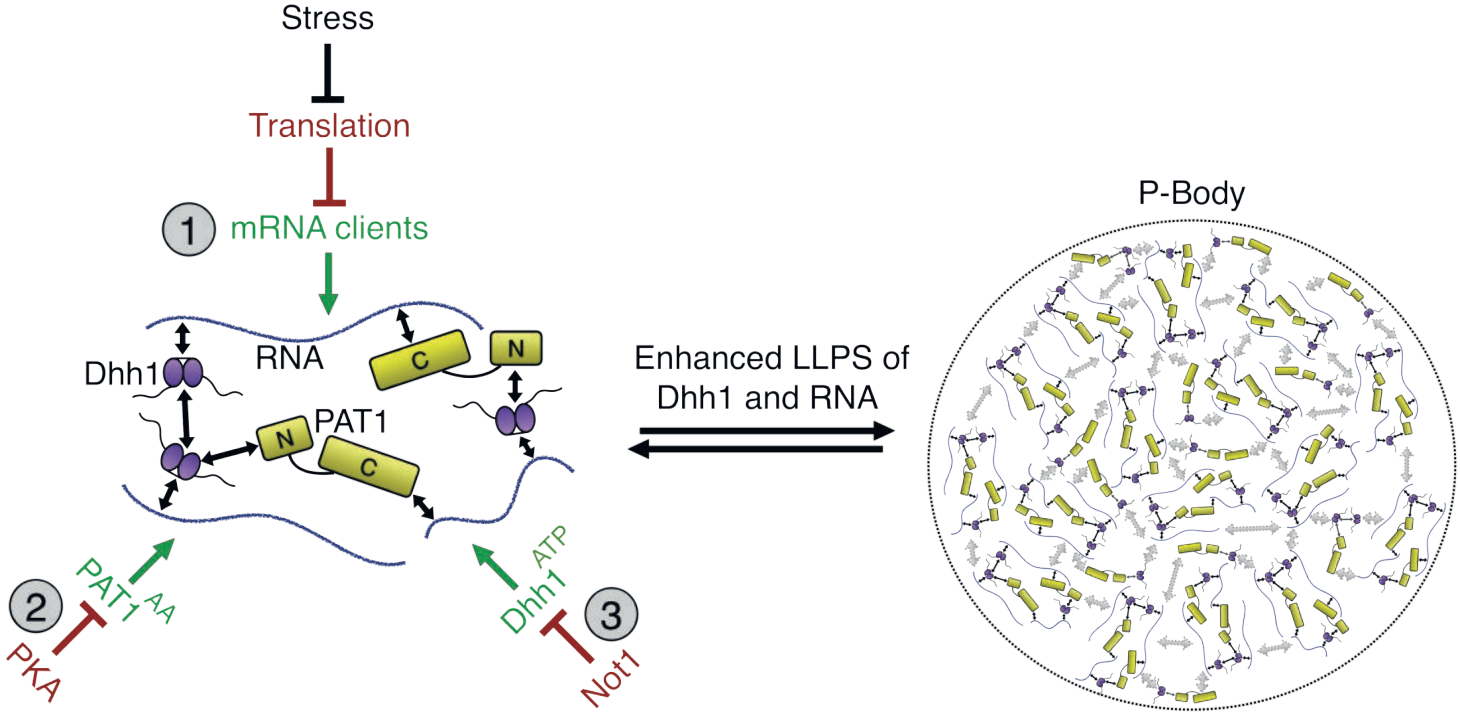

Figure 1- figure supplement 1

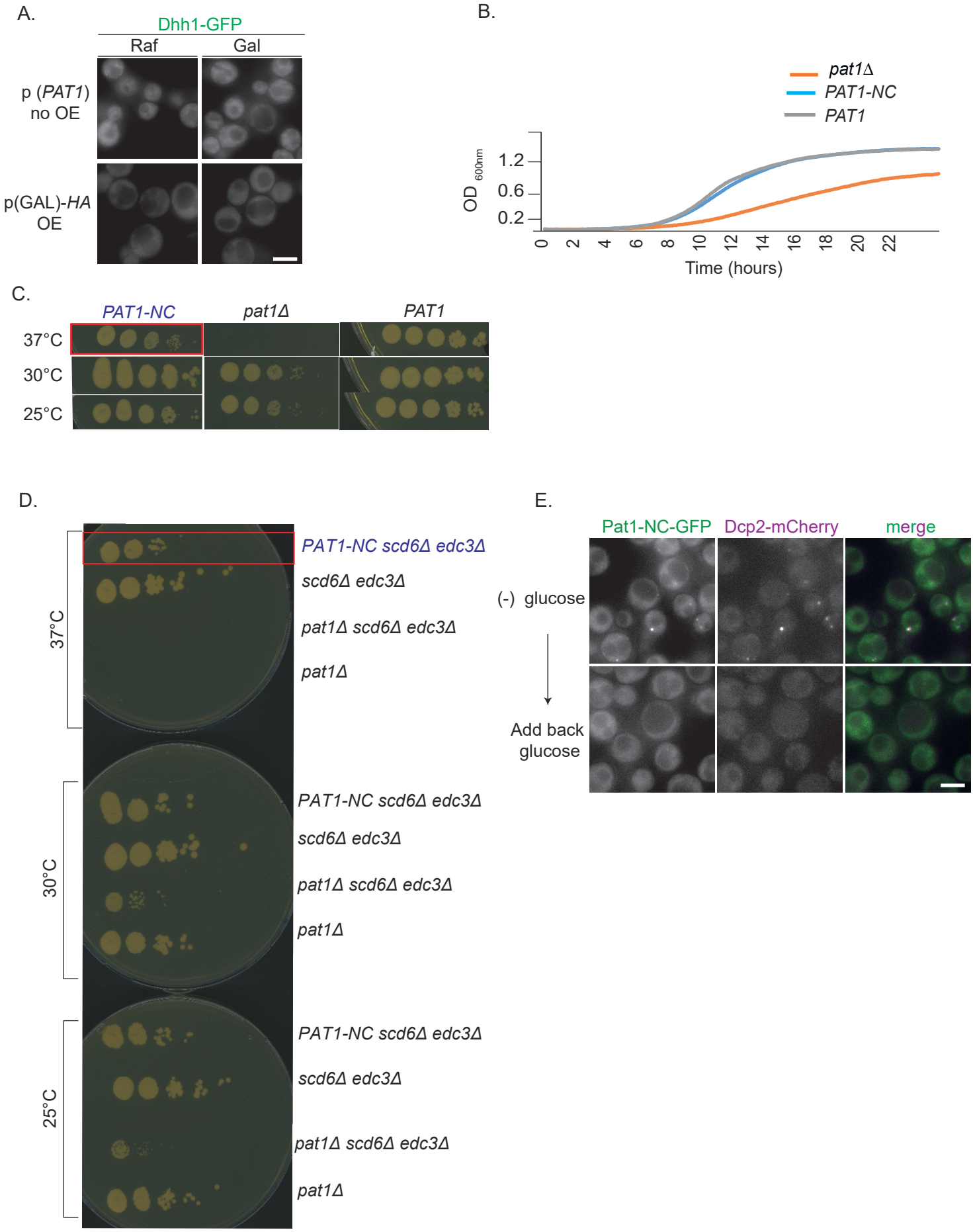

Figure 2- figure supplement 1

A.

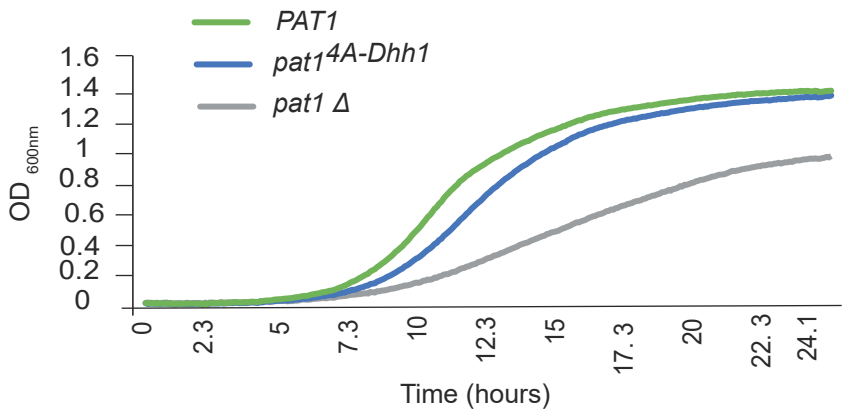

B.

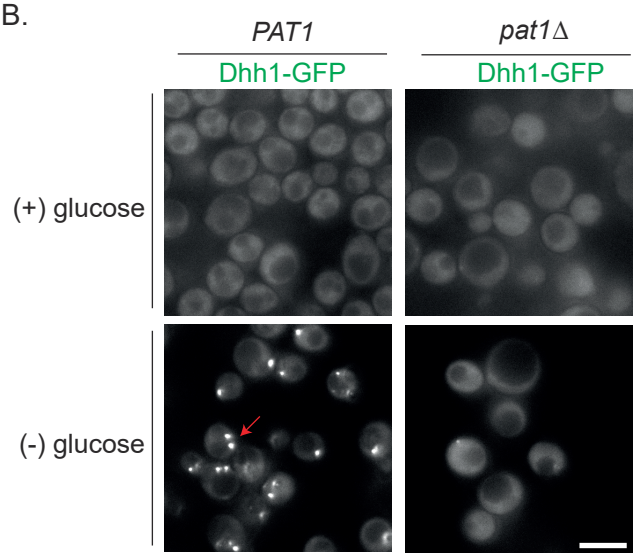

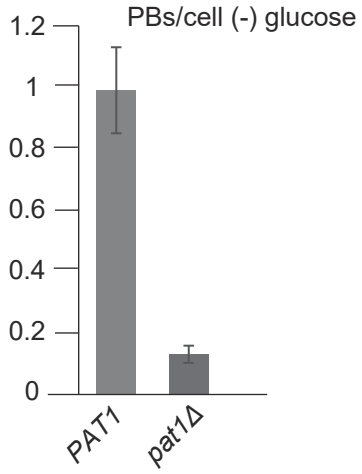

C.

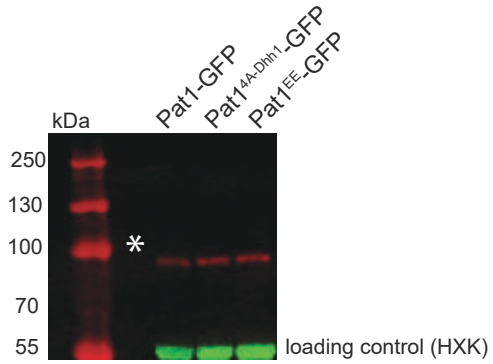

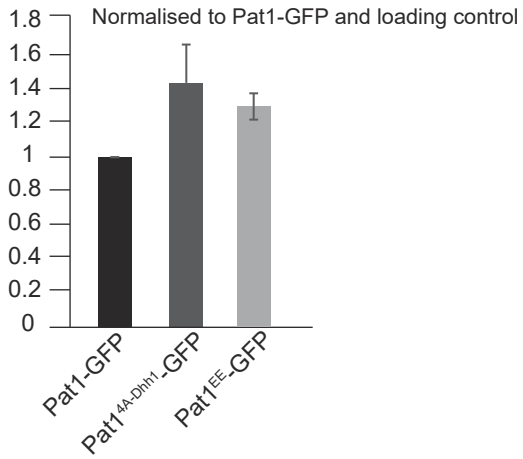

D.

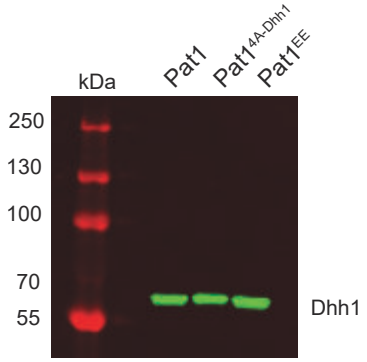

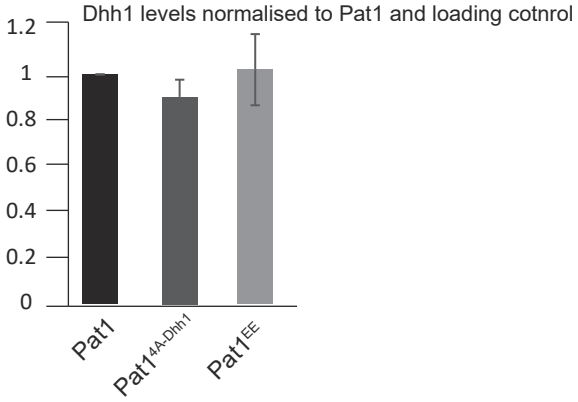

Figure 3- figure supplement 1

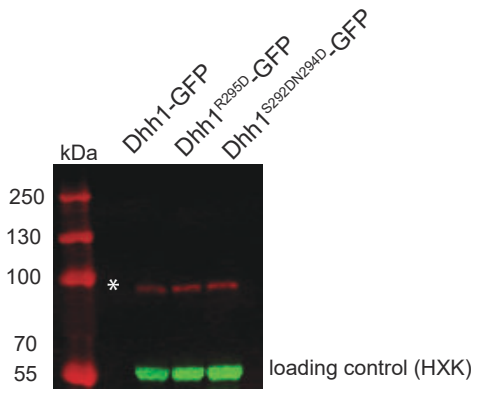

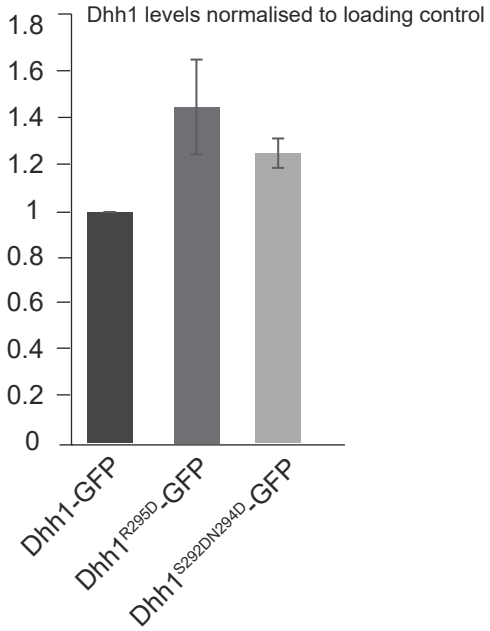

Figure 4- figure supplement 1

A.

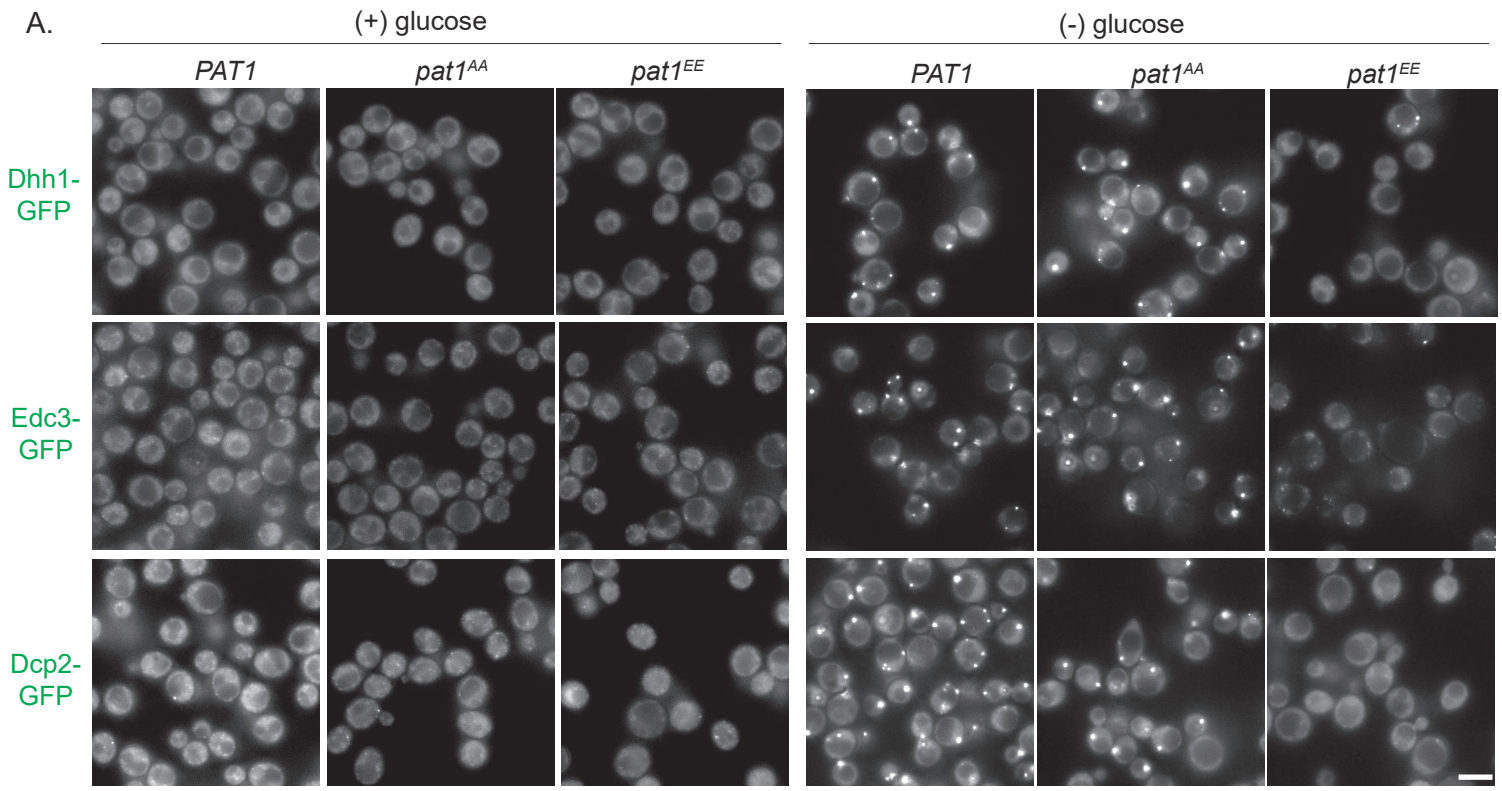

B.

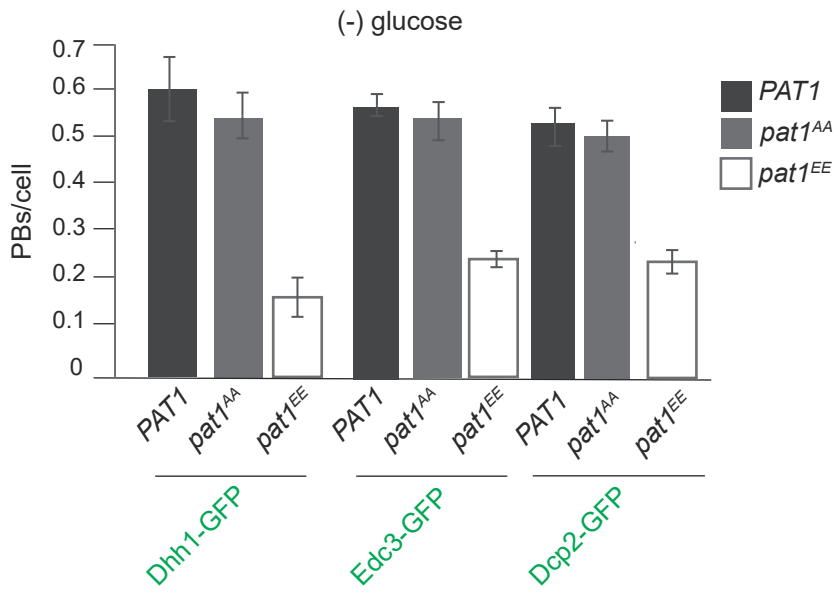

Figure 6- figure supplement 1

A.

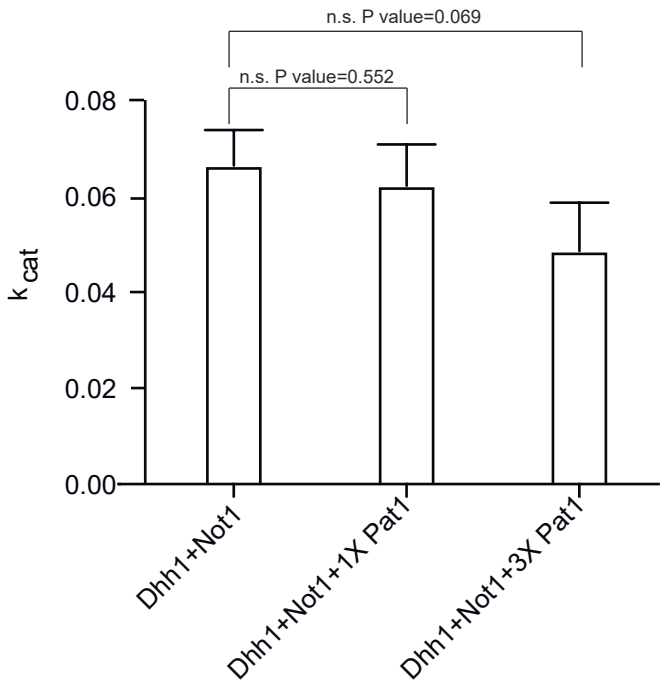

B.

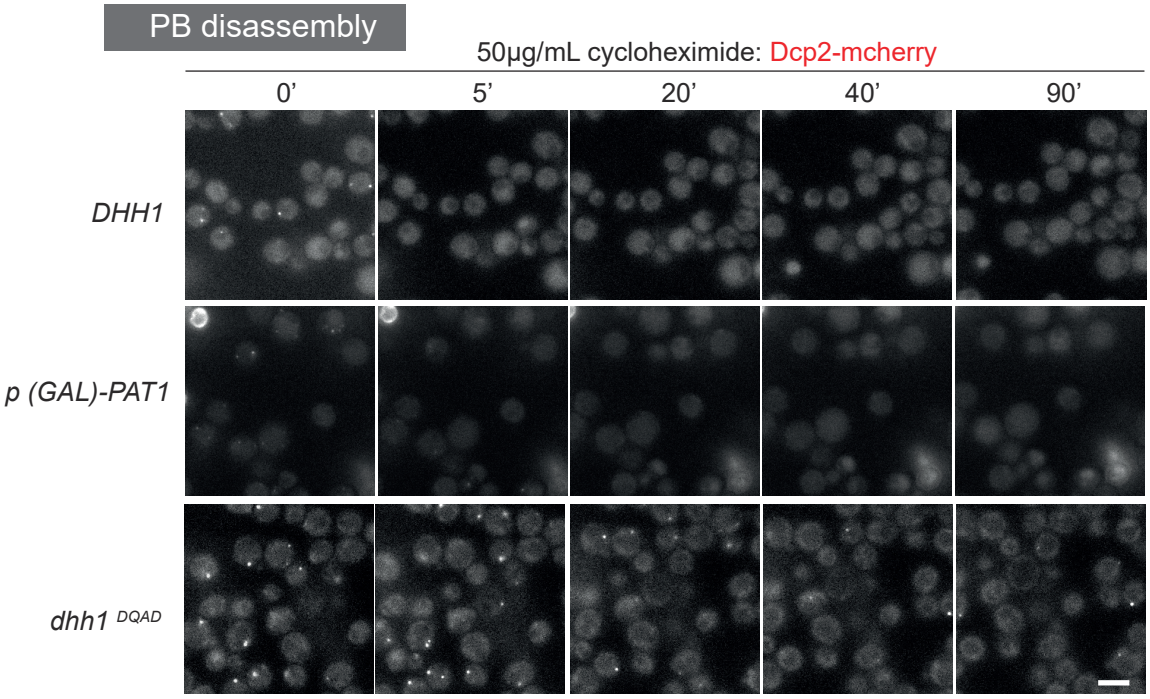

C.

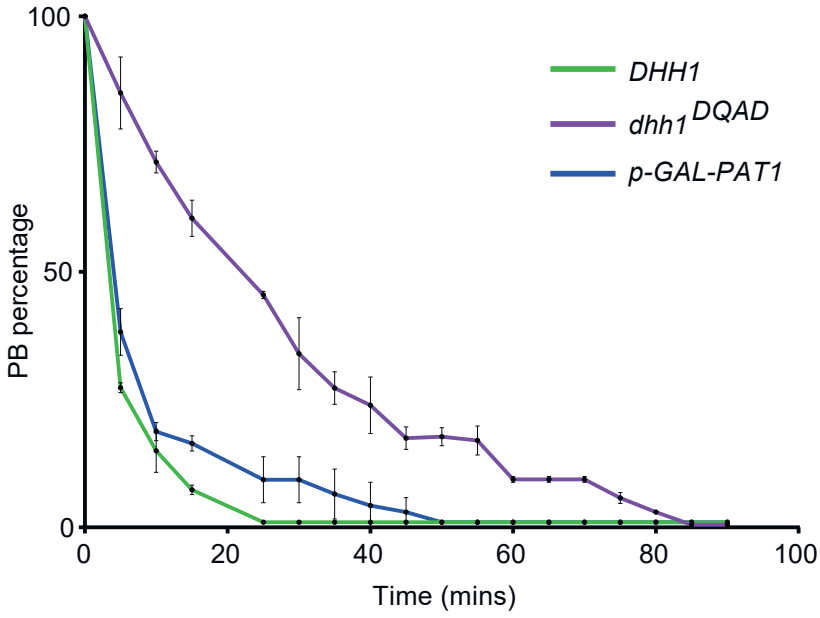

Figure 6- figure supplement 2

A.

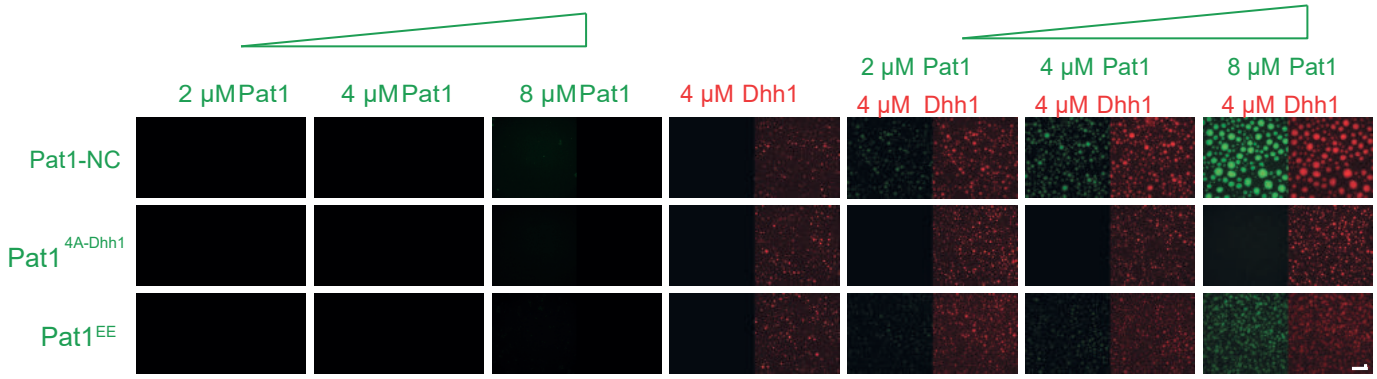

B.

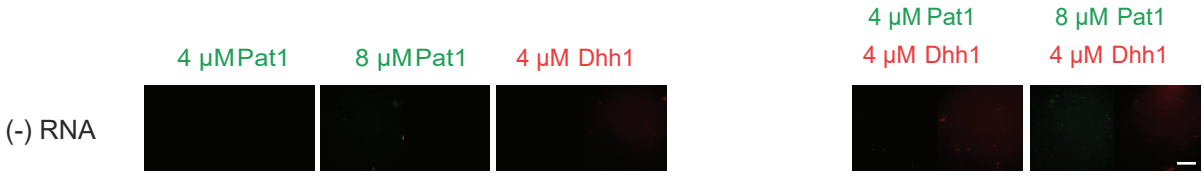

C.

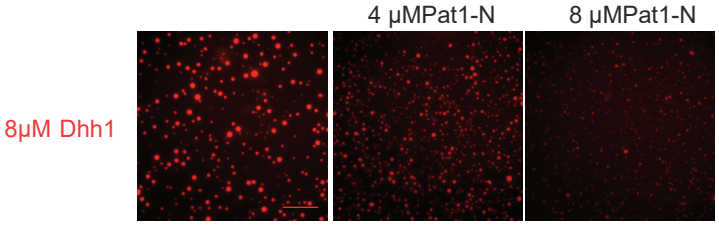

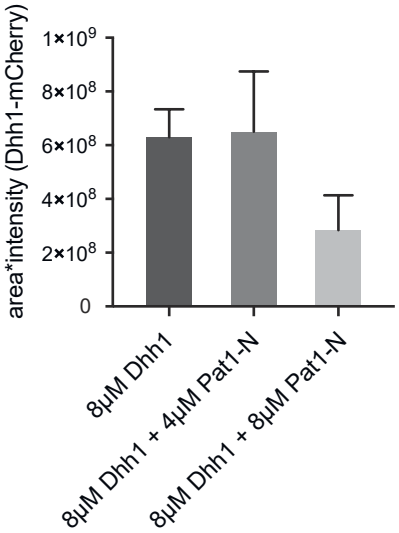

Figure 7- figure supplement 1

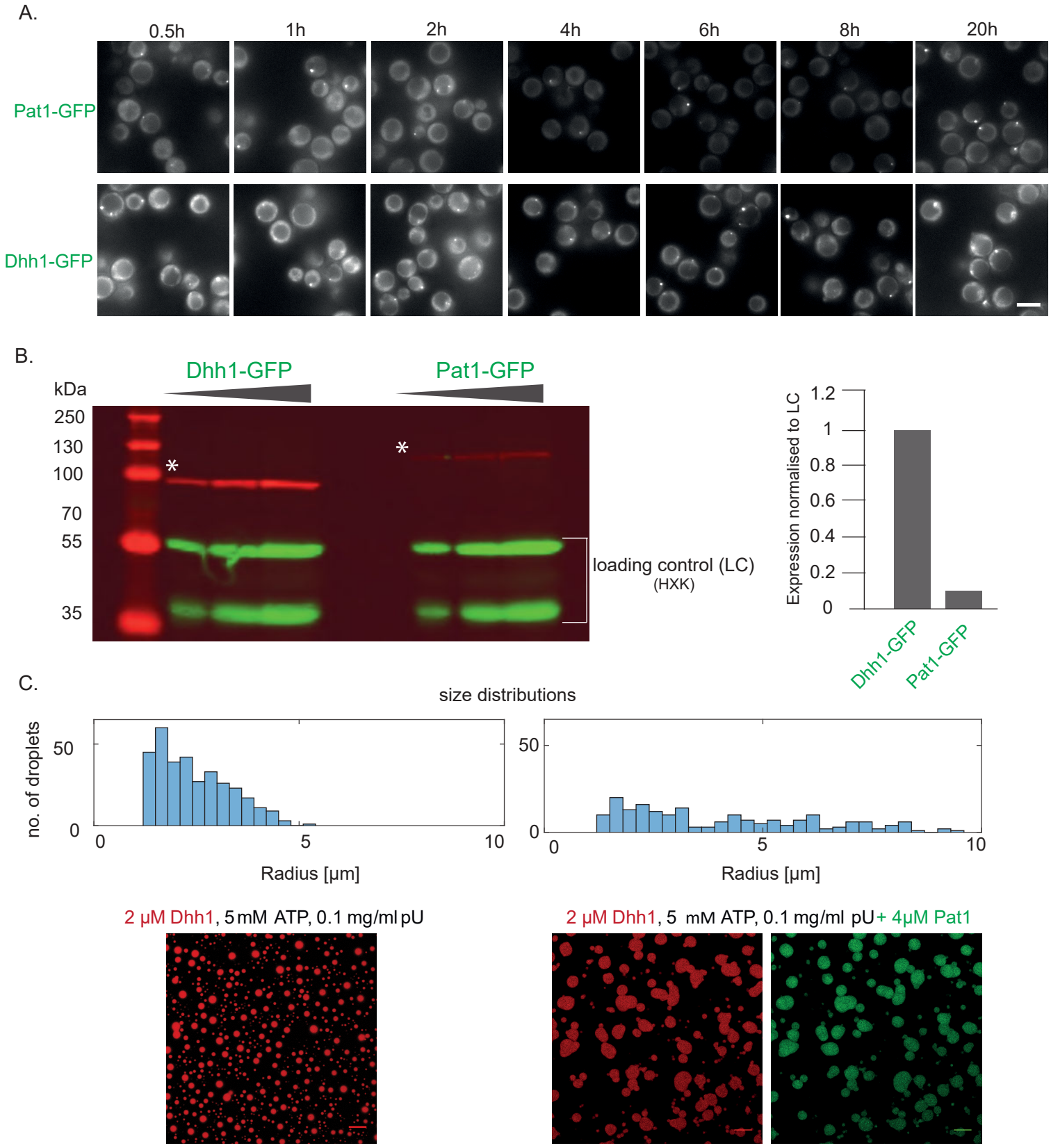

Figure 7- figure supplement 2

A.

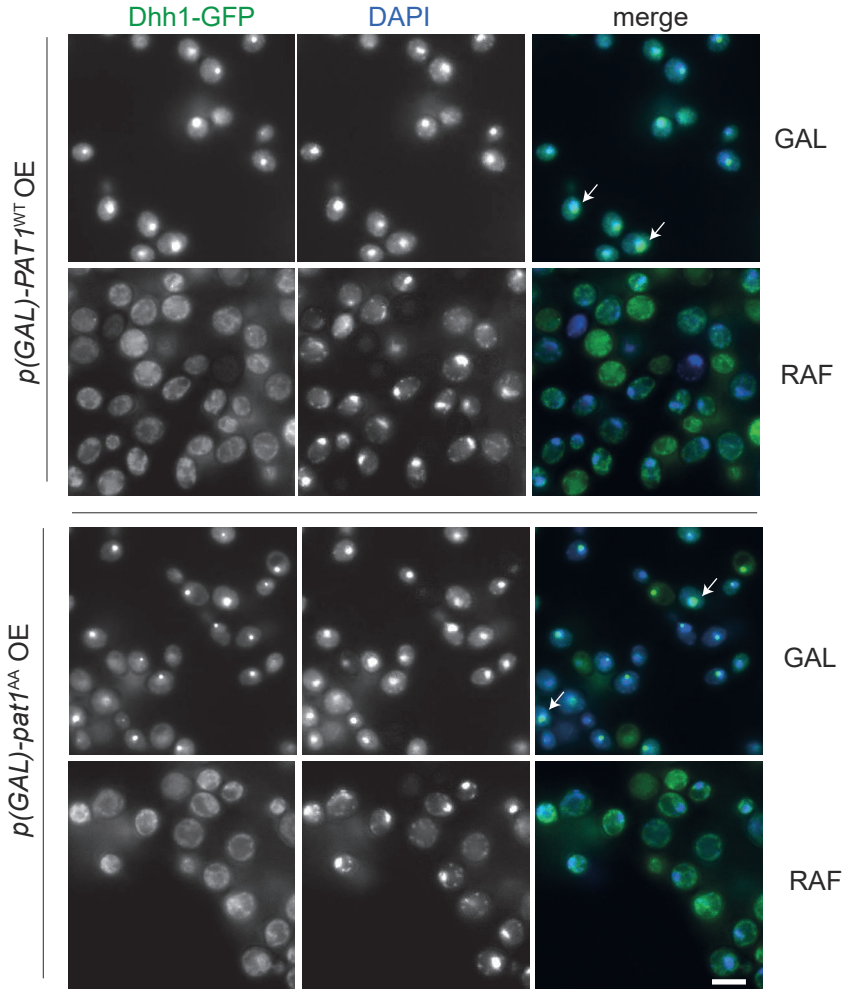

B.

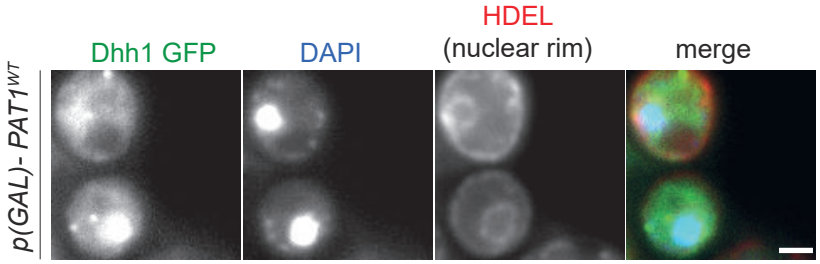
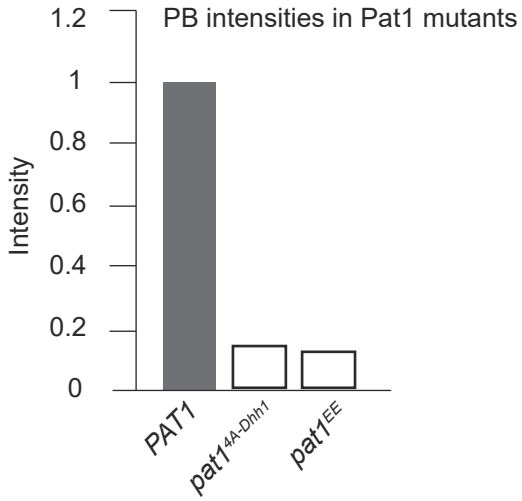
C.